VIDYA REPORT NO. 162
November 20, 1964

THEORETICAL AND EXPERIMENTAL STUDY OF THE ELASTIC BEHAVIOR OF THE HUMAN BRACHIAL AND OTHER HUMAN AND CANINE ARTERIES

by
E. Glenn Tickner
Alvin H. Sacks

prepared for
NATIONAL AERONAUTICS AND SPACE ADMINISTRATION
AMES RESEARCH CENTER
Moffett Field, California

Contract No. NAS2-1137
Vidya Project No. 9162

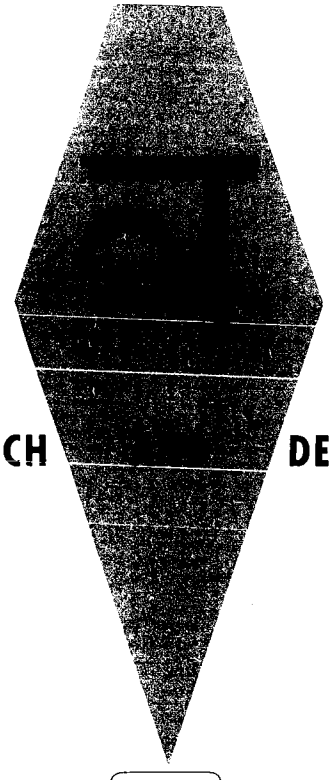

RESEARCH DEVELOPMENT

A DIVISION OF Itek CORPORATION

व VIDYA

The word Vidya, taken from the Vedanta philosophy of the Hindus, means knowledge. The symbol used to denote the Vidya organization is the letter "V" from Sanskrit, the ancient language of India.

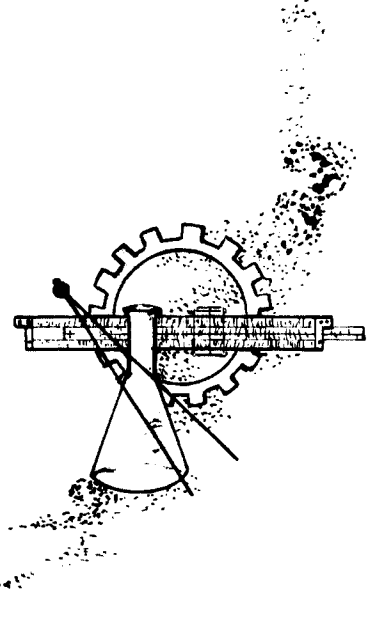

CASE FILE COPY

APPLIED MECHANICS
THERMODYNAMICS
NUMERICAL ANALYSIS
PHOTO-OPTICS
IMAGE ANALYSIS
PHYSICS

VIDYA COPY NO. 2

VIDYA REPORT NO. 162

November 20, 1964

THEORETICAL AND EXPERIMENTAL STUDY OF THE ELASTIC BEHAVIOR OF THE HUMAN BRACHIAL AND OTHER HUMAN AND CANINE ARTERIES

by
E. Glenn Tickner
Alvin H. Sacks

prepared for
NATIONAL AERONAUTICS AND SPACE ADMINISTRATION
AMES RESEARCH CENTER
Moffett Field, California

Contract No. NAS2-1137

Vidya Project No. 9162

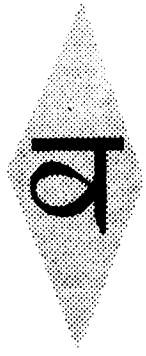

VIDYA

A DIVISION OF Itek CORPORATION

1450 PAGE MILL ROAD • PALO ALTO, CALIFORNIA
TEL: DAVENPORT 1-2455 TWX: 415 492-9270

ACKNOWLEDGMENT

A project such as this one, which involves the medical specialties of surgery, pathology, and radiology, as well as the engineering sciences, can only be carried out with the full cooperation of the medical profession. This cooperation was enthusiastically offered (without charge) by a number of local physicians, veterinarians, and X-ray specialists. In particular, we wish to thank Dr. Jon Kosek, Veterans Administration Hospital, Palo Alto, for supplying human brachial arterial specimens and consulting on the structure of the vascular wall. Other human arteries were kindly supplied by Dr. Arthur Lack, San Mateo County Hospital, and canine arteries by Dr. Ray Stofer, Palo Alto-Stanford Hospital, who also offered useful medical information. Finally, for development of the X-ray techniques employed herein, we are indebted to Mr. George Mahoney and Mr. Danny Mana of the Palo Alto-Stanford Hospital Radiology Department.

Throughout the entire project, valuable assistance was given by Vidya's medical consultant, Dr. David Bruns, and by Vidya's special consultant, Dr. William Nachbar of Stanford University, who introduced the investigators to the nonlinear membrane theory employed in the analysis.

SUMMARY

29149

A combined theoretical and experimental investigation has been carried out to determine the elastic behavior of various excised human and canine arterial segments. The specimens were subjected to the combined loads of internal pressure and axial tension, and measurements were made of the inner diameter, outer diameter, and length for each loading condition. Arteries tested included the human brachial, external iliac, superior mesenteric and splenic, as well as the canine femoral and thoracic aorta.

The results indicate that, for all specimens tested, the arterial wall behaves as a nonlinear, homogeneous, anisotropic, compressible material and can be described by six elastic constants for each level of strain. Both the circumferential and axial stiffness are found to increase with internal pressure and both approach the value for the collagenous fibres at very high internal pressure and axial weight, respectively. The radial stiffness is found to be essentially independent of either internal pressure or axial loading. The relationship of this behavior to the presence and orientation of the collagen fibres is discussed in detail.

The length of the arterial segment increases with pressure at low axial stress, but decreases with pressure at high axial stress. At in-vivo levels of internal pressure and axial stress, the artery length remains essentially unchanged, independent of loading. Further, at in-vivo levels, the artery behaves as though it were transversely isotropic, with equal stiffness in the circumferential and axial directions.

Author

TABLE OF CONTENTS

LIST OF TABLES

ACKNOWLEDGMENT

A project such as this one, which involves the medical specialties of surgery, pathology, and radiology, as well as the engineering sciences, can only be carried out with the full cooperation of the medical profession. This cooperation was enthusiastically offered (without charge) by a number of local physicians, veterinarians, and X-ray specialists. In particular, we wish to thank Dr. Jon Kosek, Veterans Memorial Hospital, Palo Alto, for supplying human brachial arterial specimens and consulting on the structure of the vascular wall. Other human arteries were kindly supplied by Dr. Arthur Lack, San Mateo County Hospital, and canine arteries by Dr. Ray Stofer, Palo Alto-Stanford Hospital, who also offered useful medical information. Finally, for development of the X-ray techniques employed herein, we are indebted to Mr. George Mahoney and Mr. Danny Mana of the Palo Alto-Stanford Hospital Radiology Department.

Throughout the entire project, valuable assistance was given by Vidya's medical consultant, Dr. David Bruns, and by Vidya's special consultant, Dr. William Nachbar of Stanford University, who introduced the investigators to the nonlinear membrane theory employed in the analysis.

LIST OF FIGURES

LIST OF SYMBOLS

a	inner radius, inches
A	ratio of elastic constants, $\frac{\beta_{23} - \beta_{13}}{\beta_{33}}$ (zero for isotropic material)
b	outer radius, inches
E_i	Young's modulus of elasticity, $\frac{d\sigma_{ii}}{d\epsilon_{ii}}$, psi
h	wall thickness, inches
I_1, I_2, I_3	strain invariants defined in Equation (4), dimensionless
k	elastic exponent, $(\beta_{11}/\beta_{33})^{1/2}$, dimensionless
l_i	dimension in the i direction ($i = 1,2,3$)
L	tube length measured between the ligatures used to mount the specimen, inches
p	internal pressure measured above atmospheric, psi or mm Hg
r	radial coordinate
r_m	mean radius $\frac{a+b}{2}$, inches
u	displacement in the radial direction
V	wall volume ($2\pi\ r_m h\ L$), in^3
w	displacement in the axial direction
W	strain energy per unit volume, (lb-in)/in^3 or psi
W_t	axial weight, lb
z	axial coordinate
α_{ij}	elastic constant obtained by inverting β_{ij}, psi^{-1}
β_{ij}	elastic constant $\lambda_j \frac{\partial \sigma_{ii}}{\partial \lambda_j}$ or $\frac{\partial \sigma_{ii}}{\partial \epsilon_{jj}}$, psi
γ	radius ratio a/b, dimensionless
ϵ_{ii}	strain in the i direction, dimensionless

θ	circumferential coordinate
λ_i	extension ratio (l_i / l_{i_o}), dimensionless
μ_{ij}	Poisson's ratio relating strain in i direction to stress in j direction ($i \neq j$), dimensionless
σ_{ii}	normal stress component in the i direction, psi

Superscript

$( )'$	partial differentiation with respect to pressure

Subscripts

o	unstressed condition ($p = W_t = o$)
1 or θ	circumferential direction
2 or z	axial direction
3 or r	radial direction

THEORETICAL AND EXPERIMENTAL STUDY OF THE ELASTIC BEHAVIOR OF THE HUMAN BRACHIAL AND OTHER HUMAN AND CANINE ARTERIES

1. INTRODUCTION

Understanding the physical structure and physiological behavior of blood vessels has long been the subject of serious study in the biological sciences. It has become increasingly clear that mathematical analysis and interpretation of such physiological phenomena as the pulse wave propagation, structural effects of aging and disease, and auscultatory blood pressures are greatly handicapped by the lack of quantitative data on the elastic behavior of arteries. Consequently, a number of investigators have performed varied tests on living, excised, and simulated parts of the arterial tree in order to deduce the elastic behavior or at least to understand the role that the elastic properties of arteries play in these phenomena (Refs. 1 through 24).

With regard to auscultatory blood pressures, the results of recent experiments in a simulated arterial system (Ref. 24) clearly indicated that auscultatory blood pressure readings exceed direct pressure readings by an amount which depends largely upon the elastic behavior (in particular the buckling pressure) of the vessel in question. Ordinarily, the vessel involved is the human brachial artery, for which elastic data appear to be virtually nonexistent. Therefore, the present investigation was initiated, primarily, to furnish such data. However, it became apparent during this study that past analytical treatments of arterial specimens have been inadequate because of the complex structure of arteries in general. The present report therefore presents a general treatment of the elastic behavior of arteries, with particular emphasis on the human brachial.

Most of the earlier mathematical analyses on elastic behavior of arterial specimens have been based upon the assumptions that the material is homogeneous, isotropic, and incompressible. It will be shown in this report that these assumptions are not justified, and that such an approach does not agree with the experimental evidence. A general nonlinear theory for thin-walled anisotropic tubes will be presented which permits the extraction of the six elastic constants for excised arterial specimens.

The results of experiments on various human and canine arteries will also be presented along with the values of these constants as obtained with the present theory.

2. THE ARTERIAL WALL

2.1 Structural Composition

The arterial wall is a very complex structure which surrounds the lumen (flow passage) of an artery. This wall is composed of several distinct annular layers, which themselves are comprised of various biological materials such as elastin, smooth muscle, collagen, and connective tissue (see Refs. 25 through 27).

Generally speaking, the arterial wall is thought of as consisting of five distinct laminas. These five layers are shown schematically in Figure 1 and are known, from the lumen outward, as the endothelium, internal elastic lamella, media, external elastic lamella, and adventitia (Ref. 25). The relative thickness of each lamina varies throughout the arterial tree so that, for some arteries, one or two layers may comprise nearly all of the wall thickness, while the remaining layers may be entirely missing. Figures 2, 3, and 4 present microphotographs which show this variation for three different arteries. The human brachial artery (Fig. 2) has a very thick media which constitutes nearly 75 percent of the total wall thickness. The canine femoral artery shown in Figure 3 has two equally thick layers (mediam and external elastic lamella) which comprise almost the entire wall, but the thoracic aorta (Fig. 4) has as its thickest layer the external elastic lamella, which makes up about 60 percent of the wall. The internal elastic lamella is virtually nonexistent in this particular artery.

The innermost lamina is the very soft endothelium which is a very thin layer, probably one cell in thickness. It cannot be seen under X100 magnification because it is only 1000 Angstroms thick (Ref. 26). The internal elastic lamella surrounds the endothelium, and it, too, comprises very little of the wall thickness of the larger arteries (see Ref. 25). This layer is primarily composed of elastin, with some connective tissue interspersed (see Ref. 28).

The next two laminas, the media and external elastic lammela, respectively, constitute the bulk of the arterial wall (see Refs. 25 through 29). The specimens already discussed (Figs. 2, 3, and 4) displayed this characteristic quite well.

The media is primarily composed of smooth muscle, but is striated with elastin and some collagen. On the other hand, the external elastic lamella, like the internal elastic lamella, has virtually no smooth muscle whatsoever. It is made up of elastin and increasing amounts of collagen,

so that its outer edge becomes completely collagenous and blends into the adventitia.

The adventitia, the outermost layer, has a high percentage of collagen and is most unique. K. J. Franklin (Ref. 30) reports that this lamina is made up of very stiff collagenous fibres, which form a double-crisscross, waveless, spiral network around the inner layers, as shown schematically in Figure 5. As indicated in the figure, their behavior is very comparable to that of the well-known "Chinese finger puzzle," in which an increasing axial load causes a thinning of the wall and a rotation of the fibers to a more nearly axial orientation. It is not known whether this structure is typical of other layers where collagen is present.

In summary, the arterial wall consists of several laminas which are composed of fairly elastic materials, elastin and smooth muscle, and the stiffer collagen fibres which form helical rings around the inner layers. The arterial wall is, therefore, clearly inhomogeneous, primarily in the radial direction.

2.2 Elastic Behavior

The importance of the elastic characteristics of living blood vessels has long been recognized by physiologists, and many attempts have been made to determine those characteristics by both static and dynamic elastic tests. For the larger arteries, the mathematical problem is that of an elastic cylindrical tube which is subjected to an elevated internal pressure, a longitudinal or axial force, and a periodic variation in internal pressure, with certain external constraints applied to the tube. Physically, this means that the artery, which has become stretched along its axis during early growth and is constrained by surrounding tissues and muscles, is subjected to an internal pressure pulse superimposed on a mean pressure which is normally about 100 mm Hg. above atmospheric pressure. The question, of course, is what are the corresponding deformations of the vessel wall, and what are the associated elastic constants.

Perhaps the earliest systematic elastic tests of arterial specimens were carried out by Roy (Ref. 1), who found that arteries exhibit the properties of that class of materials now known as elastomers. In particular, they exhibit

(a) A large elastic range (i.e., large deformations with subsequent return).

(b) A nonlinear stress-strain relation (stiffness varies with strain).

(c) A relaxation time (i.e., strain under constant stress varies with time).

(d) Anomalous thermal behavior (material contracts when heated while under tension).

Since Roy's investigations of aortic strips, many experiments have been performed to determine the variation of elastic modulus with strain for various intact vessels, both excised (Refs. 1 through 17) and in-vivo (Refs. 18 and 19). In general, all of these experiments show a nonlinear variation of diameter with pressure for the intact vessel, and in 1957, Roach and Burton published an "explanation" of this behavior (Ref. 13), which they attributed to the character of the various component materials discussed above (see Section 2.1). By differential digestion of the collagen (by formic acid) and the elastin (by crude trypsin), Roach and Burton were able to test each component material and found values of Young's modulus for elastin to be about 80 psi, as compared with the much stiffer collagen with a value of about 1500 psi.

It is interesting to note that in no case was the material volume measured. It is generally assumed that the material is incompressible, which is more or less true of rubber-like materials. Previous investigators have also generally assumed that the material is homogeneous and isotropic, and can therefore be characterized by a single value of Young's modulus for any given loading. This seems to be a particularly bold assumption, in view of the complex physical structure discussed above.

As a check on the assumption of isotropy, Lawton (Ref. 6, p. 160) tested arterial strips cut longitudinally, circumferentially, and at various angles to the tube axis. The results of these tests indicate that there is no significant effect of orientation. Lawton therefore concluded that the arterial wall is isotropic. However, since the collagenous fibres actually form a helical net around the intact arterial wall, it seems apparent that cutting this net would not only alter the elastic properties of the vessel but would remove the very mechanism of anisotropy[1] and yield results which have the appearance of isotropy. Hence, elastic tests of arterial strips cannot be used to demonstrate the elastic behavior of intact specimens. As a matter of fact, the work of Fenn (Ref. 15) strongly suggests that arteries are anisotropic.

---

[1] An anisotropic material is one whose elastic constants are directionally dependent; that is, it is one which possesses a different modulus of elasticity, Poisson's ratio, and shear modulus along each of the three orthogonal axes.

The question of homogeneity is a somewhat different matter. First, it is clear from the microphotographs discussed in Section 2.1 that the arterial wall is not really composed of a homogeneous material. On the other hand, if we seek a mathematical model which will predict the elastic behavior of an artery when subjected to various loads, we may be able to represent the cylindrical tube as made up of an equivalent homogeneous material, provided that it exhibits a different elasticity in each of three orthogonal directions, and we permit the elastic "constants" to vary with the loading. The mathematical model need not necessarily remain at constant volume, provided that we make sufficient measurements so that the volume can be determined under each loading.

The purpose of the subsequent sections of this report will be, first, to set up a mathematical model whose elastic constants may be expected to describe the elastic behavior of an artery under arbitrary loading, and, second, to set up and carry out experiments by which these constants can be determined for a given specimen. In so doing, of course, we shall find out whether the arterial wall can be described as nearly homogeneous, isotropic, and/or incompressible.

3. THEORETICAL CONSIDERATIONS

The primary aim of the analysis to be presented here is to enable one to determine the elastic constants of a given arterial specimen from measured values of the applied forces and pressures and the corresponding deformations. Because the material in question is likely to be anisotropic and exhibits nonlinear deformations, a mathematical analysis is not a simple task. In fact, the arterial wall must be considered to be characterized by at least six elastic constants (corresponding to one value of Young's modulus and one value of Poisson's ratio for each of the three coordinate directions). Furthermore, these "constants" are expected to depend upon the level of strain and are therefore not really constant at all. Consequently, we shall characterize the material of the arterial wall as anisotropic and consider large deformations, so that the elastic constants in question will refer to the local behavior of the wall at a given strain level.

The mathematical problem to be treated here is that of a thin-walled, cylindrical tube of finite length which is subjected to the combined loads of an elevated internal pressure and an applied axial force. The assumed model and the appropriate cylindrical coordinate system are shown in Figure 6.

The thin wall assumption is used so that the stresses and strains can be assumed to be uniform throughout the material. In other words, the arterial wall is treated essentially as a membrane.

Large deformation theory is required to represent the static elastic characteristics of arterial materials because these materials exhibit a nonlinear stress-displacement relationship (see sketch below). This nonlinear curve means that the modulus of elasticity (local slope of the stress-displacement curve) varies with the loading. Hence, we shall employ large deformation theory to determine the nonlinear equation relating stress and displacement and, from this equation, determine the local elastic constants from the local slopes.

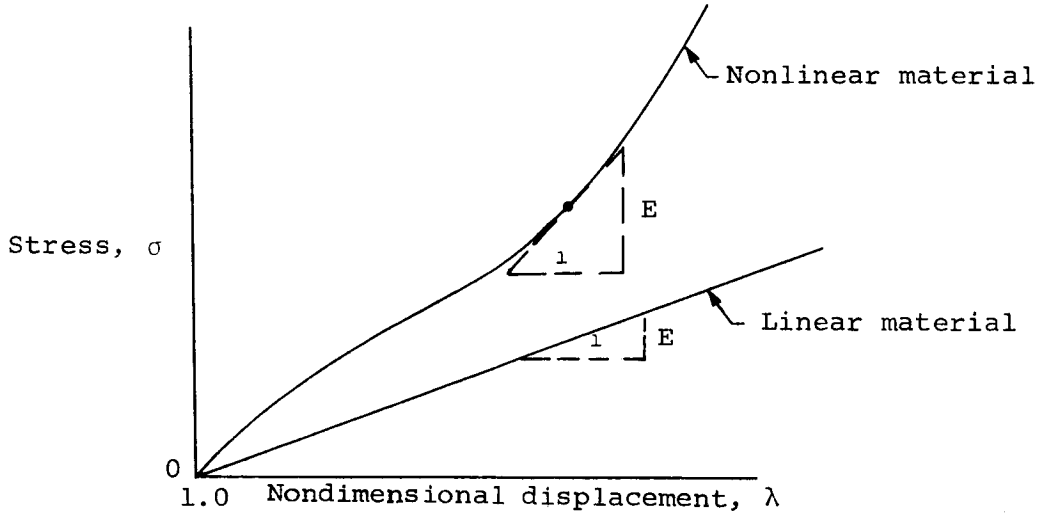

Large deformation theory is based upon the existence of a unique strain energy potential, W, which represents the elastic energy (per unit volume) stored in the material when it is brought from the unstrained configuration to its strained condition. We note that the elastic potential is a positive quantity for all real strains and has a value of zero (W = 0) at the unstrained condition. Various tests (Refs. 31, 33, or 34) show that, if the loadings are performed isothermally, an elastic potential may exist and, if so, is a single-valued function of the state of strain of the deformed body, as well as of the geometrical and elastic constants. Further, if the material is inviscid and nonplastic and if the aforementioned elastic potential exists, then the material is said to behave as an ideally elastic continuum. The real material does exhibit some viscosity and plasticity, but these are considered minimal for the low rates of loading experienced during the present static tests.

Next, we shall assume that the material is elastically homogeneous. Earlier in this report, it was pointed out that the arterial wall was definitely inhomogeneous. However, we now assume that the mean elastic behavior of the wall can be represented by an equivalent homogeneous material. Mathematically, this assumption demands that the elastic coefficients at any given load are independent of location in the specimen (see Ref. 31, p. 156 for more details), and the elastic potential has the same form throughout the material.

In summary, the elastic tube representing the artery is assumed to be

(1) A circular cylinder (axisymmetric)

(2) Thin-walled (quasi-membrane)

(3) Ideally elastic
(4) Initially unstressed and unstrained
(5) Deformed isothermally
(6) Elastically homogeneous (properties uniform throughout)

Since we are dealing with large deformations, it is convenient to represent the deformation in terms of extension ratios ($\lambda_1, \lambda_2, \lambda_3$) which are defined relative to the unstressed dimensions as follows:

$$\begin{aligned} \lambda_1 &= l_1/l_{1_0} \\ \lambda_2 &= l_2/l_{2_0} \\ \lambda_3 &= l_3/l_{3_0} \end{aligned} \tag{1}$$

The subscripts 1, 2, and 3 refer to the coordinates selected, and the zero subscript denotes the unstressed dimension.

The above ratios are directly related to the corresponding strains (ϵ_{ii}) for small displacements so that

$$\begin{aligned} \lambda_1 &= 1 + \epsilon_{11} \\ \lambda_2 &= 1 + \epsilon_{22} \\ \lambda_3 &= 1 + \epsilon_{33} \end{aligned} \tag{2}$$

The strain energy W is, in general, a function of all six components of the strain tensor; that is, it is a function of the normal strains (ϵ_{11}, ϵ_{22}, and ϵ_{33}) and the shear strains (ϵ_{12}, ϵ_{13}, and ϵ_{23}). However, because of the membrane assumption, the normal strains are assumed to be uniform throughout the material. Hence, for the axisymmetric tube being considered, a pure axial tension combined with a uniform pressure loading cannot produce any shear strains. Therefore, the shear strains are zero and the strain energy function W becomes a function of only the three normal strain components or the three extension ratios λ_1, λ_2, and λ_3. That is,

$$W = W\ (\lambda_1, \lambda_2, \text{ and } \lambda_3) \tag{3}$$

It will be noted that the extension ratios depend upon the selection of coordinates, as well as upon the loading, and that the W function defined by Equation (3), therefore, does not uniquely characterize the strain

energy of the material in question. On the other hand, it can be shown (Ref. 32) that there exist three strain invariants which are independent of the coordinate system chosen. These invariants are expressible in terms of the extension ratios of any particular coordinate system chosen. For our case, since the tube wall thickness is assumed to be very small compared with the tube diameter, we have a Cartesian coordinate system, and one can express the three invariants as follows (Ref. 31):

$$\begin{aligned} I_1 &= \lambda_1^2 + \lambda_2^2 + \lambda_3^2 \\ I_2 &= \lambda_1^2\lambda_2^2 + \lambda_1^2\lambda_3^2 + \lambda_2^2\lambda_3^2 \\ I_3 &= \lambda_1^2\lambda_2^2\lambda_3^2 \end{aligned} \tag{4}$$

The extension ratios can be defined in terms of the tube dimensions shown in Figure 6. Thus we have

$$\left.\begin{aligned} \lambda_1 &= r_m/r_{mo} \quad \text{(circumferential)} \\ \lambda_2 &= L/L_o \quad \text{(axial)} \\ \lambda_3 &= h/h_o \quad \text{(radial)} \end{aligned}\right\} \tag{5}$$

Hence, we can write the strain energy function W in its proper form

$$W = W(I_1, I_2, I_3) \tag{6}$$

so that the stored energy is uniquely defined for any loading of the given material in any coordinate system in terms of the strain invariants.

The invariant I_3 has a simple physical interpretation which can be seen by noting that the volume V of the thin tube is given by

$$V = 2\pi\, r_m h L \tag{7}$$

Similarily, the initial volume V_o is

$$V_o = 2\pi\, r_{mo} h_o L_o \tag{8}$$

so that Equations (4), (5), (7), and (8) yield

$$I_3 = \lambda_1^2\lambda_2^2\lambda_3^2 = \left(\frac{r_m}{r_{mo}}\right)^2\left(\frac{L}{L_o}\right)^2\left(\frac{h}{h_o}\right)^2 = \left(\frac{V}{V_o}\right)^2 \tag{9}$$

Thus we see that I_3 represents the square of the volume ratio, which is clearly independent of the coordinate system, and is a direct measure of the compressibility of the material. A value of $I_3 = 1$ for all loadings would represent incompressibility. The remaining two invariants, I_1 and I_2, can be shown (see Ref. 31) to be mathematically constant under proper transformations, but do not have a simple physical interpretation. All of the invariants are functions of the material and the applied loads.

The stress-strain relations are obtained by differentiation of the energy function relative to the strains, so that, for small deformations we have the familiar form (Ref. 33 or 35)

$$\sigma_{ii} = \partial W/\partial\epsilon_{ii} \tag{10}$$

For the case of an isotropic material, where W is given as

$$W = \frac{E}{2(1-2\mu)(1+\mu)}\left[(1-\mu)(\epsilon_{11}^2 + \epsilon_{22}^2 + \epsilon_{33}^2) + 2\mu(\epsilon_{11}\epsilon_{22} + \epsilon_{22}\epsilon_{33} + \epsilon_{33}\epsilon_{11})\right] \tag{11}$$

Equation (10) yields Hooke's law in the form

$$\left.\begin{aligned}
\sigma_{11} &= \frac{(1-\mu)E}{(1-2\mu)(1+\mu)}\epsilon_{11} + \frac{\mu E}{(1-2\mu)(1+\mu)}\epsilon_{22} + \frac{\mu E}{(1-2\mu)(1+\mu)}\epsilon_{33} \\
\sigma_{22} &= \frac{\mu E}{(1-2\mu)(1+\mu)}\epsilon_{11} + \frac{(1-\mu)E}{(1-2\mu)(1+\mu)}\epsilon_{22} + \frac{\mu E}{(1-2\mu)(1+\mu)}\epsilon_{33} \\
\sigma_{33} &= \frac{\mu E}{(1-2\mu)(1+\mu)}\epsilon_{11} + \frac{\mu E}{(1-2\mu)(1+\mu)}\epsilon_{22} + \frac{(1-\mu)E}{(1-2\mu)(1+\mu)}\epsilon_{33}
\end{aligned}\right\} \tag{12}$$

For the more general case of an anisotropic material with large deformations, an analogous differentiation (Ref. 32) yields (for the case of no shear strains)

$$\left.\begin{aligned}
\sigma_{11} &= \lambda_1^2\phi + \lambda_1^2(\lambda_2^2 + \lambda_3^2)\ \psi + P \\
\sigma_{22} &= \lambda_2^2\phi + \lambda_2^2(\lambda_1^2 + \lambda_3^2)\ \psi + P \\
\sigma_{33} &= \lambda_3^2\phi + \lambda_3^2(\lambda_1^2 + \lambda_2^2)\ \psi + P \\
\sigma_{ij} &= 0 \qquad i \neq j
\end{aligned}\right\} \tag{13}$$

where the quantities ϕ, ψ, and P depend upon the partial derivatives of the W function with respect to the three invariants, I_1, I_2, I_3 as given by

$$\left.\begin{aligned}
\phi &= \frac{2}{\sqrt{I_3}}\ \frac{\partial W}{\partial I_1} \\
\psi &= \frac{2}{\sqrt{I_3}}\ \frac{\partial W}{\partial I_2} \\
P &= 2\sqrt{I_3}\ \frac{\partial W}{\partial I_3}
\end{aligned}\right\} \tag{14}$$

Furthermore, it can be shown that Equation (13) reduces to Equation (12) for isotropic materials.

If the quantities ϕ, ψ, and P, which are functions of the partial derivatives of W, are known, then Equation (13) permits one to compute the stresses in terms of the extension ratios or vice versa. On the other hand, if these functions are unknown (as in the present study) but the extension ratios are known instead, then Equation (13) can be used in a different form to determine the unknown partial derivatives. Thus, solving Equations (13) for the three partial derivatives, we have

$$\left.\begin{aligned}
\frac{\partial W}{\partial I_1} &= \frac{\sqrt{I_3}}{2}\phi = \frac{\sqrt{I_3}}{2D}\left[\sigma_{11}\lambda_1^2\left(\lambda_2^2 - \lambda_3^2\right) + \sigma_{22}\lambda_2^2\left(\lambda_3^2 - \lambda_1^2\right) + \sigma_{33}\lambda_3^2\left(\lambda_1^2 - \lambda_2^2\right)\right] \\
\frac{\partial W}{\partial I_2} &= \frac{\sqrt{I_3}}{2}\psi = \frac{\sqrt{I_3}}{2D}\left[\sigma_{11}\left(\lambda_3^2 - \lambda_2^2\right) + \sigma_{22}\left(\lambda_1^2 - \lambda_3^2\right) + \sigma_{33}\left(\lambda_2^2 - \lambda_1^2\right)\right] \\
\frac{\partial W}{\partial I_3} &= \frac{P}{2\sqrt{I_3}} = \frac{1}{2D\sqrt{I_3}}\left[\sigma_{11}\lambda_2^2\lambda_3^2\left(\lambda_2^2 - \lambda_3^2\right) + \sigma_{22}\lambda_1^2\lambda_3^2\left(\lambda_3^2 - \lambda_1^2\right) + \sigma_{33}\lambda_1^2\lambda_2^2\left(\lambda_1^2 - \lambda_2^2\right)\right]
\end{aligned}\right\} \tag{15}$$

where

$$D = \lambda_1^4\left(\lambda_2^2 - \lambda_3^2\right) + \lambda_2^4\left(\lambda_3^2 - \lambda_2^2\right) + \lambda_3^4\left(\lambda_1^2 - \lambda_2^2\right)$$

It can be seen that static tests in which the three stresses and strains are measured for a given loading provide the necessary information to calculate the three partial derivatives $(\partial W/\partial I_i)$. The W function can then be determined by mapping these partial derivatives over all loadings and then generating the energy function W which satisfies the data. In order to do this, we shall assume that

$$\frac{\partial^2 W}{\partial I_i \partial I_j} = 0; \quad i \neq j \qquad (i,j = 1,2,3) \tag{16}$$

on the basis of experimental work performed on rubber-like materials (Refs. 36 through 39). This last assumption, along with that of an initial zero value of W, permits us to write W in the functional form

$$W = f_1(I_1 - 3) + f_2(I_2 - 3) + f_3(I_3 - 1) \tag{17}$$

where the functions f_1, f_2, and f_3 are unspecified except that they must pass through the origin; that is, the unloaded condition corresponds to values of I_1, I_2, and I_3 of 3.0, 3,0, and 1.0, respectively (see Eq. (4)).

For the present study, we shall represent the function W by a power series expansion of $I_1 - 3$, $I_2 - 3$, and $I_3 - 1$. That is,

$$\begin{aligned} W = {} & B_1(I_1 - 3) + B_2(I_1 - 3)^2 + \ldots + B_n(I_1 - 3)^n \\ & + C_1(I_2 - 3) + C_2(I_2 - 3)^2 + \ldots + C_n(I_2 - 3)^n \\ & + D_1(I_3 - 1) + D_2(I_3 - 1)^2 + \ldots + D_n(I_3 - 1)^n \end{aligned} \tag{18}$$

Experimentally, we find that $n = 3$ is sufficient to describe the behavior of all arteries tested.

The coefficients of the W function in Equation (18) can be determined from the stress-strain data, since the partial derivatives of W are related to the stresses and deformations by Equations (15). Thus, if the partial derivative $\partial W/\partial I_i$ obtained from Equation (15) using the experimental values of stresses and extension ratios can be fitted by a second-order curve to yield

$$\frac{\partial W}{\partial I_1} = A_1 + A_2(I_1 - 3) + A_3(I_1 - 3)^2 \tag{19}$$

then the corresponding coefficients of the W function are given by

$$W = \int \frac{\partial W}{\partial I_1} d(I_1 - 3) + f(I_2, I_3) \tag{20}$$

so that substitution of Equation (19) gives

$$W = A_1(I_1 - 3) + \frac{A_2}{2}(I_1 - 3)^2 + \frac{A_3}{3}(I_1 - 3)^3 + f(I_2, I_3) \tag{21}$$

Hence, from Equations (18) and (21), we see that

$$B_1 = A_1; \quad B_2 = A_2/2; \quad B_3 = A_3/3 \tag{22}$$

The remaining constants of Equation(18) are found in a similar manner from the derivatives $\partial W/\partial I_2$ and $\partial W/\partial I_3$ so that W is defined over the test domain.

At a given strain level, the elastic constants are determined from the local slopes of the stresses; that is, the change in stress at a given strain level can be expressed as

$$d\sigma_{11} = \left(\frac{\partial \sigma_{11}}{\partial \lambda_1}\right)_p d\lambda_1 + \left(\frac{\partial \sigma_{11}}{\partial \lambda_2}\right)_p d\lambda_2 + \left(\frac{\partial \sigma_{11}}{\partial \lambda_3}\right)_p d\lambda_3 \tag{23}$$

where the subscript p means that the derivatives are taken at a fixed pressure level. This expression can also be written in the form

$$d\sigma_{11} = \lambda_1 \left(\frac{\partial \sigma_{11}}{\partial \lambda_1}\right)_p \left(\frac{d\lambda_1}{\lambda_1}\right) + \lambda_2 \left(\frac{\partial \sigma_{11}}{\partial \lambda_2}\right)_p \left(\frac{d\lambda_2}{\lambda_2}\right) + \lambda_3 \left(\frac{\partial \sigma_{11}}{\partial \lambda_3}\right)_p \frac{d\lambda_3}{\lambda_3} \tag{24}$$

and we observe that $d\lambda_1/\lambda_1$ is simply the change in strain; that is,

$$d\epsilon_{11} = \frac{d\lambda_1}{\lambda_1}; \quad d\epsilon_{22} = \frac{d\lambda_2}{\lambda_2}; \quad d\epsilon_{33} = \frac{d\lambda_3}{\lambda_3} \tag{25}$$

Hence, substitution of Equation (25) into Equation (24), yields the perturbation stress-strain equation,

$$d\sigma_{11} = \beta_{11}\, d\epsilon_{11} + \beta_{12}\, d\epsilon_{22} + \beta_{13}\, d\epsilon_{33} \tag{26}$$

where

$$\beta_{11} = \lambda_1 \frac{\partial \sigma_{11}}{\partial \lambda_1}, \quad \beta_{12} = \lambda_2 \frac{\partial \sigma_{11}}{\partial \lambda_2}, \quad \beta_{13} = \lambda_3 \frac{\partial \sigma_{11}}{\partial \lambda_3} \tag{27}$$

Equation (27) is then a perturbation Hooke's law for a nonlinear, anisotropic material. The remaining two equations are determined in exactly the same manner, so that the stress-strain equation takes the form

$$d\sigma_{ik} = \beta_{ij} d\epsilon_{jj} \delta_{ik} (i,j,k = 1,2,3) \tag{28}$$

where δ_{ik} is the Kroenecker delta defined as

$$\delta_{ik} = \begin{vmatrix} 1 & 0 & 0 \\ 0 & 1 & 0 \\ 0 & 0 & 1 \end{vmatrix} \tag{29}$$

From these equations, we define each coefficient of the β_{ij} matrix as follows:[2]

$$\left.\begin{aligned} \beta_{11} &= \lambda_1 \frac{\partial \sigma_{11}}{\partial \lambda_1}; \quad \beta_{12} = \lambda_2 \frac{\partial \sigma_{11}}{\partial \lambda_2}; \quad \beta_{13} = \lambda_3 \frac{\partial \sigma_{11}}{\partial \lambda_3} \\ \beta_{21} &= \lambda_1 \frac{\partial \sigma_{22}}{\partial \lambda_1}; \quad \beta_{22} = \lambda_2 \frac{\partial \sigma_{22}}{\partial \lambda_2}; \quad \beta_{23} = \lambda_3 \frac{\partial \sigma_{22}}{\partial \lambda_3} \\ \beta_{31} &= \lambda_1 \frac{\partial \sigma_{33}}{\partial \lambda_1}; \quad \beta_{32} = \lambda_2 \frac{\partial \sigma_{33}}{\partial \lambda_2}; \quad \beta_{33} = \lambda_3 \frac{\partial \sigma_{33}}{\partial \lambda_3} \end{aligned}\right\} \tag{30}$$

The elastic coefficients are therefore determined by partial differentiation of the stress Equation (13) in terms of the known extension ratios and the W function constructed from the experimental data. The expanded form of the β's in terms of measured quantities and the coefficients of the W function is not presented here, owing to its length, but is presented in Appendix A.

The final determination of the β's, in reality, satisfies our initial requirements; that is, we are now able to determine the local elastic constants from the original displacement and pressure data and to write these in terms of a usable Hookean equation (Eq. (26)). (Appendix B provides

[2]Note that these coefficients represent a rather special case, since the shear coefficients (β_{ik} i=1,2,3 and, k=4,5,6; see Ref 34) do not appear. This is a consequence of the symmetric loading treated here and of the thin-wall (membrane) assumption (see p. 6). It should also be noted that the nine β's of Equation (30) actually reduce to six independent constants, owing to reciprocity (Ref. 33) since $\beta_{ij} = \beta_{ji}$.

an example of their use.) If desired, one can also calculate the more familiar Young's Modulus E_i and Poisson's ratio μ_{ij} from the computed β_{ij} for the three coordinate directions 1,2,3 (θ,z, and r). For the assumed material, these quantities are given by (see Ref. 34)

$$E_i = 1/\alpha_{ii}; \quad \mu_{ji} = -\alpha_{ij}/\alpha_{jj} \tag{31}$$

where α_{ij} refers to the coefficients of the stress-strain equation when written in the form

$$d\epsilon_{ik} = \delta_{ik} [\alpha_{ij}] \, d\sigma_{ii} \tag{32}$$

Comparison of this equation with Equation (28) shows that the α-matrix is the inversion of the β-matrix; that is,

$$[\alpha_{ij}] = [\beta_{ij}]^{-1} \tag{33}$$

Therefore, Young's Modulus E_i and Poisson's ratio μ_{ij} are extracted by inverting the β-matrix of Equation (30) and applying Equation (31). For an isotropic material, we would, of course, find that

$$\left.\begin{aligned} E_1 = E_2 = E_3 \quad &\text{and} \\ \mu_{12} = \mu_{13} = \mu_{23} = \mu_{21} = \mu_{31} = \mu_{32} \end{aligned}\right\} \tag{34}$$

4. EXPERIMENTAL TESTS AND APPARATUS

The purpose of these experiments was to determine the geometric and elastic properties of various human and canine arteries. Both static and dynamic tests were carried out, but the latter are not reported herein.

4.1 Selection and Preparation of Test Specimens

In all, 14 different arteries were actually tested. (See table below).

ARTERY SPECIMENS

Human	Canine
Brachial (4)[3]	Thoracic Aorta (2)
Mesenteric (2)	Femoral (2)
Splenic (2)	
Iliac (1)	
Femoral (1)	

All arteries were tested within a few hours after death, and in only one case was a specimen accepted for study that was not pathologically normal. The normality of each specimen was checked by the assisting pathologists and by Vidya's medical consultant, Dr. D. L. Bruns, who is a cardio-vascular specialist.

Table I lists the clinical information on each arterial segment, as well as the time elapsed from death to excision and testing. About one-half of these arteries were excised and tested within 6 hours after death, and the remainder were excised within 6 hours and tested within 2 days. During this time, they were placed in normal saline and kept refrigerated at 10° C. The in-situ length of each artery was measured prior to excision so that the natural extension ratios could be calculated.

All of the branch arteries of the excised specimen were cut long intentionally (approximately 1/4-in.), so that they could be ligated (i.e., tied off) at some distance from the main artery being tested. Ligating the branches at their tips proved very useful throughout the tests, because it minimized the local stress concentrations at their junctions with the test specimen. Figure 7 shows this effect for two different thoracic aortas, one of which was tied off at the tip of the branching vessel and the other near the junction. The differences in the local tube expansion at the juncture of the branch are apparent in the photographs. The branches on the specimen at the left were ligated at the juncture, and the specimen is considerably deformed under pressure. On the other hand, the branches of the

[3]The number in the paranthesis refers to the number of specimens tested.

specimen on the right were ligated near their outer extremities, and the specimen remains essentially a cylindrical tube.

Prior to testing, each specimen was cleaned of all the surrounding tissue by carefully stripping away the excess material until the adventitia was exposed. Next, the branch arteries were ligated and the plexiglass end pieces were fitted to each end of the artery. One of these plexiglass pieces was hollowed for pressurizing the specimen. The other end piece was a solid plug. After installation of the plugs, the artery was pressurized with air and placed in saline to check for air leaks. If any leaks developed, they were corrected by retying the leaky branch. Sometimes, excessive leakage could not be corrected by this technique because the leaks were too close to the arterial wall. It was then necessary to shorten the test specimen by removing the faulty section. All samples were kept in normal saline at 10° C until testing began.

4.2 Static Tests

A photographic technique was employed to determine the static elastic characteristics of various human and canine arteries. Each test specimen was exposed to soft X-rays at various internal pressures. The physical arrangement of the experimental setup is shown in Figure 8. The developed film furnished all the information required for direct measurement of the three pertinent dimensions: length, radius, and thickness. Figures 9, 10, and 11 show the positive contact prints of the X-ray negatives for a series of pressure-displacement tests for three different arteries.

Prior to testing, the specimen was removed from the refrigerator and brought up to room temperature by placing it in a large container of warm saline (21° to 25° C) and held there for 5 minutes. All tests were performed at room temperature (21° to 25° C).

Since the artery wall thickness was to be measured by X-ray photography, and since water, blood, and saline all have roughly the same density as the arterial wall, it was decided to pressurize all test specimens with air, and all saline was carefully removed from each specimen just prior to testing. This procedure insured sufficiently high resolution of the inner artery wall on the X-ray film to permit accurate measurements of the wall thickness.

The specimen was then placed in its holder (see Fig. 8) and oriented so that it lay flat against the vertical film. This was necessary for the unweighted tests, because some specimens were curved (see Fig. 10) so that their projected length on the film would otherwise not agree with their centerline length. Addition of axial weights straightened the artery and eliminated the problem.

Each specimen was initially pressurized to 300 mm Hg. and deflated to zero several times. This cycling eliminated hysteresis in the pressure-displacement data and yielded repeatable experimental data. Bergel (Ref. 7) and Remington (Ref. 17) have observed and discussed this phenomenon in their reports.

The actual tests were a simple matter of X-raying the specimen at various internal pressures with a fixed axial weight and, then, repeating with other axial weights. Generally, three or four axial weights were used. A 1- to 2-minute pause[4] was taken between X-rays in order to insure that relaxation effects had subsided and that true static data were obtained.

Periodically throughout the tests the specimen was bathed with saline to keep it from drying out.

The final step in testing was to stretch and fix each specimen at its in-situ length, and retake the pressure-displacement data.

Although the specimens were kept in normal saline solution and refrigerated, some tests were repeated at 2-day intervals to ascertain whether rigor mortis effects might change the elastic behavior.

[4] Zatzman, et al. (Ref. 40) and our own observations indicated that nearly all relaxation effects in arterial segments subsided after 1 minute.

5. INSTRUMENTATION AND CALIBRATION

5.1 Aneroid Manometer

The aneroid manometer used to measure internal pressure was a standard medical Tycos Aneroid Manometer. It was calibrated (statically) against a column of mercury and found to be within the manufacturers specifications ($\pm$1 mm Hg. at 300 mm Hg.).

5.2 X-ray Apparatus

The X-ray assembly used in these studies was a Westinghouse dental X-ray product. The settings required to obtain proper film exposures, when the film and test specimen were placed 25 ($\pm$1/16) inches away, was found to be 60 mAs at 42 kV. The film used throughout the tests was Kodak Industrial Film, Type AA.

6. DATA REDUCTION

The exposed X-ray films, along with the recorded values of internal pressure and axial weight, served as the raw data. In the interests of increased accuracy, each negative was magnified approximately 15 times on an Itek 18.24 Reader-Printer, which furnished 2- by 4-foot positive prints for measurement purposes. A full-scale portion of such a print is shown in Figure 12. Note that the inner and outer edges of the artery wall are clearly discernible. A reference cylinder of known diameter was included in the picture to give the exact magnification of the specimen. Because the test specimens are not always straight cylindrical tubes, the inner and outer diameters were usually determined by using a planimeter to measure the inner and outer cross-sectional areas over a considerable length of the test specimen. This length was taken as the largest length over which the diameters are relatively unaffected by presence of the two ligatures used to mount the specimen to the end plugs. In cases for which the specimen was very nearly cylindrical, the inner and outer diameters were read directly at several positions and averaged over the length. The length measurement used to determine axial extensions was taken to be the centerline axial distance between these two ligatures.

7. TECHNIQUE FOR DETERMINING THE ELASTIC PARAMETERS

If the three components of stress and strain could be measured directly, then the determination of the strain energy function W and the associated elastic constants from the experimental data would be a relatively straightforward, though lengthy, procedure as outlined in Section 3. However, as the stresses and strains cannot be measured directly, it is necessary to deduce them from the experimental data. One of these stresses, σ_{11} (sometimes referred to as the "hoop stress"), is simply related to the measured pressures and displacements (only for the case of zero axial weight) by the hoop stress equation. This equation can be derived by taking the limit of Equation (B-18) as the wall thickness approaches zero. The remaining two stresses are approximated by the mean axial stress (end force over cross-sectional area) and mean radial stress, $(-p + 0)/2$. Hence, for the zero weight case, the stresses are written as:

$$\sigma_{11} = pa/h \tag{35a}$$

$$\sigma_{22} = pa^2/2r_m h \tag{35b}$$

$$\sigma_{33} = -p/2 \tag{35c}$$

Therefore, for the unweighted case, we can indeed determine all of the stresses and displacements and, from these, determine the strain-energy function W through its partial derivatives by use of Equations (15), (18), (19), and (22). With axial weights, however, Equations (35a) and (35b) no longer hold, because they become functions of the weight as well as the pressure.

It will be recalled that the energy function W must apply for arbitrary loadings of a given material. Hence, if the W function determined from the unweighted data is to be used for extracting the elastic constants, that same function must be valid for the weighted specimen as well. Therefore, we shall first determine a W function for the unweighted specimen by curve-fitting the displacement data as a function of internal pressure as follows:[5]

$$\left.\begin{aligned} a &= a_1 + a_2 p + a_3 p^2 \\ b &= b_1 + b_2 p + b_3 p^2 \\ L &= z_1 + z_2 p + z_3 p^2 \end{aligned}\right\} \tag{36}$$

[5] It was found that a least-squares, second-order curve fit was sufficient for all data taken in these tests.

where a, b, and L refer to the inner and outer radii and the measured axial length, respectively, and the subscripted quantities are the desired curve-fit constants. By using these curve fits, the associated extension ratios, and the simplified stress Equations (35), the W function is obtained from its partial derivatives in the manner described previously (see Eqs. (15) to (22)).

By using this W function, the stresses σ_{22} and σ_{33} for the weighted cases are calculated (using Eq. (13)) and compared with the approximated membrane stresses, which are determined by the mean axial force $(W_t + \pi a^2 p)$ per unit area, and the mean radial stress and are given as

$$\left.\begin{aligned} \sigma_{22} &= \frac{a^2 p}{2 r_m h} + \frac{W_t}{2\pi r_m h} \\ \sigma_{33} &= -p/2 \end{aligned}\right\} \qquad (37)$$

where W_t is the axial weight. If the deviations of these two stresses are outside of the experimental accuracy, the W function constants (B_3, C_3, and D_3) are readjusted and the stresses for all loadings, including the unweighted case, are recalculated until satisfactory agreement is obtained. In this manner, the final W function constants were developed for each specimen, from which the elastic constants can be extracted. About one-half of the final W function constants were determined on the first curve fit. The remainder required anywhere from 2 to 10 iterations.

STEP 1 - CURVE-FITTING THE DISPLACEMENT DATA

It was not always possible to approximate the displacement data with Equation (36) (even for zero weight) to the specified tolerances (see table of uncertainties below) over the entire range of internal pressures; therefore, the data were curve-fitted over most of the test domain and limits (maximum and minimum pressures) were placed on these curve-fit equations.

EXPERIMENTAL UNCERTAINTIES

Pressure (mm Hg.)	Diameter (in.)	Length (in.)	Thickness (in.)
± 1	± 0.002	± 0.002	± 0.004

In general, these pressure limits are widely separated (approximately from 70 to 240 mm Hg.), so that the data are fitted over the range of pressures ordinarily measured on the arterial side of the human and canine vascular systems. Table II shows all the constants and the acceptable pressure limits for all specimens tested.

STEP 2 - DETERMINING THE UNSTRESSED DIMENSIONS

The partial derivatives of W for the zero weight tests are calculated from the stress-displacement equations (see Eq. (15)). In order to define the extension ratios appearing therein, we must know the dimensions (a_o, b_o, and L_o) of the unstressed specimens (at $p = 0$ and $W_t = 0$). Generally, this information was obtained directly from the X-ray film for the unloaded condition, but sometimes at this condition, owing to the lack of internal pressure, the tube was not of circular cross section. Hence, it became necessary to define equivalent dimensions by extrapolating from the lowest pressures at which the tube was cylindrical. In such cases, the tube length L_o was assumed to be unaffected by the oblateness, and was taken to be the measured value. This leaves the unstressed radii, a_o and b_o, to be determined by extrapolating from the low internal pressure (10 to 50 mm Hg.) data. The final values of a_o, b_o, and L_o are also tabulated in Table II for each specimen. After the initial displacements were determined, the partial derivatives of W were computed in the previously described manner. Next, these computed derivatives were fitted with a second-order, least-squares curve. A comparison between the computed derivatives as given from the experimental data and Equation (15) and the curve-fit derivatives, is shown in Table III. The W function constants (for the unweighted case) are generated by equating the derivative curve-fit constants to the corresponding W function constants, as shown in Equation (22). The finalized values which are applicable between certain limits of the invariants (I_1, I_2, and I_3) are given in Table IV.

STEP 3 - DETERMINATION OF THE ELASTIC CONSTANTS

After the W function has been fixed (see Table IV), the β's, α's, E's, and μ's are calculated for all loadings. This is done by first computing the β matrix as indicated in Appendix A. The α matrix is determined by inverting the computed β matrix, and the customary elastic constants (E's and μ's) are calculated from Equation (31).

Certain additional checks can be made on the finalized β_{ij} and W function, and a discussion of these is found in Appendix C.

8. EXPERIMENTAL RESULTS AND DISCUSSION

8.1 Experimental Displacement Data

The measured values of internal and external radii and axial length for some typical test specimens are plotted in Figures 13 and 14. The observed variations of artery dimensions with internal pressure have been approximated by second-order, least-squares curve-fits (see Section 7.1), as shown in the figures. Since the analysis of Section 3 requires a knowledge of the unstressed dimensions (a_o, b_o, and L_o) for each specimen at zero pressure and zero axial weight, these quantities are indicated by the darkened data points.

Other test specimens yielded similar curves not shown in these figures. Rather than presenting all such plots for each specimen subjected to several axial weights, the resulting curve-fit constants (a_i, b_i, z_i, $i = 1,2,3$), and the unstressed dimensions (a_o, b_o, and L_o) are tabulated for each specimen in Table II with the appropriate pressure limits between which the curve-fit equations are valid. These pressure limits are necessary, because it was not possible to fit all the data within the experimental accuracy with a single, second-order curve. However, the data were successfully fitted from pressures of 40 to 270 mm Hg., which covers the normal operating range of pressure in both the human and canine arterial systems.

At first glance, some of the coefficients appear to be quite small (see Table II), but it should be remembered that these coefficients are multiplied by the square of the pressure. Further, it will be noted that the slopes of the curves of radii versus pressure (Figs. 13 and 14) become very small at higher pressures and that a zero slope infers infinite stiffness. Hence, a small change in the slope of the curve fit produces a large change in calculated elastic constants.

With no axial weight applied to the specimen, the radii and length continually rise with increasing pressure, but the wall thickness decreases with increasing pressure. Figure 15 shows this decrease in thickness clearly. It can be seen from Figures 13 and 14 that the rate of change of dimensions is greatest over the first 60 mm Hg. and becomes quite small at the highest pressure levels. In general, the distentional behavior of all the specimens within the first 60 mm Hg. are similar with the possible exception of the thoracic aortas. The thoracic aortas exhibit more of an "S" shaped radius versus pressure curve, commonly referred to as a sigmoid, as shown in Figure 14(a). This type of behavior results in an inflection point in the radius and length data at about 50 mm Hg. However, for pressures

above this inflection point, the thoracic aorta behaves in the same manner as the other specimens. Therefore, the thoracic aorta data were curve-fitted only for pressures above the inflection point. Since the sigmoid effect is evident only below 50 mm Hg., it is considered to be of no consequence in describing the elastic behavior of arteries.

If the arterial wall were composed of an incompressible, isotropic material, as suggested in the literature, and does not experience an axial force, then the length of a specimen should not change with pressure (see Ref. 15). However, for zero axial weight condition, it is seen from Figures 13 and 14 that the length increases with internal pressure for all specimens. Hence, we conclude that arteries <u>are not</u> incompressible, isotropic materials. It will be noted that, generally, the length approaches the in-situ length as the internal pressure becomes very high. In some cases, such as Figure 13(a), this does not appear to be true. However, it should be mentioned that we have no way of placing experimental tolerances on the in-situ measurements, so discrepencies of 10 percent, such as those found in Figure 13(a), are possible.

The addition of an axial weight to an unpressurized specimen results in lengthening the artery and decreasing its radii and thickness. Most specimens were exposed to a range of axial weights which stretched them to values greater than their in-situ length. In some cases, excessive weights caused such a decrease in radius that the specimen developed axial wrinkles. In such cases, the displacement data were rejected, since the specimen was no longer a cylindrical tube. (Such was the case for all of the canine femoral arteries.)

The pressure-displacement data for the weighted specimens (Figs. 13 and 14) were also curve-fitted with a second-order curve, and, in general, all of the weighted specimens exhibited an increase in radii and a slight decrease in thickness (Fig. 13), but a <u>decrease</u> in length with increasing pressure. The fact that the specimen becomes shorter with increasing pressure may seem somewhat surprising, but is associated with the anisotropic nature of the arterial wall. (The physical reasons for this behavior will be discussed later in this section). It will also be noted that the length of the weighted specimens tends to approach the in-situ length with increasing internal pressure, so that the artery length of both the unweighted and weighted specimens approach the same value at the highest tested pressure levels (300 mm Hg.). Such observations are not new. McDonald (Ref. 6) noted a similar result for unweighted specimens.

Since the unweighted specimen increases in length toward the in-situ value and the heavily weighted specimen decreases in length toward the in-situ value, it follows that there will be some intermediate weight for which the length of the specimen will be constant at the in-situ length (see Fig. 16). Therefore, this weight for which the length remains constant must correspond to the axial tethering force in the body. Hence, we conclude that length changes in arteries in vivo are minimal. As a check on the above reasoning, the weight required for zero change in length with pressure (the nulling weight) was obtained for each specimen (by cross-plotting the experimental data), and these weights were compared with those required to stretch the specimen to its in-situ length. This comparison is tabulated below, and it can be seen that the agreement is quite close, except for Brachial II.

COMPARISON OF THE TETHERING FORCE AND THE NULLING WEIGHT

Specimen	Tethering Force (grams)	Nulling Weight (grams)
Brachial I	45	41
Brachial II	200	20
Brachial III	16	20
Brachial IV	20	22
External Iliac	21	20
Splenic I	45	50
Thoracic Aorta I	94	--
Thoracic Aorta II	130	150
Superior Mesenteric	28	32
Femoral I	50	--
Femoral II	50	52
Femoral III	20	20

(It is now suspected that an error was made in the length measurement for that specimen, either before or after excision, but the specimen was unfortunately discarded before this suspicion could be verified.) These results appear to clarify Lawton and Greene's (Ref. (14) observation that, in some cases, an artery contracts in length during systole. This behavior would be quite typical of a specimen exposed to a tethering force somewhat greater than the "nulling weight," and it seems reasonable to assume that such was the case.

Although the absolute wall thickness in all cases decreases significantly over the first 80 mm Hg. of pressure, it becomes nearly constant (see Figs. 15 and 17) for all higher pressures, irrespective of the axial

weight. This constant value is roughly given at 100 mm Hg. as 0.019 $\pm$0.005 inch for all specimens except the canine femoral arteries, which were not included owing to their smaller diameters. Such a figure may prove useful in future analyses where knowledge of the wall thickness is required. The nearly constant wall thickness does not necessarily imply that the radial modulus of elasticity is infinite, because the radial modulus of elasticity, as determined from the analysis presented in Section 3, is extremely sensitive to very small changes of the wall thickness, especially for specimens with thin walls.

8.2 Comparison of Dimensional Data

It would be highly desirable to compare the dimensional displacement data presented herein, whenever possible, with similar data found in the literature in order to check the validity of the measured wall thickness, diameter, and length. However, such information is nearly nonexistent in the literature, since most investigators who performed static elastic tests on whole arteries did not measure all of these quantities. Instead, some have measured the inner volume, others have determined the outer diameter and length, still others did not present their raw displacement data. To our knowledge, no one previously has measured the variation of radius, length, and thickness, simultaneously, with loading. Generally, most investigators would measure two of the three dimensions and make an assumption about the third. Invariabily, the assumption concerns the behavior of the most difficult item to measure, that is, the variation of wall thickness with pressure. Consequently, it is of interest to compare the wall-thickness measurements with the limited data which are available.

Apparently, Bergel (Ref. 7) was one of the investigators who did measure the wall thickness and outer radius for various specimens at only one pressure (100 mm Hg.), but he did not tabulate each quantity. Instead, he tabulated the ratio of thickness to outer radius, at the one pressure, for many canine arteries. This can serve as a useful nondimensional comparison.

Fenn (Ref. 15) also has published values of wall thickness and radius at one pressure (0 mm Hg.), so his data can also be compared to the equivalent test data presented herein. Table V shows these comparisons of h/b for both Fenn's and Bergel's data.

In general, we note that, whenever direct comparisons are possible, the data presented herein are in excellent agreement with Bergel's data ($\pm$5 percent), but they do not check Fenn's data at all. In fact, Fenn's data exceed those presented here by about 50 to 80 percent. However, since

the number of comparisons per type of artery are limited to one or two, and since the arterial dimensions are known to vary from person to person, one cannot place much importance on these observations or make of any positive conclusions. Further comparisons are impossible, owing to the lack of similar data.

The in-situ extension ratio (the ratio of the in-situ length to the excised length) is also presented in Table V. Again, the data taken in the present study agree quite well with Bergel's data for the specimens which can be compared.

8.3 Volume of the Arterial Wall

We have already discussed the fact that much of the earlier experimental and analytical work concerning arteries was based upon the assumption that arteries are incompressible. The analysis of Appendix B indicates that such a material must be characterized as an isotropic material with a Poisson's ratio of 0.50, or a transversely isotropic material in the r, θ plane. No other type of material (i.e., either isotropic with $\mu \neq 0.50$ or anisotropic) can exhibit a constant volume under load. Since the radius, thickness, and length of each test specimen were all measured in the present tests, we can calculate the volume of the material at each load and determine the compressibility of the material by comparing that volume with the volume at the unloaded condition. The results of these calculations revealed that, in nearly every case, the material volume changed by a significant amount (20 to 40 percent) when the specimen was exposed to loads comparable with those experienced in the body. Figure 18 shows the arterial wall volume as a function of pressure for several specimens at various axial weights.

The volume of the wall depends upon all three normal stresses (σ_θ, σ_z, and σ_r) and, if the material is anisotropic, upon the six local elastic constants. Various combinations of these stresses and elastic constants can cause either an increase or a decrease in volume. For example, consider the loaded specimen to be anisotropic and, for the sake of discussion, let the values of Poisson's ratio be very small. The local strains in the wall will then depend upon the ratio of the three stresses to their corresponding moduli of elasticity, so that

$$\epsilon_\theta = \frac{\sigma_\theta}{E_\theta}; \qquad \epsilon_z = \frac{\sigma_z}{E_z}; \qquad \epsilon_r = \frac{\sigma_r}{E_r} \tag{38}$$

The change in volume is given by the sum of these strains, that is

$$\Delta V/V = \epsilon_\theta + \epsilon_z + \epsilon_r \tag{39}$$

For a positive internal pressure and a tensile axial load, two of these terms (ϵ_θ and ϵ_z) are positive because σ_θ, σ_z, E_θ, and E_z are all positive. But the radial strain ϵ_r is negative because σ_r is negative (i.e., the wall is in compression). Therefore, the relative magnitudes of $(\epsilon_\theta + \epsilon_z)$ and ϵ_r will dictate whether the change in volume is positive or negative. Hence, both increases and decreases in volume can occur, and such was the case with some of the specimens tested herein.

In general, the volume decreases, which means that the radial strain dominates the volume expression. However, the radial stress is smaller than the circumferential or longitudinal stresses. Hence, the elastic modulus in the radial direction must be much smaller than in the other two directions.

8.4 Elastic Constants

8.4.1 Young's Modulus

The nonlinear theory developed in Section 3 enables one to extract the six elastic constants (the β's) from the experimental data. By proper manipulation (see Section 3), these elastic constants can be used to determine the three Young's Moduli of elasticity (one modulus for each of the three orthogonal coordinates, r, θ, z) and the corresponding Poisson's ratios. The resulting moduli are plotted as functions of pressure in Figures 21 through 34 for each artery tested.

For the tests with no axial weight (Figs. 19 through 34), we see that the circumferential modulus of elasticity E_θ increases with pressure. With the single exception of Figure 20(a), the axial modulus E_z also increases with pressure, while the radial modulus E_r stays roughly constant. Generally, E_θ is greater than E_z, and both of these are greater than E_r. For Brachial II (Fig. 20(a)), we see that the E_z and E_r decrease with an increase in pressure. The reasons for this apparent trend are not known. However, we note that this particular specimen has the highest h/r_m, so that perhaps the membrane assumption is not quite as valid as with other specimens.

The general trends of the elastic constants can be associated with the presence of the individual biological materials in the wall. It was pointed out in Section 2 that arteries are composed of annular layers of material of

nearly the same elasticity, with the exception of the much stiffer collagenous fibres. These fibres form a double criss-cross helical net around the inner layers and can be characterized by the "finger puzzle" effect (see Fig. 5). Since increased internal pressure causes a larger increase in circumferential (hoop) stress than in longitudinal (axial) stress (see Appendix B for exact equations), the net result of increased internal pressure is to reorient the fibres in the direction of maximum stress so that they tend to align themselves circumferentially, thereby making the material effectively stiffer in that direction. Hence, E_θ increases more rapidly with pressure than does E_z (see Fig. 21(a)). The high internal pressure tends to compress the inner layers so that the actual tube thickness is diminished considerably. The collagenous fibres, which are thin chords acting in the θ-z plane, do not affect either the radial compression[6] or the radial elastic modulus, E_r. (See Figs. 19 through 34.)

For all specimens, we find that, at low pressures, all three elastic constants appear to have, roughly, the same low Young's Modulus, (20 to 100 psi). We also note from Reference 7, that this is approximately the value of Young's Modulus of elasticity for elastin and smooth muscle. Therefore, it would appear that, near the unloaded condition, the elastic moduli of arterial specimens take on the nearly isotropic characteristics of elastin and smooth muscle, and the material is said to behave as an isotropic material. McDonald (Ref. 6) has speculated that, under such conditions, the stiff collagenous fibres are slack and do not affect the elastic behavior.

With the addition of axial weight, it can be seen from Figure 21(b) that the axial modulus E_z increases. This increase is presumably associated with the orientation of the collagenous fibres toward the axial direction, but, as the internal pressure is increased, these fibres tend to rotate back toward the circumferential direction, and E_θ increases (see Fig. 21(b)). Hence, at some internal pressure (the "crossover" pressure), E_θ becomes equal to E_z. The crossover pressure increases with axial weight, as seen in Figures 21(b) and 21(c), since a higher pressure is required to reorient the fibres from a more nearly axial alignment. It would seem reasonable that, at the crossover pressure, the collagenous

[6] This is analogous to compressing a large block of rubber with a flat piece of metal in the middle, normal to the applied load. One must compress the rubber to nearly the thickness of the metal before noticing its presence.

fibres are symmetrically arranged at 45° to the z-axis, so that the material would behave identically in the axial and circumferential directions.

A comparison of the stresses and extension ratios at the data points taken closest to the crossover pressure (as determined from crossplots) indicates that both the stresses and the extension ratios are essentially equal in the axial and circumferential directions (see Table below).

COMPARISON OF σ_θ AND σ_z, AND λ_1 AND λ_2 NEAR THE CROSSOVER PRESSURE FOR SEVERAL SPECIMENS

Vessel	W_t (grams)	P (mm Hg.)	σ_θ (psi)	σ_z (psi)	λ_1	λ_2	P crossover from crossplots (mm Hg.)
Splenic IB	20	100	9.7	9.5	1.20	1.20	100
Brachial IIA	20	110	8.5	7.8	1.13	1.17	120
	100	230	21	24	1.12	1.19	226
Brachial IIIA	20	100	21	20	1.23	1.21	96
	50	150	27	28	1.24	1.25	155
Brachial IVA	32.4	100	17	16	1.30	1.30	100
	55.9	130	26	26	1.31	1.31	132

It should be noted from Figures 19 to 34 that the radial modulus of elasticity is relatively unaffected by either internal pressure or axial weight. This suggests that the stiffer collagenous fibres, which lie essentially normal to the radial direction, do not affect the elastic constant in the radial direction.

When a specimen is exposed to a very high axial and/or circumferential stress, one would expect that the corresponding elastic constants E_z and/or E_θ will gradually approach the values of the collagenous fibres themselves as the fibres become aligned with the direction of stresses. Figures 20(d), 22(c), and 23(b) are test cases with high axial stresses and much lower hoop stresses, and Figures 24(c), 33, and 34 are other test cases with the opposite characteristics, that is, high hoop stress and low axial stress. From these figures, we note values of E_z vary from 400 psi to 2000 psi and E_θ from 300 psi to 1000 psi. Various investigators (see Refs. 6 and 7) have tabulated elastic constants for the collagenous fibres and found values of Young's modulus varying from 400 to 1500 psi. In general, we see that, for very high loadings (stresses), the moduli of elasticity do approach these established values of collagenous materials.

In summary, the general behavior of the anisotropic elastic moduli seem to be associated with the orientation of the collagenous fibres. Arteries appear to be initially isotropic, with a modulus of elasticity equivalent to that found for elastin and smooth muscle (about 60 psi). For the in-vivo loads where σ_θ approximately equals σ_z, the specimens behave as transversely isotropic materials. For other loads, where σ_θ does not equal σ_z, the test specimens behave anisotropically, having a greater elastic modulus in the direction associated with the higher stress. The radial modulus is the lowest of the three and is essentially constant for all loadings, being unaffected by the orientation of the collagenous fibres.

8.4.2 Poisson's ratio

It is difficult to say much about the various Poisson's ratios (μ) presented in Figures 19 through 34, except that, in general, their values are realistic. A realistic value of μ falls between +1.0 and -1.0. These limits can be established by considering the bulk modulus of elasticity for a special anisotropic material, one which possesses identical values of μ_{ij} in all planes, ($\mu_{rz} = \mu_{zr} = \mu_{r\theta} = \mu_{\theta r} = \mu_{\theta z} = \mu_{z\theta}$). By considering the two limiting values of the bulk modulus (0 and ∞), one finds that the corresponding values of μ are given as -1.0 and +1.0, respectively. Although we normally do not think of a Poisson's ratio as being negative, for an anisotropic material it simply indicates that a positive normal stress in one direction can generate a positive normal strain in one of the other two orthogonal directions.

In some instances, the μ's do not fall within realistic limits over portions of the pressure range. The reason for the unrealistic μ's can be shown from the approximate form of μ_{ij}

$$\mu_{ij} \cong -\beta_{ij}/\beta_{ii} \quad i \neq j \left(i,j, = 1,2,3\right) \tag{40}$$

We note that, when β_{ii} becomes small, the μ's exceed a realistic limit of 1.0. Consequently, there are small bands of the pressure range in which the value of μ cannot be calculated; such was the case for Brachial II, 20-gram weight (see Fig. 29(b)). For this reason, it is perhaps better to use the well-behaved, though less familiar, β's, rather than the more conventional E's and μ's. Figure 35 shows the variation of the elastic coefficients β_{ij} with internal pressure for two different specimens.

8.5 Transverse Isotropy

A cursory glance at any of the Young's Moduli shown in Figures 19 through 34 shows that arteries generally behave as anisotropic materials. There are, however, conditions at which E_θ becomes equal to E_z, and $\mu_{r\theta}$ becomes approximately equal to μ_{rz}. When this occurs, the material can be said to be transversely isotropic.[7] Such conditions are characterized by equal circumferential and longitudinal stresses and extension ratios, (see Table on p. 30) which cause the collagen fibres to make a 45° angle with respect to the longitudinal axis. When an additional axial weight is added at this condition, the fibres reorient themselves toward the axial direction, and the material becomes stiffer in that direction. However, by increasing the internal pressure again, a new condition of transverse isotropy can be found which corresponds to a higher internal pressure for each larger axial weight. If the pressurization were to continue, the elastic moduli and stresses would cross over one another so that the circumferential stress and elastic modulus would exceed the corresponding longitudinal stress and modulus. Hence, it is possible to construct a plot of the "crossover" pressure as a function of axial force acting on each specimen, which in reality gives us the conditions for transverse isotropy.

Figure 36 shows the conditions for transverse isotropy for three different arterial specimens. These curves are intended to indicate the particular combination of pressure and axial weight that will cause the material to behave as transversely isotropic. If a particular combination of axial force and internal pressure places the load point to the left of this curve, then the material is anisotropic and $E_z > E_\theta$. Loads to the right of this curve cause the material to be anisotropic, but, in this case, $E_\theta > E_z$.

It is interesting to note that, in all cases, the crossover pressure which corresponds to the axial force necessary to stretch the specimen to its in-situ length (see Fig. 36) falls within the normal in-vivo arterial pressure range, namely pressures of 80 to 120 mm Hg. This observation is also true of the other specimens tested, which are not plotted in Figure 36.

---

[7] Strictly speaking, transverse isotropy also implies that all the shear moduli β_{ik} (i = 1,2,3 ; k = 4,5,6) are identically zero. This point has not been clearly demonstrated.

Hence, excised arteries subjected to in-vivo loadings seem to behave as transversely isotropic materials. It should be noted that, for the condition of transverse isotropy, arteries can be represented by four elastic constants rather than six because $\beta_{11} = \beta_{22}$ and $\beta_{13} = \beta_{23}$. Furthermore, for this condition, the axial length remains constant with variations in internal pressure (see Fig. 16 and Section 8.1).

8.6 Age Effects

There are many parameters which affect the elastic characteristics of arteries. One such parameter which has been studied extensively (Ref. 20) is the artery calendar age. Although we cannot furnish quantitative data on this subject, we have been able to study four normal brachial arteries from people of different ages. A comparison of these brachial data is shown in Figure 37, which displays the variation of the three anisotropic moduli of elasticity as functions of the internal pressure for specimens stretched to their in-situ lengths. These specimens were considered to be pathologically normal. From Figure 37, we note a consistent trend with age; namely, that the values of E_θ, E_z, and E_r at any internal pressure above 80 mm Hg. increase with age. This effect seems to indicate that an aging process takes place in the elastic and smooth muscle and not the collagen.

8.7 Change of the Elastic Constants of Excised Arteries With Time After Removal From the Body

One of the items studied during this program was the effect of time after removal of the specimen from the body. To study this aspect of the problem, static-elastic tests were performed on several specimens with a 2- to 6-day waiting period between tests. The specimen was kept in a normal saline solution at 10° C during this period.

The table below shows the specimens which were tested at more than one time after death. The letter A or B which modifies the specimen number indicates the first or second test, respectively.

TIME AFTER DEATH TO THE STATIC-ELASTIC TESTS

Specimen tested	Time after death to test (hr)
Brachial IVA	6
Brachial IVB	151
Splenic IA	40
Splenic IB	94
Femoral IIA	2
Femoral IIB	54
Thoracic IIA	3
Thoracic IIB	55

In general, no measurable change was detected in the elastic constants with time after death. In many cases, the W function determined from the first test also satisfied the data for the second test (see Table IV for the W function constants). For the cases in which the first W function constants would not satisfy the data for the second test, such as with Brachial IVA and Brachial IVB, it was found that the W function constants did not change significantly, and, more importantly, that the various moduli were nearly identical.

In summary, although the first test was generally within 1 or 2 hours after death, it was found that the elastic constants do not change significantly with time, at least for times up to 6 days, if the specimen is kept in normal saline under refrigeration.

8.8 Shortcoming of the Analysis

In some special cases, the analysis presented in Section 3 was not successful. That is, the strains calculated from the computed elastic constants, using a thick-wall tube analysis, did not check the measured strains (see Appendix B). Those specimens which did not yield satisfactory elastic data were the human femoral artery and the canine femoral arteries under high axial loads. Both specimens gave similar difficulties in extracting the anisotropic elastic constants, namely, those of inaccuracies in the experimental data (see Section 7). Since the nonlinear analysis is extremely sensitive to the input displacements, a small error in input data produces large errors in the resulting elastic constants. Owing to the small dimensions of the canine femoral arteries, the heavy axial weights reduced the wall thickness to about 0.010 inch, producing a $\pm$33-percent measurement error. The human femoral artery was highly sclerosed and was so stiff that its displacements were too small to generate enough variation of the strain invariants to obtain a proper W function curve fit.

In any case, it is felt that the problem lies with accuracy of the measurements rather than with the analyses.

9. CONCLUSIONS

Experiments have been carried out and an analysis has been developed for determining the elastic behavior of excised human and canine arterial segments subjected to combined internal pressure and axial tension. The dimensional measurements taken to deduce the elastic behavior included the inner diameter, outer diameter, and length of each specimen for each loading condition. Arteries tested included the human brachial, femoral, external iliac, superior mesenteric and splenic, as well as the canine femoral and thoracic aorta. The results of the present investigation lead to the following conclusions:

(1) In all of the arteries tested, the elastic behavior of the arterial wall can be represented by a nonlinear, homogeneous, anisotropic, compressible material.

(2) A description of this elastic behavior requires six elastic constants at each level of strain. These correspond to three values of Young's Modulus and three values of Poisson's ratio.

(3) The anisotropic behavior seems to be associated with the presence of the collagenous fibres which form a double criss-cross network around the inner layers and change their orientation with loading.

(4) The circumferential stiffness approaches that of the stiff collagenous fibres at very high internal pressures, irrespective of axial loading, and the axial stiffness also approaches that of the collagenous fibres at very high axial stress, irrespective of internal pressure.

(5) The radial stiffness is essentially unaltered by loading and remained roughly at the value of elastin and smooth muscle.

(6) The three values of Young's Modulus (radial, circumferential, and axial) all appear to increase with age.

(7) The artery length may increase or decrease with increasing internal pressure, depending upon the applied axial stress.

(8) At in-vivo levels of internal pressure and axial stress, the artery length is evidently independent of the internal pressure.

(9) At in-vivo levels of internal pressure and axial stress, the arterial wall behaves as though it were transversely isotropic, with the same value of Young's Modulus in the axial and circumferential directions.

(10) The elastic behavior of excised arteries was found to be unaffected by time after death when they were kept in normal saline under refrigeration.

10. RECOMMENDATIONS FOR FUTURE WORK

The present investigation has yielded the static elastic behavior of various excised human and canine arteries. Although this information is only a first step toward a full understanding of the dynamic elastic behavior of the living cardiovascular system, it does lay the groundwork for a systematic approach to that goal. In particular, the following recommendations are offered for future work in this area of research:

(1) During the present experimental program, oscillatory test data on a number of excised specimens were obtained but were not analyzed, since such an analysis requires the results of the static analysis. Now that the static analysis is complete, it would seem appropriate to analyze the dynamic test data, which requires extending the present analysis to oscillatory internal pressures.

(2) The question of the difference between the elastic behavior of excised arteries and arteries in vivo remains unanswered. It is therefore recommended that experimental studies be undertaken on sacrificial animals, such as dogs or sheep, to make elastic tests of various arteries in vivo and repeat the tests after excision. The measurements to be made would be internal pressure, the axial stress, the artery length, and its inner and outer diameter. The force measurements could be made by exposing the artery, employing strain gages, and measuring the compressive axial stress required to cancel the natural tethering stress. Various axial loads could then be applied, and the internal pressure could be varied by injecting drugs into the anesthetized animal.

(3) As a diagnostic technique, it would be highly desirable to determine the elastic behavior of the arteries of a human patient without resorting to surgery. Perhaps the most promising approach for such a technique lies in the measurement of pulse-wave velocity. However, the mathematical expressions for pulse-wave velocity along a realistic artery have not yet been developed. Since the present study indicates that arteries in vivo behave as transversely isotropic, thin-walled tubes, one can treat them as having a single Young's Modulus by ignoring the radial elastic effects. However, that single modulus is a function of the internal pressure. This effect produces waves which change their shape along the tube and travel at a different velocity from that of classical theory. It is therefore recommended that a theoretical analysis of this problem be undertaken.

(4) It is known that the elastic behavior of veins is quite different from that of arteries, and that veins are essentially collapsible vessels whose internal volume varies greatly and comprises the "venous reservoir." In view of the importance of this behavior with regard to such conditions as venous pooling of blood, and in view of the general dirth of knowledge regarding venous elastic properties, it is recommended that the present study be extended to veins in order to determine their elastic behavior.

REFERENCES

1. Roy, C. S.: The Elastic Properties of the Arterial Wall. Jour. Physiol., vol. 3, Nov. 1880, pp. 125-160.

2. Wood, G. C.: Some Tensile Properties of Elastic Tissue. Biochimica Et Biophysica Acta, col. 15, pp. 311-324, 1954.

3. Zon, L.: The Elasticity of the Aorta. Master's Thesis, Univ. of Minn., 1932.

4. Lawton, R. W.: The Thermoelastic Behavior of Isolated Aortic Strips of the Dog. Circ. Research, 1954, pp. 344-53.

5. Lawton, R. W.: Measurements on the Elasticity and Damping of Isolated Aortic Strips of the Dog. Report No. NADC-MA-5603, A.M.A.L., U.S. Navy Air Dev. Center, 1956.

6. McDonald, D. A.: Blood Flow in Arteries. Williams & Wilkins Co., Baltimore, 1960.

7. Bergel, D. H.: The Static Elastic Properties of the Arterial Wall. Jour. Physiol., vol. 156, 1961.

8. Hass, G. M.: Elastic Tissue - Parts I and II. Archives of Pathology, vol. 34, 1942, pp. 807-981.

9. Hass, G. M.: Elastic Tissue. Archives of Pathology, vol. 35, 1943, pp. 29-45.

10. Hinke, J. A. M. and Wilson, M. L.: A Study of Elastic Properties of a 550-μ Artery in Vitro. Amer. Jour. of Physiol., vol. 203, 1962, pp. 1153-1160.

11. Patel, D. J., Schilder, D. P., and Mallos, A. J.: Mechanical Properties and Dimensions of the Major Pulmonary Arteries. Jour. of Applied Physiol., vol. 15, no. 1, Jan. 1960, pp. 92-96.

12. Hallock, P. and Benson, I. C.: Studies on the Elastic Properties of Human Isolated Aorta. Jour. of Clinical Investigation, vol. 16, 1937, pp. 595-602.

13. Roach, M. R. and Burton, A. C.: The Reason for the Shape of the Distensibility Curves of Arteries. Can. J. Biochem. Physiol., vol. 35, no. 8, 1957, pp. 681-690.

14. Lawton, R. W. and Greene, L. C.: A Method for the In Situ Study of Aortic Elasticity in the Dog. Rept. No. NADC-MA-5603, A.M.A.L., U.S. Navy Air Dev. Center, 1956.

15. Fenn, W. O.: Changes in Length of Blood Vessels on Inflation. Tissue Elasticity. ed. Remington, J., 1957, pp. 154-167.

16. Evans, R. L.: Elasticity of Vessel Walls. Amer. Jour. Physiol., vol. 187, 1956, pp. 597.

17. Remington, J. W.: Hysteresis Loop Behavior of the Aorta and Other Extensible Tissues. Amer. Jour. Physiol., vol. 180, 1955, pp. 83-95.

18. Richards, T. G.: Determination of the Elastic Properties of the Peripheral Vessels in Vivo. Jour. of Physiol., vol. 122, no. 2, 1953, pp. 291-301.

19. Peterson, L. H., Jensen, R. E., and Parnell, J.: Mechanical Properties of Arteries in Vivo. Circ. Research, vol. 8, May 1960, pp. 622-639.

20. Hallock, P.: Arterial Elasticity in Man in Relation to Age as Evaluated by the Pulse-Wave Velocity Method. Archives Internal Medicine, vol. 54, 1934, pp. 770-798.

21. Van Citters, R. L.: Longitudinal Waves in the Walls of Fluid-Filled Elastic Tubes. Cir. Research, vol. 8, no. 6, Nov. 1960.

22. Clark, J. H.: The Elasticity of Veins. Amer. Jour. of Physiol., vol. 105, 1933, pp. 418-427.

23. Burton, A. C.: On the Physical Equilibrium of Small Blood Vessels. Amer. Jour. of Physiol., vol. 164, 1951, pp. 319-329.

24. Sacks, A., Raman, K., Burnell, J., and Tickner, E.: Auscultatory Versus Direct Pressure Measurement for Newtonian Fluids and for Blood in Simulated Arteries. Vidya Rep. No. 119, Dec. 1963.

25. Maximow, A. A. and Bloom, W.: Histology. Saunders Co., 7th Ed., Philadelphia, 1957.

26. Stedman's Medical Dictionary, 1957 Ed. Williams & Wilkins Co., Baltimore, 1957.

27. Bloom, W. and Fawcitt, D. W.: Histology. Saunders Co., 8th Ed., Philadelphia, 1962.

28. Abramson, D. I.: Blood Vessels and Lymphatics. Academic Press, New York, 1962.

29. Lansing, A. I.: The Arterial Wall. The Williams and Wilkins Co., 1959.

30. Franklin, K. J.: A Monograph on Veins. Thomas Co., Springfield, Ill., 1937.

31. Green, A. E. and Zerna, W.: Theoretical Elasticity. Clarendon Press, Oxford, 1960.

32. Green, A. E. and Adkins, J. E.: Large Elastic Deformations and Nonlinear Continuum Mechanics. Clarendon Press, Oxford, 1960.

33. Love, A. E. H.: A Treatise on the Mathematical Theory of Elasticity. Dover Publications, New York, 1944.

34. Lekhnitskii, S. G.: Theory of Elasticity of an Anisotropic Elastic Body. Holden Day, Inc., San Francisco, 1963.

35. Timoshenko, S. and Goodier, J. N.: Theory of Elasticity. McGraw-Hill Book Co., New York, 1951.

36. Mooney, M.: A Theory of Large Elastic Deformation. Jour. of Applied Physics, vol. 11, 1940, p. 582.

37. Rivlin, R. S.: Torsion of a Rubber Cylinder. Jour. Applied Phys., vol. 18, 1947, p. 444.

38. Rivlin, R. S. and Saunders, D. W.: Large Elastic Deformations of Isotropic Materials. Phil. Trans. A, 243, 1951, p. 251.

39. Gent, A. N. and Rivlin, R. S.: Experiments on Mechanics of Rubber. Proc. Phys. Soc. B., 1952, p. 487.

40. Zatzman, M. et al.: Time Course of Stress Relaxation in Isolated Arterial Segments. Amer. Jour. of Physiol., vol. 177, 1954.

41. Kline, S. J. and McClintock, F. A.: Describing Uncertainties in Single-Sample Experiments. Mech. Eng. 75, 3, 1953.

TABLE I

CLINICAL INFORMATION ON THE ARTERIES TESTED

Arteries	Species	Age (yr)	Weight (lb)	Blood pressure (mm Hg.)	Death by	Time after death to first test (hr)	Date of test	Excised length (in.)	In-situ length* (in.)	In-situ extension ratio
Thoracic Aorta I	Canine (male)	1	30	---	Bleeding	4	1/8/64	1.38 ±0.06	2.0 ±0.1	1.4
Femoral I	Canine (male)	1	30	---	Bleeding	3		0.91 ± .06	1.5 ± .1	1.7
Splenic I	Human (male)	58	240	---	Coronary	40	1/11/64	1.29 ± .05	1.5	1.2
Super Mesenteric I	Human (male)	58	---	---	Coronary	42		1.35 ± .05	1.5	1.1
Brachial I	Human (male)	38	155	140/70	Pneumo-coccal-meningitis	10	1/14/64	2.35 ± .05	2.95	1.25
Thoracic Aorta II	Canine (male)	3	40	---	Bleeding	3	1/20/64	1.41 ± .06	2.0 ± .1	1.4
Femoral II						2		1.09 ± .06	1.75 + .1	1.6
Brachial II	Human (male)	40	155	210/110	Diabetes and uremia	3	1/22/64	2.85	3.96	1.4
Brachial III	Human (male	44	158	130/70	Cardiac surgery	1	1/29/64	3.35	3.96	1.2
External Iliac I	Human (female)	45	150	---	CO poisoning	21	1/30/64	1.55 ± .06	2.0	1.3
Splenic II						20		1.28 ± .06	3.2	1.3
Superior Mesenteric II						18		1.95 ± .06	2.3	1.2
Brachial IV	Human (male)	67	137	90/60	Coronary	6	3/9/64	2.85 ± .05	3.5	1.2
Femoral III						5		2.45 ± .05	2.85	1.2

*All in-situ measurements with unspecified tolerances were determined by the various pathologist prior to excision, so we cannot place any tolerances on these measurements.

TABLE II

DATA CURVE-FIT CONSTANTS

BRACHIAL I A

AXIAL WEIGHT = 0 P(MAX)=302 P(MIN)= 79

A(0)= 4.050-2	A(1)= 4.268-2	A(2)= 2.253-4	A(3)=-4.032-7
B(0)= 7.055-2	B(1)= 7.055-2	B(2)= 1.432-4	B(3)=-2.546-7
L(0)= 7.132-1	Z(1)= 7.242-1	Z(2)= 5.299-4	Z(3)=-9.254-7

AXIAL WEIGHT = 50 P(MAX)=300 P(MIN)= 60

A(0)= 4.050-2	A(1)= 6.627-2	A(2)= 3.279-5	A(3)=-1.306-8
B(0)= 7.055-2	B(1)= 8.133-2	B(2)= 3.452-5	B(3)=-3.497-8
L(0)= 7.132-1	Z(1)= 9.244-1	Z(2)=-1.165-4	Z(3)= 1.691-7

BRACHIAL II A

AXIAL WEIGHT = 0 P(MAX)=298 P(MIN)= 20

A(0)= 7.500-2	A(1)= 9.381-2	A(2)= 7.329-5	A(3)=-1.211-7
B(0)= 1.125-1	B(1)= 1.231-1	B(2)=-5.212-6	B(3)= 9.059-8
L(0)= 1.220+0	Z(1)= 1.271+0	Z(2)= 8.159-4	Z(3)=-1.060-6

AXIAL WEIGHT = 20 P(MAX)=300 P(MIN)= 20

A(0)= 7.500-2	A(1)= 8.497-2	A(2)= 9.744-5	A(3)=-1.597-7
B(0)= 1.125-1	B(1)= 1.115-1	B(2)= 6.210-5	B(3)=-9.680-8
L(0)= 1.220+0	Z(1)= 1.431+0	Z(2)= 4.596-5	Z(3)= 1.410-7

AXIAL WEIGHT =100 P(MAX)=300 P(MIN)= 59

A(0)= 7.500-2	A(1)= 6.862-2	A(2)= 1.790-4	A(3)=-2.644-7
B(0)= 1.125-1	B(1)= 1.003-1	B(2)= 5.735-5	B(3)=-1.098-8
L(0)= 1.220+0	Z(1)= 1.499+0	Z(2)=-1.010-4	Z(3)=-1.099-8

AXIAL WEIGHT = T P(MAX)=286 P(MIN)= 60

A(0)= 7.500-2	A(1)= 6.055-2	A(2)= 3.165-4	A(3)=-6.724-7
B(0)= 1.125-1	B(1)= 8.064-2	B(2)= 2.466-4	B(3)=-5.078-7
L(0)= 1.220+0	Z(1)= 1.311+0	Z(2)=-4.663-4	Z(3)= 1.250-6

Example: The displacements (a, b, and L) are given by

$$a = a_1 + a_2 p + a_3 p^2$$

$$b = b_1 + b_2 p + b_3 p^2$$

$$L = z_1 + z_2 p + z_3 p^2$$

where

$A(1) = a_1 = 4.050 - 2 = 4.050 \times 10^{-2} = 0.04050$ inch/mm Hg.

$A(2) = a_2 = 4.268 - 2 = 0.04268$ inch/(mm Hg.)^2

Etc.

TABLE II.- CONTINUED.

BRACHIAL IIIA

AXIAL WEIGHT = 0 P(MAX)=292 P(MIN)= 39

A(0)= 6.500-2	A(1)= 8.438-2	A(2)= 6.721-5	A(3)=-9.244-8
B(0)= 8.800-2	B(1)= 9.940-2	B(2)= 5.423-5	B(3)=-9.650-8
L(0)= 1.000+0	Z(1)= 1.016+0	Z(2)= 1.032-3	Z(3)=-1.734-6

AXIAL WEICHT = 20 P(MAX)=308 P(MIN)= 20

A(0)= 6.500-2	A(1)= 7.687-2	A(2)= 1.465-4	A(3)=-2.964-7
B(0)= 8.800-2	B(1)= 8.905-2	B(2)= 1.437-4	B(3)=-3.071-7
L(0)= 1.000+0	Z(1)= 1.252+0	Z(2)=-5.161-4	Z(3)= 1.138-6

AXIAL WEIGHT = 50 P(MAX)=300 P(MIN)= 19

A(0)= 6.500-2	A(1)= 6.841-2	A(2)= 1.981-4	A(3)=-3.794-7
B(0)= 8.800-2	B(1)= 8.035-2	B(2)= 1.964-4	B(3)=-4.016-7
L(0)= 1.000+0	Z(1)= 1.343+0	Z(2)=-4.965-4	Z(3)=-7.681-7

AXIAL WEIGHT = T P(MAX)=299 P(MIN)= 60

A(0)= 6.500-2	A(1)= 7.298-2	A(2)= 1.376-4	A(3)=-2.305-7
B(0)= 8.800-2	B(1)= 8.296-2	B(2)= 1.379-4	B(3)=-2.533-7
L(0)= 1.000+0	Z(1)= 1.305+0	Z(2)= 1.592-8	Z(3)=-5.307+0

BRACHIAL IV A

AXIAL WEIGHT = 0 P(MAX)=300 P(MIN)= 27

A(0)= 7.810-2	A(1)= 1.050-1	A(2)= 7.666-5	A(3)=-9.734-8
B(0)= 1.045-1	B(1)= 1.248-1	B(2)= 3.302-5	B(3)=-2.057-8
L(0)= 1.628+0	Z(1)= 1.789+0	Z(2)= 1.903-3	Z(3)=-3.756-6

AXIAL WEIGHT=32.4 P(MAX) =300 P(MIN)= 20

A(0)= 7.810-2	A(1)= 1.019-1	A(2)= 1.316-4	A(3)=-2.737-7
B(0)= 1.045-1	B(1)= 1.167-1	B(2)= 1.040-4	B(3)=-2.078-7
L(0)= 1.628+0	Z(1)= 2.199+0	Z(2)=-1.006-3	Z(3)= 2.141-6

AXIAL WEIGHT=55.9 P(MAX)=300 P(MIN)= 50

A(0)= 7.810-2	A(1)= 9.053-2	A(2)= 2.368-4	A(3)=-4.894-7
B(0)= 1.045-1	B(1)= 1.123-1	B(2)= 1.260-4	B(3)=-2.297-7
L(0)= 1.628+0	Z(1)= 2.176+0	Z(2)=-4.053-4	Z(3)= 7.690-7

TABLE II.- CONTINUED.

BRACHIAL IV B

AXIAL WEIGHT = 0 P(MAX)=251 P(MIN)= 52

A(0)= 7.810-2	A(1)= 9.129-2	A(2)= 1.257-4	A(3)=-2.196-7
B(0)= 1.045-1	B(1)= 1.130-1	B(2)= 6.975-5	B(3)=-6.059-8
L(0)= 1.628+0	Z(1)= 1.681+0	Z(2)= 1.960-3	Z(3)=-3.670-6

AXIAL WEIGHT = 20 P(MAX)=250 P(MIN)= 46

A(0)= 7.810-2	A(1)= 9.150-2	A(2)= 1.580-4	A(3)=-4.281-7
B(0)= 1.045-1	B(1)= 1.112-1	B(2)= 1.014-4	B(3)=-2.582-7
L(0)= 1.628+0	Z(1)= 1.950+0	Z(2)= 1.744-6	Z(3)= 3.442-7

AXIAL WEIGHT = 50 P(MAX)=251 P(MIN)= 60

A(0)= 7.810-2	A(1)= 9.274-2	A(2)= 8.731-5	A(3)=-1.364-7
B(0)= 1.045-1	B(1)= 1.096-1	B(2)= 5.840-5	B(3)=-4.314-8
L(0)= 1.628+0	Z(1)= 2.090+0	Z(2)=-7.885-4	Z(3)= 2.489-6

AXIAL WEIGHT =100 P(MAX)=250 P(MIN)= 64

A(0)= 7.810-2	A(1)= 8.131-2	A(2)= 2.230-4	A(3)=-5.184-7
B(0)= 1.045-1	B(1)= 9.962-2	B(2)= 1.780-4	B(3)=-3.884-7
L(0)= 1.628+0	Z(1)= 2.173+0	Z(2)=-2.468-4	Z(3)=-9.551-8

ILIAC EXTERNAL I

AXIAL WEIGHT = 0 P(MAX)=306 P(MIN)= 20

A(0)= 7.250-2	A(1)= 8.960-2	A(2)= 2.306-4	A(3)=-5.010-7
B(0)= 1.110-1	B(1)= 1.204-1	B(2)= 1.475-4	B(3)=-3.096-7
L(0)= 9.500-1	Z(1)= 1.003+0	Z(2)= 2.054-3	Z(3)=-4.440-6

AXIAL WEIGHT = 20 P(MAX)=302 P(MIN)= 20

A(0)= 7.250-2	A(1)= 9.686-2	A(2)= 1.484-4	A(3)=-2.718-7
B(0)= 1.110-1	B(1)= 1.219-1	B(2)= 1.060-4	B(3)=-1.703-7
L(0)= 9.500-1	Z(1)= 1.226+0	Z(2)= 1.583-4	Z(3)=-1.025-8

AXIAL WEIGHT = 50 P(MAX)=260 P(MIN)= 52

A(0)= 7.000-2	A(1)= 8.448-2	A(2)= 7.279-5	A(3)=-8.751-8
B(0)= 9.500-2	B(1)= 1.002-1	B(2)= 7.892-5	B(3)=-1.390-7
L(0)= 6.700-1	Z(1)= 7.899-1	Z(2)=-2.632-4	Z(3)= 1.048-6

AXIAL WEIGHT =100 P(MAX)=294 P(MIN)= 80

A(0)= 7.250-2	A(1)= 9.468-2	A(2)= 1.272-4	A(3)=-1.991-7
B(0)= 1.110-1	B(1)= 1.165-1	B(2)= 1.177-4	B(3)=-1.926-7
L(0)= 9.500-1	Z(1)= 1.384+0	Z(2)=-2.501-4	Z(3)= 4.457-7

AXIAL WEIGHT = T P(MAX)=305 P(MIN)= 20

A(0)= 7.250-2	A(1)= 9.793-2	A(2)= 1.698-4	A(3)=-3.430-7
B(0)= 1.110-1	B(1)= 1.184-1	B(2)= 1.290-4	B(3)=-2.584-7
L(0)= 9.500-1	Z(1)= 1.260+0	Z(2)= 1.338-8	Z(3)= 0.000+0

TABLE II.- CONTINUED.

HUMAN SPLENIC IA

AXIAL WEIGHT = 0 P(MAX)=300 P(MIN)= 20

A(0)= 7.000-2	A(1)= 8.471-2	A(2)= 1.129-4	A(3)=-2.534-7
B(0)= 9.500-2	B(1)= 1.053-1	B(2)= 8.284-5	B(3)=-1.633-7
L(0)= 6.700-1	Z(1)= 7.141-1	Z(2)= 6.695-4	Z(3)=-1.685-6

AXIAL WEIGHT = 50 P(MAX)=260 P(MIN)= 52

A(0)= 7.000-2	A(1)= 8.448-2	A(2)= 7.279-5	A(3)=-8.751-8
B(0)= 9.500-2	B(1)= 1.002-1	B(2)= 7.892-5	B(3)=-1.390-7
L(0)= 6.700-1	Z(1)= 7.899-1	Z(2)=-2.632-4	Z(3)= 1.048-6

HUMAN SPLENIC I B

AXIAL WEIGHT = 0 P(MAX)=251 P(MIN)= 90

A(0)= 7.000-2	A(1)= 8.221-2	A(2)= 1.305-4	A(3)=-2.842-7
B(0)= 9.500-2	B(1)= 9.741-2	B(2)= 1.637-4	B(3)=-4.033-7
L(0)= 5.540-1	Z(1)= 5.929-1	Z(2)= 4.696-4	Z(3)=-9.262-7

AXIAL WEIGHT = 20 P(MAX)=350 P(MIN)= 54

A(0)= 7.000-2	A(1)= 7.324-2	A(2)= 2.301-4	A(3)=-4.472-7
B(0)= 9.500-2	B(1)= 9.078-2	B(2)= 2.130-4	B(3)=-4.639-7
L(0)= 5.540-1	Z(1)= 6.706-1	Z(2)=-9.137-5	Z(3)= 2.161-7

THORACIC AORTA I A

AXIAL WEIGHT = 0 P(MAX)=184 P(MIN)= 40

A(0)= 1.300-1	A(1)= 1.064-1	A(2)= 1.288-3	A(3)=-3.880-6
B(0)= 1.553-1	B(1)= 1.361-1	B(2)= 1.069-3	B(3)=-3.121-6
L(0)= 3.670-1	Z(1)= 3.456-1	Z(2)= 1.244-3	Z(3)=-3.990-6

AXIAL WEIGHT = 50 P(MAX)=200 P(MIN)= 40

A(0)= 1.300-1	A(1)= 1.129-1	A(2)= 1.118-3	A(3)=-3.165-6
B(0)= 1.553-1	B(1)= 1.405-1	B(2)= 8.847-4	B(3)=-2.306-6
L(0)= 3.670-1	Z(1)= 4.613-1	Z(2)=-3.705-4	Z(3)= 3.984-6

THORACIC AORTA I B

AXIAL WEIGHT = 0 P(MAX)=200 P(MIN)= 50

A(0)= 1.300-1	A(1)= 1.187-1	A(2)= 8.912-4	A(3)=-2.060-6
B(0)= 1.600-1	B(1)= 1.485-1	B(2)= 7.327-4	B(3)=-1.637-6
L(0)= 5.500-1	Z(1)= 5.535-1	Z(2)= 1.304-3	Z(3)=-3.813-6

THORACIC AORTA II A

AXIAL WEIGHT = 0 P(MAX)=260 P(MIN)= 50

A(0)= 1.320-1	A(1)= 1.314-1	A(2)= 1.132-3	A(3)=-2.178-6
B(0)= 1.820-1	B(1)= 1.762-1	B(2)= 9.129-4	B(3)=-1.775-6
L(0)= 2.600+0	Z(1)= 2.362+0	Z(2)= 1.169-2	Z(3)=-2.311-5

AXIAL WEIGHT = 50 P(MAX)=300 P(MIN)= 50

A(0)= 1.320-1	A(1)= 1.154-1	A(2)= 1.345-3	A(3)=-2.702-6
B(0)= 1.820-1	B(1)= 1.503-1	B(2)= 1.150-3	B(3)=-2.270-6
L(0)= 2.600+0	Z(1)= 2.512+0	Z(2)= 1.142-2	Z(3)=-2.262-5

TABLE II.- CONTINUED.

HUMAN SPLENIC I A

AXIAL WEIGHT = 0	P(MAX)=300	P(MIN)= 20		
A(0)= 7.000-2	A(1)= 8.471-2	A(2)= 1.129-4	A(3)=-2.534-7	
B(0)= 9.500-2	B(1)= 1.053-1	B(2)= 8.284-5	B(3)=-1.633-7	
L(0)= 6.700-1	Z(1)= 7.141-1	Z(2)= 6.695-4	Z(3)=-1.685-6	
AXIAL WEIGHT = 50	P(MAX)=260	P(MIN)= 52		
A(0)= 7.000-2	A(1)= 8.448-2	A(2)= 7.279-5	A(3)=-8.751-8	
B(0)= 9.500-2	B(1)= 1.002-1	B(2)= 7.892-5	B(3)=-1.390-7	
L(0)= 6.700-1	Z(1)= 7.899-1	Z(2)=-2.632-4	Z(3)= 1.048-6	

HUMAN SPLENIC I B

AXIAL WEIGHT = 0	P(MAX)=251	P(MIN)= 90		
A(0)= 7.000-2	A(1)= 8.221-2	A(2)= 1.305-4	A(3)=-2.842-7	
B(0)= 9.500-2	B(1)= 9.741-2	B(2)= 1.637-4	B(3)=-4.033-7	
L(0)= 5.540-1	Z(1)= 5.929-1	Z(2)= 4.696-4	Z(3)=-9.262-7	
AXIAL WEIGHT = 20	P(MAX)=350	P(MIN)= 54		
A(0)= 7.000-2	A(1)= 7.324-2	A(2)= 2.301-4	A(3)=-4.472-7	
B(0)= 9.500-2	B(1)= 9.078-2	B(2)= 2.130-4	B(3)=-4.639-7	
L(0)= 5.540-1	Z(1)= 6.706-1	Z(2)=-9.137-5	Z(3)= 2.161-7	

THORACIC AORTA I A

AXIAL WEIGHT = 0	P(MAX)=184	P(MIN)= 40		
A(0)= 1.300-1	A(1)= 1.064-1	A(2)= 1.288-3	A(3)=-3.880-6	
B(0)= 1.553-1	B(1)= 1.361-1	B(2)= 1.069-3	B(3)=-3.121-6	
L(0)= 3.670-1	Z(1)= 3.456-1	Z(2)= 1.244-3	Z(3)=-3.990-6	
AXIAL WEIGHT = 50	P(MAX)=200	P(MIN)= 40		
A(0)= 1.300-1	A(1)= 1.129-1	A(2)= 1.118-3	A(3)=-3.165-6	
B(0)= 1.553-1	B(1)= 1.405-1	B(2)= 8.847-4	B(3)=-2.306-6	
L(0)= 3.670-1	Z(1)= 4.613-1	Z(2)=-3.705-4	Z(3)= 3.984-6	

THORACIC AORTA I B

AXIAL WEIGHT = 0	P(MAX)=200	P(MIN)= 50		
A(0)= 1.300-1	A(1)= 1.187-1	A(2)= 8.912-4	A(3)=-2.060-6	
B(0)= 1.600-1	B(1)= 1.485-1	B(2)= 7.327-4	B(3)=-1.637-6	
L(0)= 5.500-1	Z(1)= 5.535-1	Z(2)= 1.304-3	Z(3)=-3.813-6	

THORACIC AORTA II A

AXIAL WEIGHT = 0	P(MAX)=260	P(MIN)= 50		
A(0)= 1.320-1	A(1)= 1.314-1	A(2)= 1.132-3	A(3)=-2.178-6	
B(0)= 1.820-1	B(1)= 1.762-1	B(2)= 9.129-4	B(3)=-1.775-6	
L(0)= 2.600+0	Z(1)= 2.362+0	Z(2)= 1.169-2	Z(3)=-2.311-5	
AXIAL WEIGHT = 50	P(MAX)=300	P(MIN)= 50		
A(0)= 1.320-1	A(1)= 1.154-1	A(2)= 1.345-3	A(3)=-2.702-6	
B(0)= 1.820-1	B(1)= 1.503-1	B(2)= 1.150-3	B(3)=-2.270-6	
L(0)= 2.600+0	Z(1)= 2.512+0	Z(2)= 1.142-2	Z(3)=-2.262-5	

TABLE II.- CONTINUED.

THORACIC AORTA II B

AXIAL WEIGHT = 0 P(MAX)=250 P(MIN)= 50

A(0)= 1.230-1	A(1)= 9.565-2	A(2)= 1.722-3	A(3)=-3.965-6
B(0)= 1.730-1	B(1)= 1.418-1	B(2)= 1.460-3	B(3)=-3.382-6
L(0)= 2.120+0	Z(1)= 1.826+0	Z(2)= 1.156-2	Z(3)=-2.504-5

AXIAL WEIGHT = T P(MAX)=250 P(MIN)= 50

A(0)= 1.230-1	A(1)= 9.380-2	A(2)= 1.764-3	A(3)=-4.227-6
B(0)= 1.730-1	B(1)= 1.363-1	B(2)= 1.541-3	B(3)=-3.727-6
L(0)= 2.120+0	Z(1)= 2.739+0	Z(2)= 2.026-3	Z(3)= 1.055-6

HUMAN SUP MESENTERIC

AXIAL WEIGHT = 0 P(MAX)=300 P(MIN)= 60

A(0)= 9.600-2	A(1)= 1.094-1	A(2)= 1.696-4	A(3)=-2.367-7
B(0)= 1.250-1	B(1)= 1.355-1	B(2)= 1.284-4	B(3)=-1.844-7
L(0)= 5.500-1	Z(1)= 5.949-1	Z(2)= 1.828-4	Z(3)=-4.682-7

AXIAL WEIGHT = 20 P(MAX)=259 P(MIN)= 21

A(0)= 9.600-2	A(1)= 1.119-1	A(2)= 1.283-4	A(3)=-3.408-7
B(0)= 1.250-1	B(1)= 1.352-1	B(2)= 1.209-4	B(3)=-2.907-7
L(0)= 5.500-1	Z(1)= 5.544-1	Z(2)= 8.548-4	Z(3)=-2.247-6

FEMORAL I A

AXIAL WEIGHT = 0 P(MAX)=250 P(MIN)= 23

A(0)= 5.400-2	A(1)= 5.332-2	A(2)= 1.716-4	A(3)=-4.532-7
B(0)= 6.680-2	B(1)= 6.657-2	B(2)= 1.232-4	B(3)=-2.982-7
L(0)= 9.280-1	Z(1)= 8.936-1	Z(2)= 1.595-3	Z(3)=-3.226-6

FEMORAL II A

AXIAL WEIGHT = 0 P(MAX)=301 P(MINT= 80

A(0)= 6.200-2	A(1)= 8.024-2	A(2)= 7.336-5	A(3)=-1.130-7
B(0)= 7.500-2	B(1)= 9.774-2	B(2)=-1.031-5	B(3)= 3.429-8
L(0)= 8.300-1	Z(1)= 6.679-1	Z(2)= 1.823-3	Z(3)=-1.466-6

FEMORAL II B

AXIAL WEIGHT = 0 P(MAX)=200 P(MIN)= 50

A(0)= 5.700-2	A(1)= 7.227-2	A(2)= 1.836-4	A(3)=-4.063-7
B(0)= 7.800-2	B(1)= 9.261-2	B(2)= 7.750-5	B(3)=-1.620-7
L(0)= 7.200-1	Z(1)= 6.245-1	Z(2)= 2.627-3	Z(3)=-3.906-6

AXIAL WEIGHT = 20 P(MAX)=300 P(MIN)= 50

A(0)= 5.700-2	A(1)= 7.377-2	A(2)= 1.394-4	A(3)=-2.779-7
B(0)= 7.800-2	B(1)= 8.419-2	B(2)= 1.112-4	B(3)=-2.304-7
L(0)= 7.200-1	Z(1)= 1.022+0	Z(2)=-1.206-4	Z(3)= 6.499-7

TABLE II.- CONCLUDED.

HUMAN FEMORAL III

AXIAL WEIGHT = 0 P(MAX)=200 P(MIN)= 50			
A(0)= -----	A(1)= 1.171-1	A(2)= 5.014-5	A(3)=-5.045-8
B(0)= -----	B(1)= 1.471-1	B(2)= 1.271-4	B(3)=-1.708-7
L(0)= 1.050+0	Z(1)= 1.073+0	Z(2)= 8.346-4	Z(3)=-2.133-6
AXIAL WEIGHT = 20 P(MAX)=200 P(MIN)= 50			
A(0)= -----	A(1)= 1.098-1	A(2)= 1.315-4	A(3)=-2.754-7
B(0)= -----	B(1)= 1.580-1	B(2)=-2.790-5	B(3)= 2.797-7
L(0)= 1.050+0	Z(1)= 1.136+0	Z(2)= 3.780-4	Z(3)=-5.199-7
AXIAL WEIGHT = 50 P(MAX)=200 P(MIN)= 49			
A(0)= -----	A(1)= 1.146-1	A(2)= 2.975-5	A(3)= 1.162-7
B(0)= -----	B(1)= 1.561-1	B(2)= 5.558-5	B(3)=-1.535-7
L(0)= 1.050+0	Z(1)= 1.180+0	Z(2)= 1.648-4	Z(3)=-2.814-7
AXIAL WEIGHT =100 P(MAX)=200 P(MIN)= 50			
A(0)= -----	A(1)= 1.134-1	A(2)= 1.335-4	A(3)=-3.487-7
B(0)= -----	B(1)= 1.473-1	B(2)= 1.537-4	B(3)=-5.205-7
L(0)= 1.050+0	Z(1)= 1.215+0	Z(2)= 8.790-5	Z(3)=-3.622-7

TABLE III

COMPARISON OF THE COMPUTED AND CURVE-FIT PARTIAL DERIVATIVES

Curve-fit constants used to compute $\partial W/\partial I_1$

B(1)= 9.4437712E+00 B(2)=-2.6532887E+01 B(3)= 8.4045130E+01

p	I_1	$\partial W/\partial I_1$	$\partial W/\partial I_1$ (curve-fit)
8.0000000E+01	3.1294099E+00	6.3733320E+00	6.7990263E+00
1.0000000E+02	3.1754404E+00	8.2578011E+00	7.8944498E+00
1.2000000E+02	3.2166439E+00	1.0216174E+01	9.781263(00
1.3000000E+02	3.2353849E+00	1.1216134E+01	1.0922716E+01
1.5000000E+02	3.2690527E+00	1.3243111E+01	1.3418200E+01
1.9000000E+02	3.3206904E+00	1.7320726E+01	1.8356278E+01
2.2000000E+02	3.3452673E+00	2.0302322E+01	2.1178830E+01
2.6300000E+02	3.3587815E+00	2.4281831E+01	2.2860671E+01

Curve-fit constants used to compute $\partial W/\partial I_2$

C(1)=-3.5674805E+00 C(2)=-9.2478551E+00 C(3)=-2.5272090E+01

p	I_2	$\partial W/\partial I_2$	$\partial W/\partial I_2$ (curve-fit)
8.0000000E+01	2.8833054E+00	-2.3070669E+00	-2.4415689E+00
1.0000000E+02	2.9498764E+00	-3.0630928E+00	-2.8308879E+00
1.2000000E+02	3.0079971E+00	-3.8544077E+00	-3.7202412E+00
1.3000000E+02	3.0337420E+00	-4.2588998E+00	-4.2778812E+00
1.5000000E+02	3.0783371E+00	-5.0773690E+00	-5.4816424E+00
1.9000000E+02	3.1387572E+00	-6.7095095E+00	-7.5936264E+00
2.2000000E+02	3.1578850E+00	-7.8844960E+00	-8.3775986E+00
2.6300000E+02	3.1451681E+00	-9.4188080E+00	-7.8502025E+00

Curve-fit constants used to compute $\partial W/\partial I_3$

D(1)=-1.5817267E+01 D(2)=-4.0867958E+01 D(3)=-3.4145444E+01

p	I_3	$\partial W/\partial I_3$	$\partial W/\partial I_3$ (curve-fit)
8.0000000E+01	6.8739370E-01	-4.6821624E-01	-2.7645900E-01
1.0000000E+02	6.9066190E-01	-3.8458184E-01	-3.3537330E-01
1.2000000E+02	6.8991550E-01	-2.6874055E-01	-3.2172560E-01
1.3000000E+02	6.8805440E-01	-2.0345684E-01	-2.8819300E-01
1.5000000E+02	6.8141750E-01	-6.6079810E-02	-1.7439000E-01
1.9000000E+02	6.5703640E-01	1.9888270E-01	1.6620400E-01
2.2000000E+02	6.2985990E-01	3.5344204E-01	4.0231800E-01
2.6300000E+02	5.7964090E-01	4.5161913E-01	4.4048900E-01

Example: $\partial W/\partial I_1(\text{curve-fit}) = B_1 + 2B_2(I_1-3) + 3B_3(I_1-3)^2$

where

$B_1 = B(1) = 9.4437712E + 00 = 9.4437712\times10^{0} = 9.4437712$

$B_2 = B(2) = -2.6532887E + 01 = -2.6532887\times10^{1} = -26.532887$

Etc.

TABLE IV

W-FUNCTION CONSTANTS

Vessel	Constants				I(max)	I(min)
BRACHIAL IA	B(1)= 4.263+0	B(2)=-3.126+0	B(3)= 3.648+0	I(1)=	4.0	3.2
	C(1)=-1.076+0	C(2)= 9.508-1	C(3)=-2.265-1	I(2)=	4.3	3.2
	D(1)=-1.106+0	D(2)= 4.221+0	D(3)=-1.190+1	I(3)=	0.9	0.7
BRACHIAL IIA	B(1)= 1.440+1	B(2)= 2.064+1	B(3)= 3.931+1	I(1)=	3.4	2.9
	C(1)=-1.391+1	C(2)=-1.026+1	C(3)=-2.451+0	I(2)=	3.4	2.4
	D(1)= 9.929+0	D(2)= 4.882+0	D(3)=-2.270+0	I(3)=	0.9	0.4
BRACHIAL IIIA	B(1)= 9.444+0	B(2)=-2.653+1	B(3)= 8.405+1	I(1)=	3.2	3.4
	C(1)=-3.567+0	C(2)=-9.248+0	C(3)=-2.527+1	I(2)=	3.1	2.8
	D(1)=-1.582+1	D(2)=-4.087+1	D(3)=-3.415+1	I(3)=	5.8	4.3
BRACHIAL IVA	B(1)=-1.729+1	B(2)= 7.358+0	B(3)= 2.849+1	I(1)=	3.7	3.4
	C(1)= 3.502+1	C(2)=-4.063+1	C(3)= 8.836+0	I(2)=	3.8	3.6
	D(1)= 2.600+0	D(2)= 1.155+0	D(3)=-3.936+0	I(3)=	1.0	0.6
BRACHIAL IVB	B(1)= 1.267+0	B(2)= 5.173+1	B(3)=-1.563+1	I(1)=	3.5	3.1
	C(1)=-6.886+0	C(2)=-1.861+1	C(3)= 8.365+0	I(2)=	3.8	3.0
	D(1)= 8.404+0	D(2)= 6.814-2	D(3)=-5.025+1	I(3)=	1.1	0.7
EXTERNAL ILIAC I	B(1)= 7.459+0	B(2)=-1.651+1	B(3)= 2.529+1	I(1)=	4.1	3.2
	C(1)=-2.579+0	C(2)= 2.110+0	C(3)=-3.824+0	I(2)=	4.7	3.4
	D(1)= 1.849+0	D(2)= 3.030+1	D(3)= 7.644-1	I(3)=	1.1	0.6
SPLENIC IA AND IB	B(1)= 2.966+0	B(2)=-7.101+0	B(3)= 3.687+1	I(1)=	3.6	3.1
	C(1)= 3.430+0	C(2)=-1.090+1	C(3)= 1.756+0	I(2)=	4.3	2.9
	D(1)=-9.570-2	D(2)= 7.822+0	D(3)= 8.233-1	I(3)=	1.3	0.7
THORACIC AORTA I A	B(1)= 1.792+1	B(2)=-1.243+1	B(3)= 6.241+0	I(1)=	4.9	3.2
	C(1)=-1.224+1	C(2)= 8.853+0	C(3)=-2.394+0	I(2)=	6.8	3.3
	D(1)=-2.623+0	D(2)= 5.485+0	D(3)= 1.282+1	I(3)=	1.9	1.0

Example: The W function for Brachial IA is given as

$$W = B_1(I_1-3) + B_2(I_1-3)^2 + B_3(I_1-3)^3 + C_1(I_2 - 3) + C_2(I_2-3)^2 + C_3(I_2-3)^3 + D_1(I_3-1) + D_2(I_3-1)^2 + D_3(I_3-1)^3$$

where

$$B(1) = B_1 = 4.263 + 0 = 4.263\times10^0 = 4.263$$

$$C(1) = C_1 = -1.076 + 0 = -1.076\times10^0 = -1.076$$

Etc.

TABLE IV.- CONCLUDED.

THORACIC AORTA I B	B(1)= 3.091+1	B(2)=-2.837+1	B(3)= 1.358+1	I(1)= 4.0	3.1
	C(1)=-2.089+1	C(2)= 1.848+1	C(3)=-5.872+0	I(2)= 4.3	3.1
	D(1)= 1.320+1	D(2)= 1.348+2	D(3)= 3.643+2	I(3)= 1.0	0.8
THORACIC AORTA II A	B(1)= 9.471+0	B(2)=-2.932+0	B(3)= 1.092+0	I(1)= 5.6	3.1
	C(1)=-1.909+0	C(2)= 1.258-1	C(3)=-2.319-2	I(2)= 7.8	2.7
	D(1)=-8.051-1	D(2)= 1.452+0	D(3)=-6.617-1	I(3)= 1.0	0.5
THORACIC AORTA II B	B(1)= 1.844+1	B(2)=-6.572+0	B(3)= 1.131+0	I(1)= 6.2	3.3
	C(1)=-1.695+0	C(2)= 2.819-1	C(3)=-2.117-2	I(2)= 9.5	3.4
	D(1)=-1.733+0	D(2)= 2.344+0	D(3)=-1.461+0	I(3)= 1.2	0.9
SUPERIOR MESENTERIC	B(1)=-6.279+0	B(2)=-1.538+1	B(3)= 8.382+1	I(1)= 3.5	3.0
	C(1)= 8.471+0	C(2)=-4.262+0	C(3)=-8.313+0	I(2)= 3.9	2.9
	D(1)=-7.098+0	D(2)= 1.717+1	D(3)= 2.240+0	I(3)= 1.4	0.9
FEMORAL I A	B(1)= 1.171+1	B(2)= 3.804+1	B(3)= 4.594+1	I(1)= 3.5	3.0
	C(1)=-5.609+0	C(2)=-2.791+1	C(3)= 2.030+0	I(2)= 3.7	3.0
	D(1)= 3.281+0	D(2)= 1.140+2	D(3)=-2.109+2	I(3)= 1.2	1.0
FEMORAL II A	B(1)= 3.812+1	B(2)=-1.018+2	B(3)= 1.128+2	I(1)= 3.8	3.4
	C(1)= 1.767+1	C(2)=-2.176+1	C(3)=-7.347+0	I(2)= 4.0	3.5
	D(1)=-5.392+0	D(2)= 2.014+0	D(3)= 2.757+1	I(3)= 0.9	0.6
FEMORAL II B	B(1)= 2.564+1	B(2)=-4.927+1	B(3)= 3.400+1	I(1)= 4.2	3.3
	C(1)=-4.083+0	C(2)= 7.837+0	C(3)=-5.520+0	I(2)= 4.7	3.4
	D(1)=-1.100+0	D(2)=-4.290+1	D(3)=-6.430+1	I(3)= 1.0	0.4

TABLE V

COMPARISON OF PRESENT MEASUREMENTS WITH OTHER DATA

Vessel	Species	Relative wall thickness h/b at 0 mm Hg. and unweighted		Relative wall thickness h/b at 100 mm Hg. and unweighted		In-situ extension ratios (in-situ length/excised length) L_e/L_o	
		Data	Ref. 15	Data	Ref. 7	Data	Ref. 7
Thoracic Aorta	Canine	0.231(2)	---	0.099(2)	0.105(15)	1.40(2)	1.47(22)
Femoral Artery	Canine	.183(2)	0.334(1)	.111(2)	.115(11)	1.65(2)	1.72(22)
Abdominal Aorta	Canine	---	.194(1)	---	.105(9)	---	1.51(7)
Carotid Artery	Canine	---	.263(1)	---	.132(13)	---	1.54(29)
Iliac Artery	Human	.347(1)	---	.184(1)	---	1.30(1)	---
Brachial Artery	Human	.318(4)	---	.167(4)	---	1.26(4)	---
Splenic Artery	Human	.263(1)	.474(1)	.165(1)	---	1.25(2)	---
Superior Mesenteric Artery	Human	.232(1)	.344(1)	.153(1)	---	1.15(2)	---
Femoral Artery (somewhat sclerosed)	Human	---	---	.230(1)	---	1.17(1)	---

Figures in brackets refer to the number of specimens measured.

TABLE VI

COMPUTER OUTPUT OF THE ELASTIC CONSTANTS FOR BRACHIAL III

PRESSURE= 100.00 MM HG WEIGHT= 0.00 GRAMS

A = 9.0173471E-02	B = 1.0385758E-01	L = 1.1014488E+00
AO= 6.5000000E-02	BO= 8.8000000E-02	LO= 1.0000000E+00
LAMBDA 1= 1.26817	LAMBDA 2= 1.10144	LAMBDA 3= .59496
W= 3.4457071E+00	W(CHECK)=3.0561319E+00	

BETA(1,1)= 7.8289814E+01	BETA(1,2)=-6.4852066E+01	BETA(1,3)=-9.8850779E+01
BETA(2,1)=-6.8208814E+01	BETA(2,2)=-8.2269395E+01	BETA(2,3)=-1.0689836E+02
BETA(3,1)=-8.5387956E+01	BETA(3,2)=-9.9988770E+01	BETA(3,3)=-7.3748761E+01

ALFA(1,1)= 8.3006059E-03	ALFA(1,2)=-9.1624657E-03	ALFA(1,3)= 2.1550325E-03
ALFA(2,1)=-8.6724006E-03	ALFA(2,2)= 2.5531076E-02	ALFA(2,3)=-2.5382880E-02
ALFA(3,1)= 2.1474390E-03	ALFA(3,2)=-2.4006596E-02	ALFA(3,3)= 1.8359484E-02

E(R)= 5.4467761E+01	E(T)= 1.2047313E+02	E(Z)= 3.9167953E+01
MU12= 1.0447912E+00	MU13=-2.5870869E-01	MU23= 9.4028922E-01
MU31=-1.1737979E-01	MU32= 1.3825486E+00	MU21= 3.5887502E-01

BETA(1,1)= 7.8289814E+01	BETA(1,2)=-6.1575440E+01	BETA(1,3)=-9.2119365E+01
BETA(2,1)=-6.1575440E+01	BETA(2,2)=-8.2269395E+01	BETA(2,3)=-1.0344356E+02
BETA(3,1)=-9.2119365E+01	BETA(3,2)=-1.0344356E+02	BETA(3,3)=-7.3748761E+01

ALFA(1,1)= 8.2958723E-03	ALFA(1,2)=-8.9310271E-03	ALFA(1,3)= 2.1647376E-03
ALFA(2,1)=-8.9310270E-03	ALFA(2,2)= 2.5531911E-02	ALFA(2,3)=-2.4656566E-02
ALFA(3,1)= 2.1647376E-03	ALFA(3,2)=-2.4656566E-02	ALFA(3,3)= 1.8320967E-02

E(R)= 5.4582271E+01	E(T)= 1.2054187E+02	E(Z)= 3.9166672E+01
MU12= 1.0765626E+00	MU13=-2.6094151E-01	MU23= 9.6571563E-01
MU31=-1.1815629E-01	MU32= 1.3458113E+00	MU21= 3.4978960E-01

Example: Beta (1,1) = β_{11} = 7.8289814E + 01 = 78289814x10^{1} = 78.289814 psi

Alpha (1,1) = α_{11} = 8.3006059E - 03 = 8.3006059x10^{-3}

= 0.0083006059 $(psi)^{-1}$

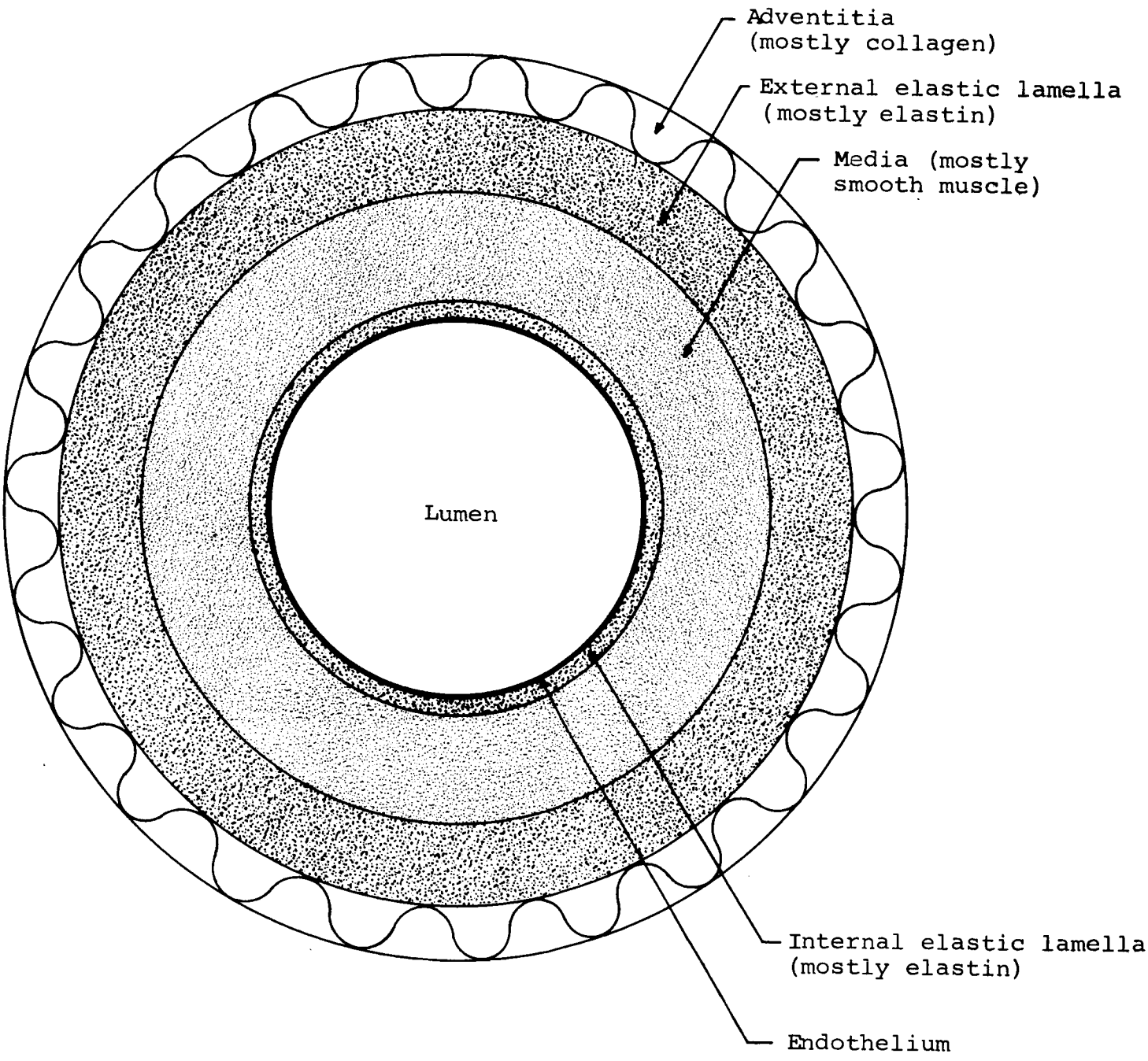

Figure 1.- The five layers of the arterial wall.

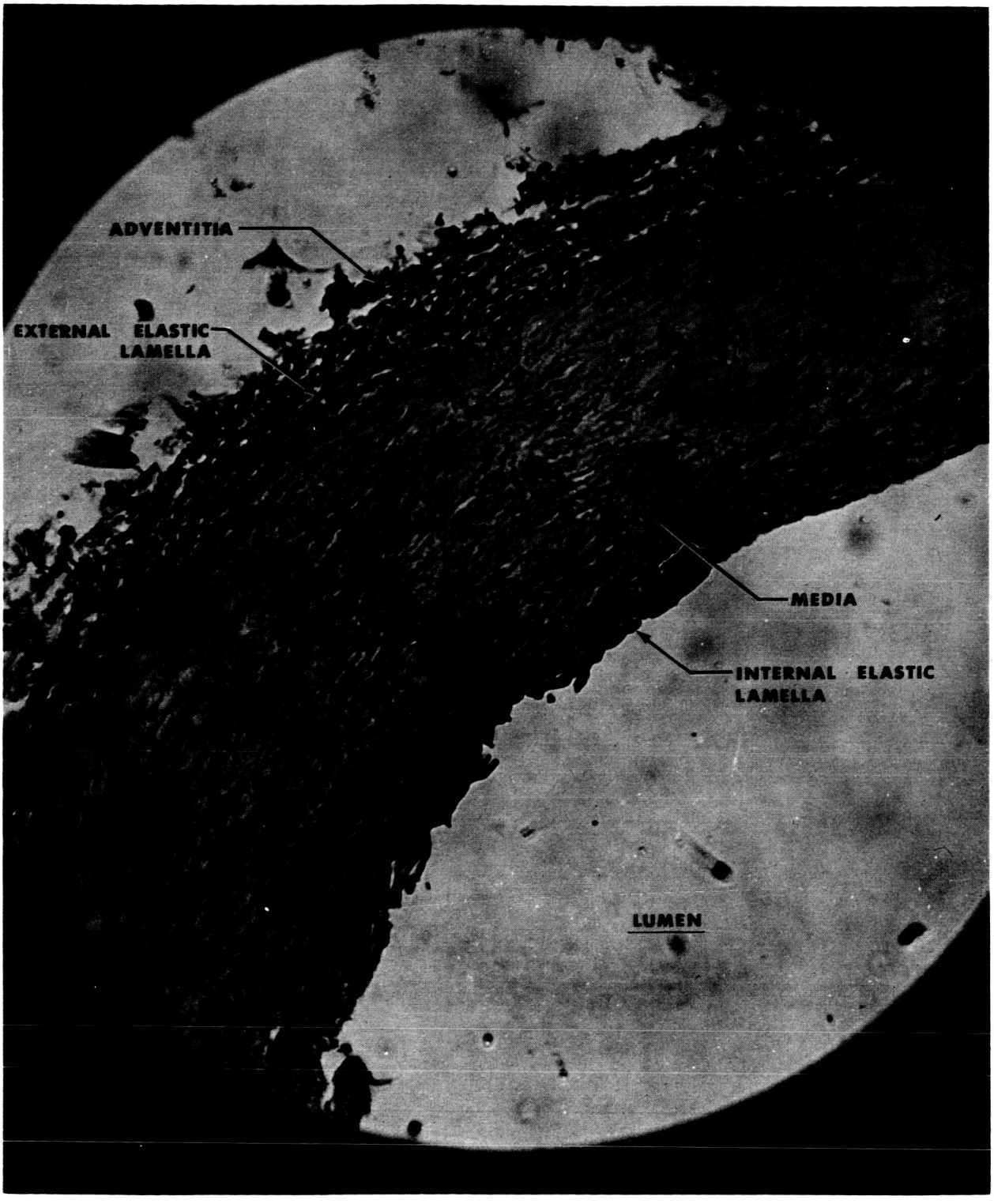

Figure 2.- Microphotograph of Human Brachial II, magnification 125X.

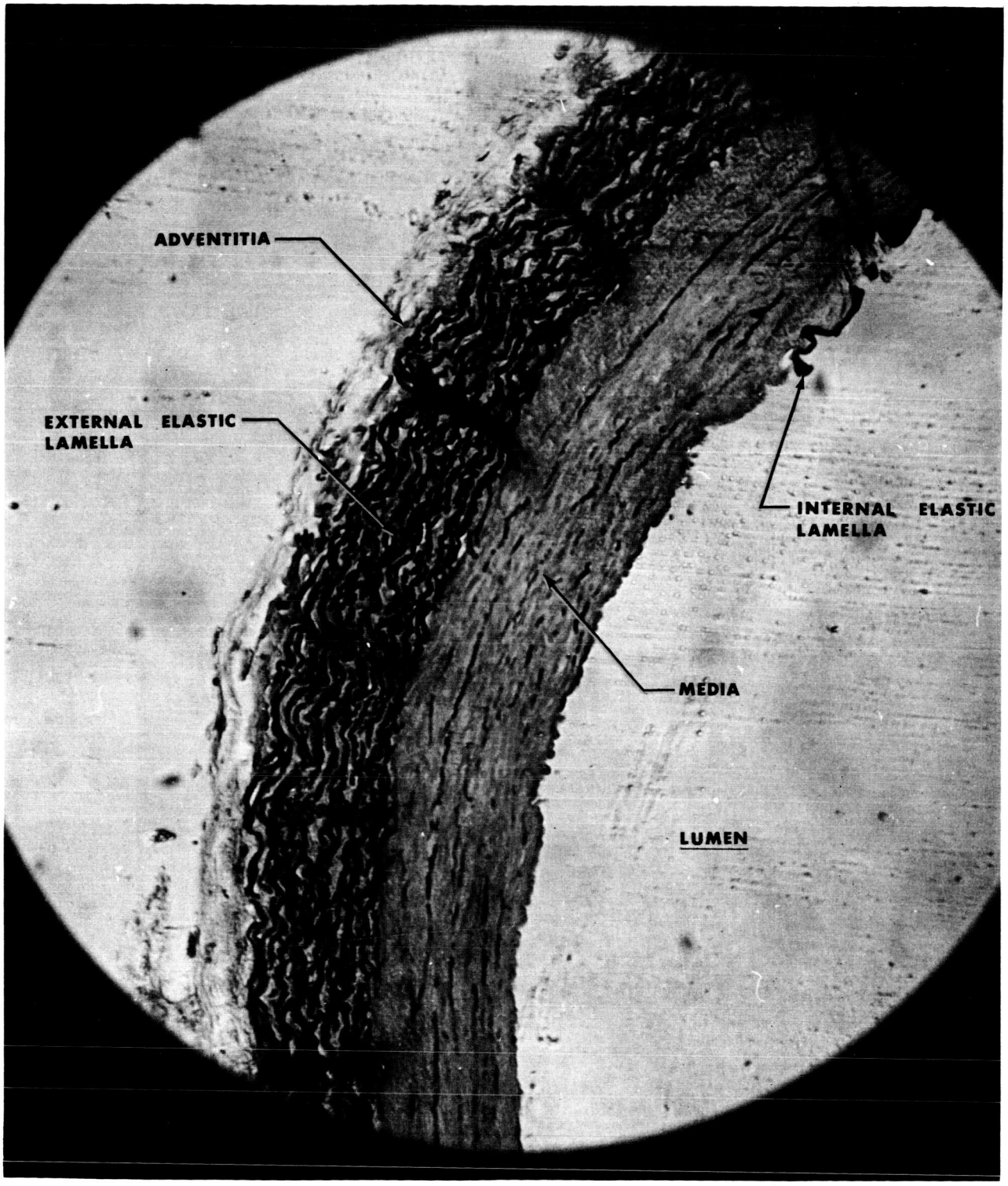

Figure 3.- Microphotograph of Canine Femoral I, magnification 125X.

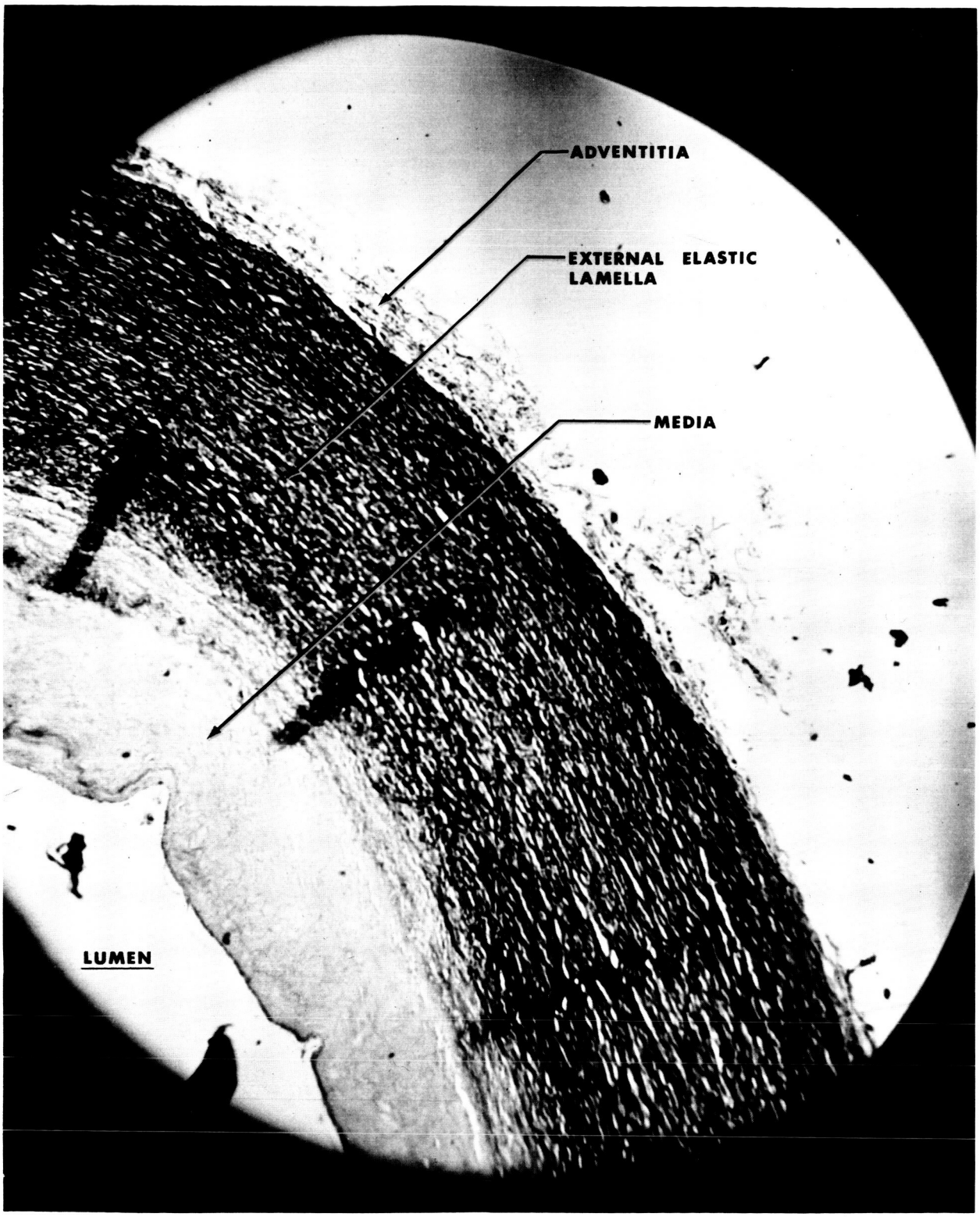

Figure 4.- Microphotograph of Canine Thoracic Aorta I, magnification 62X.

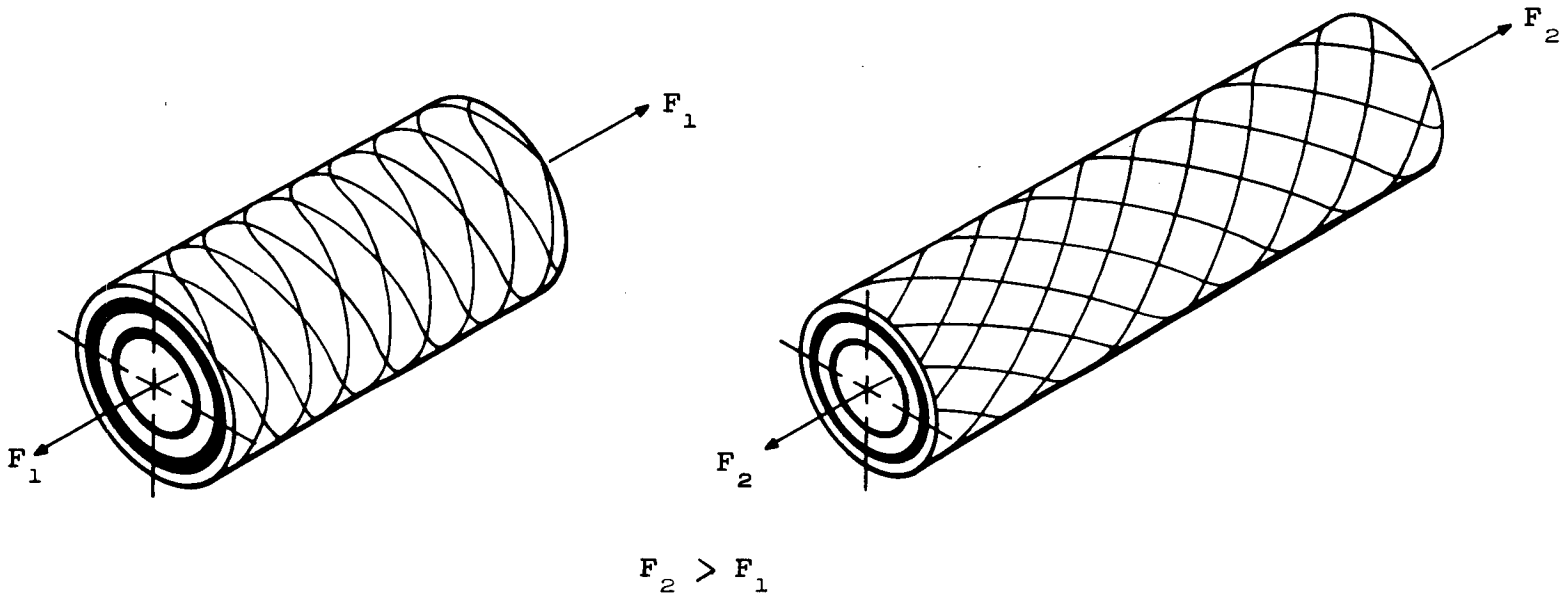

Figure 5.- Arrangements of the collagenous fibres in an artery for two different axial forces (from Ref. 30).

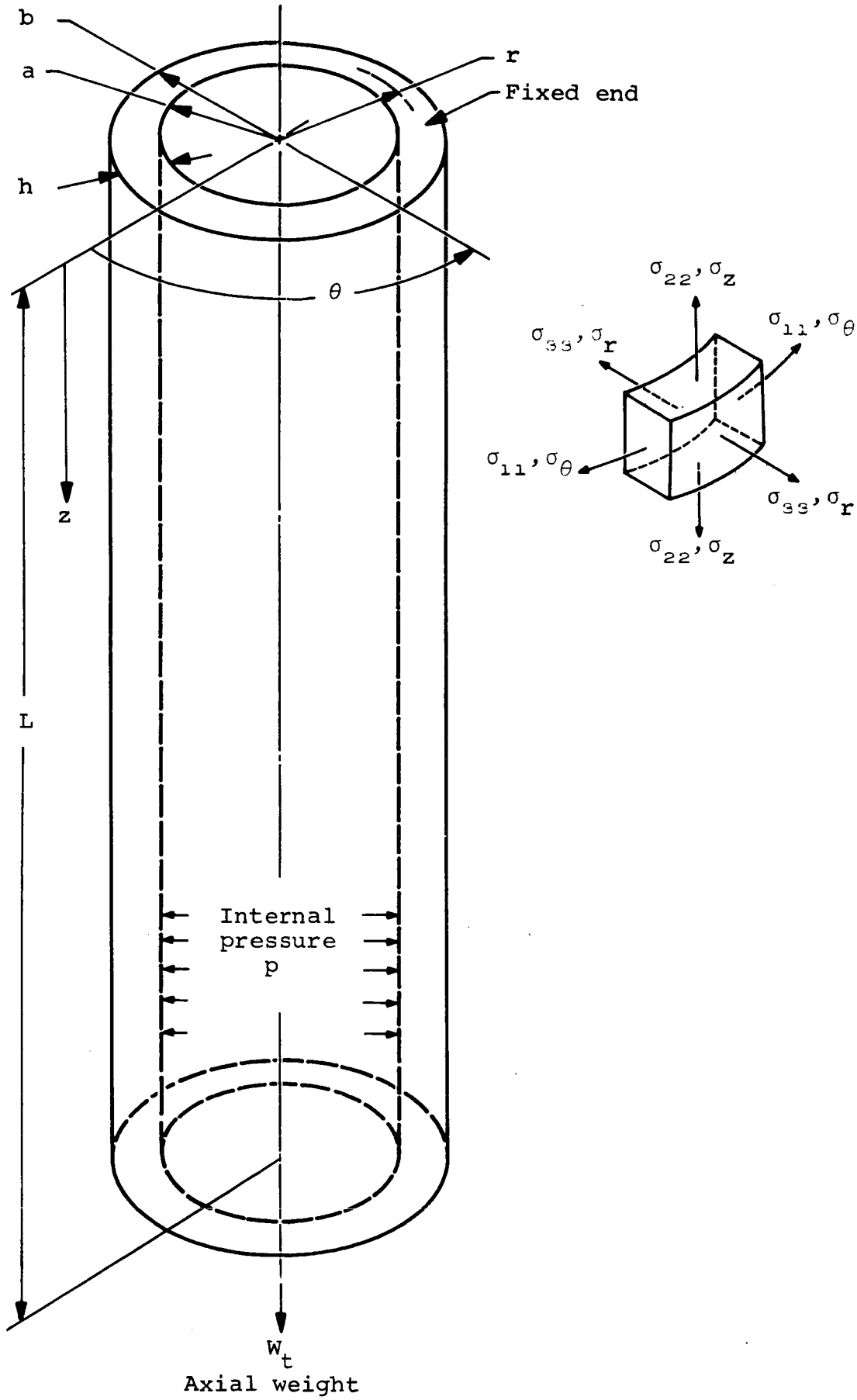

Figure 6.- Mathematical model, coordinate system, and stress components.

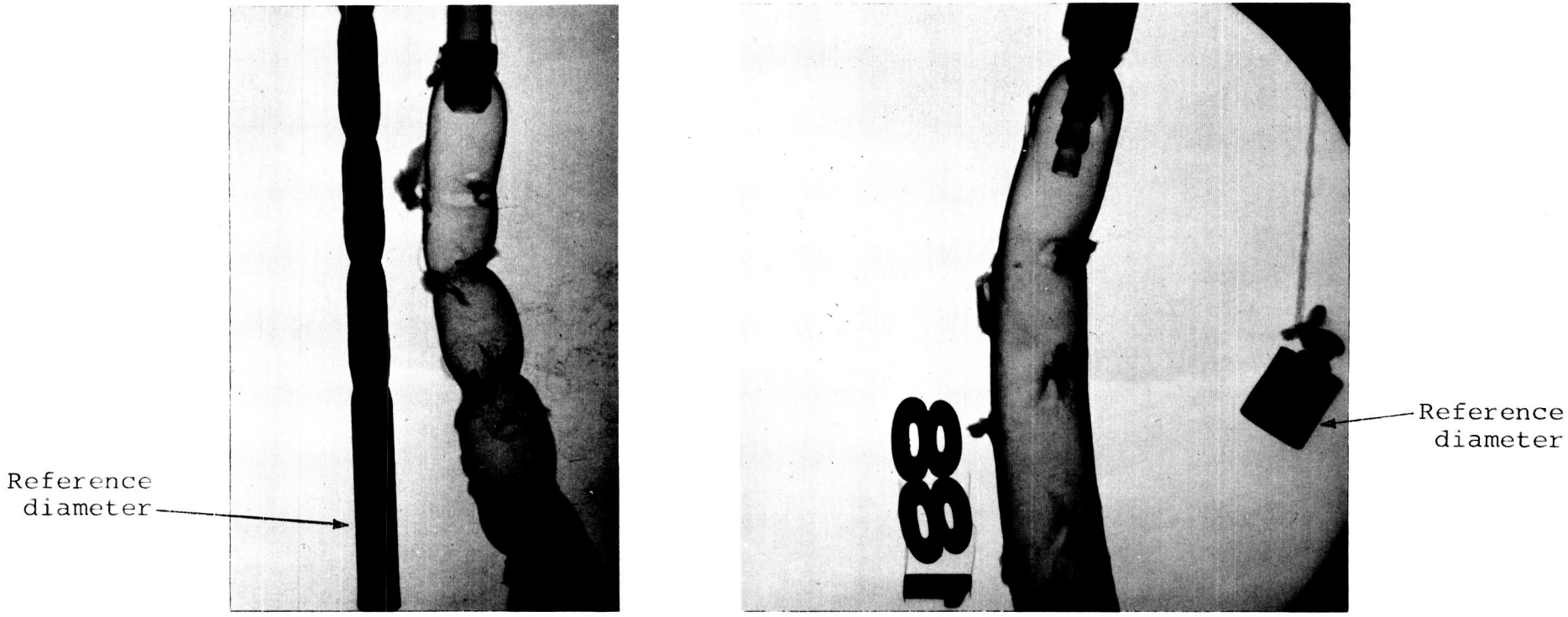

(a) Branches ligated at juncture Thoracic Aorta IA, p = 200 mm Hg.

(b) Branches ligated at extremities Thoracic Aorta IIA, p = 200 mm Hg.

Figure 7.- Effects of ligation location on local stress concentrations for two different Thoracic Aortas.

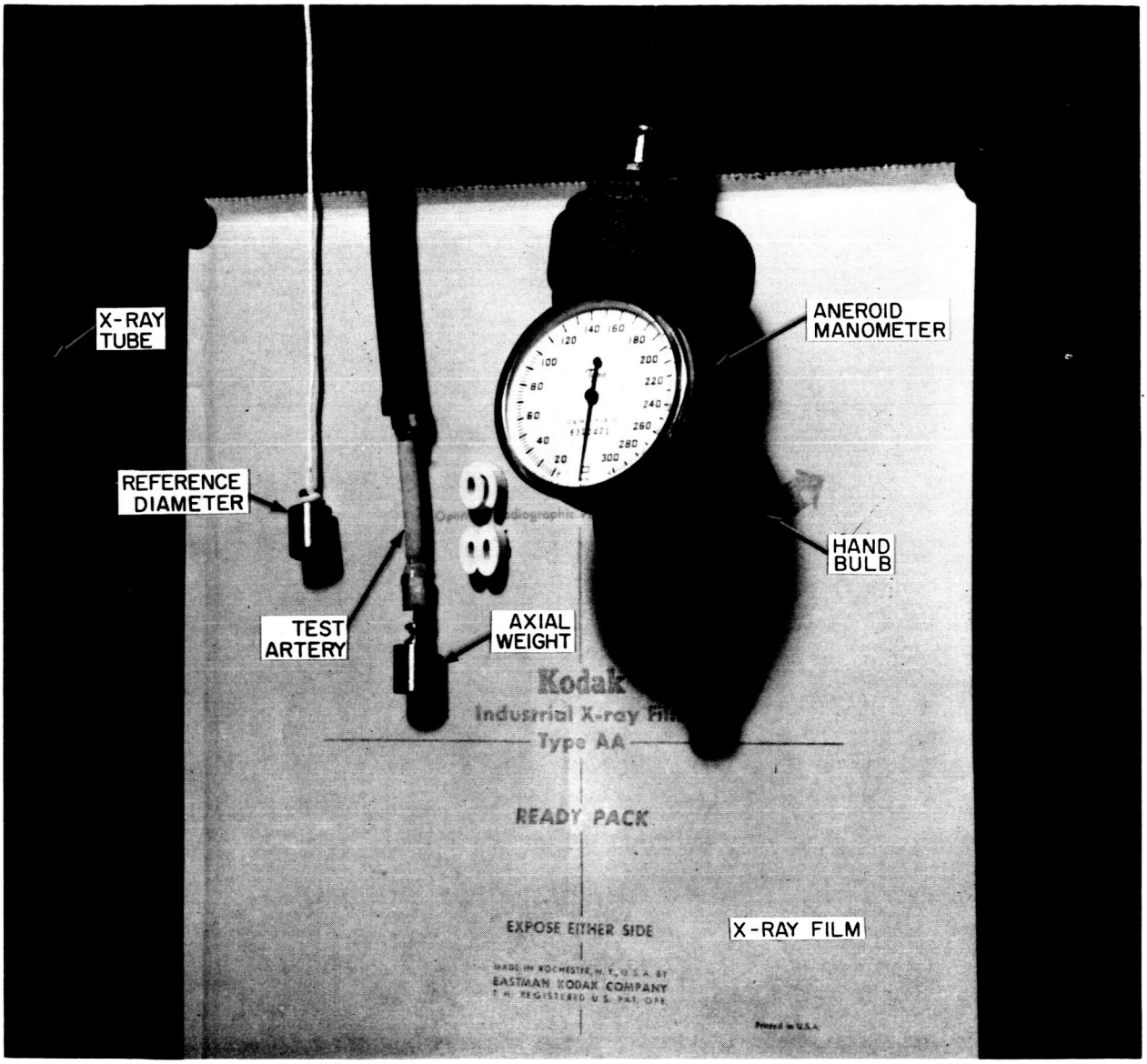

Figure 8.- Experimental setup for static elastic tests.

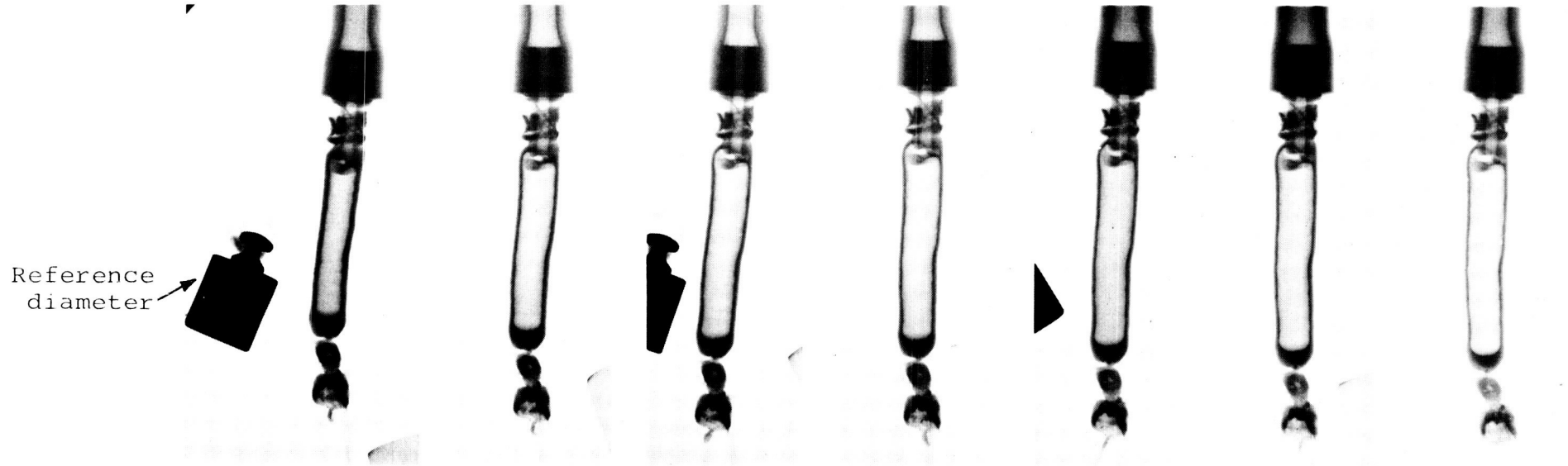

p_o = 0 mm Hg. 40 mm Hg. 100 mm Hg. 150 mm Hg. 200 mm Hg. 250 mm Hg. 300 mm Hg.

Figure 9.- X-ray photographs of Human Brachial II for various internal pressures with no axial weight.

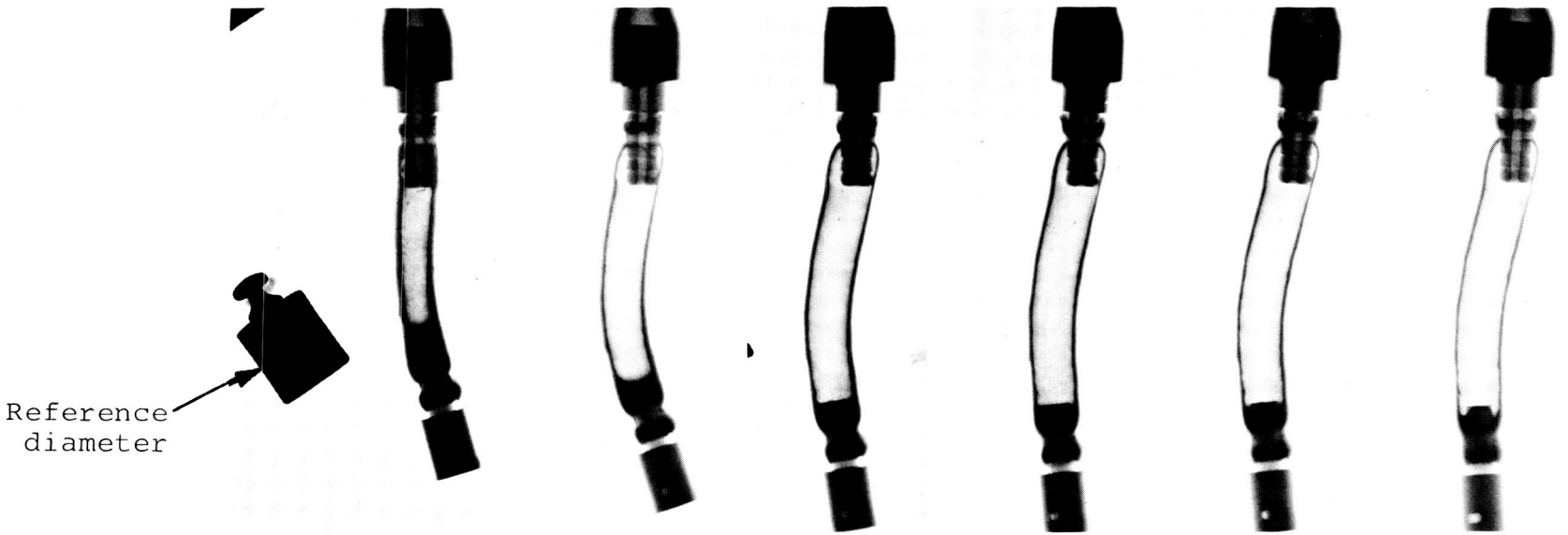

p_o = 0 mm Hg. 42 mm Hg. 100 mm Hg. 130 mm Hg. 160 mm Hg. 278 mm Hg.

Figure 10.- X-ray photographs of Human Iliac I for various internal pressures with no axial weight.

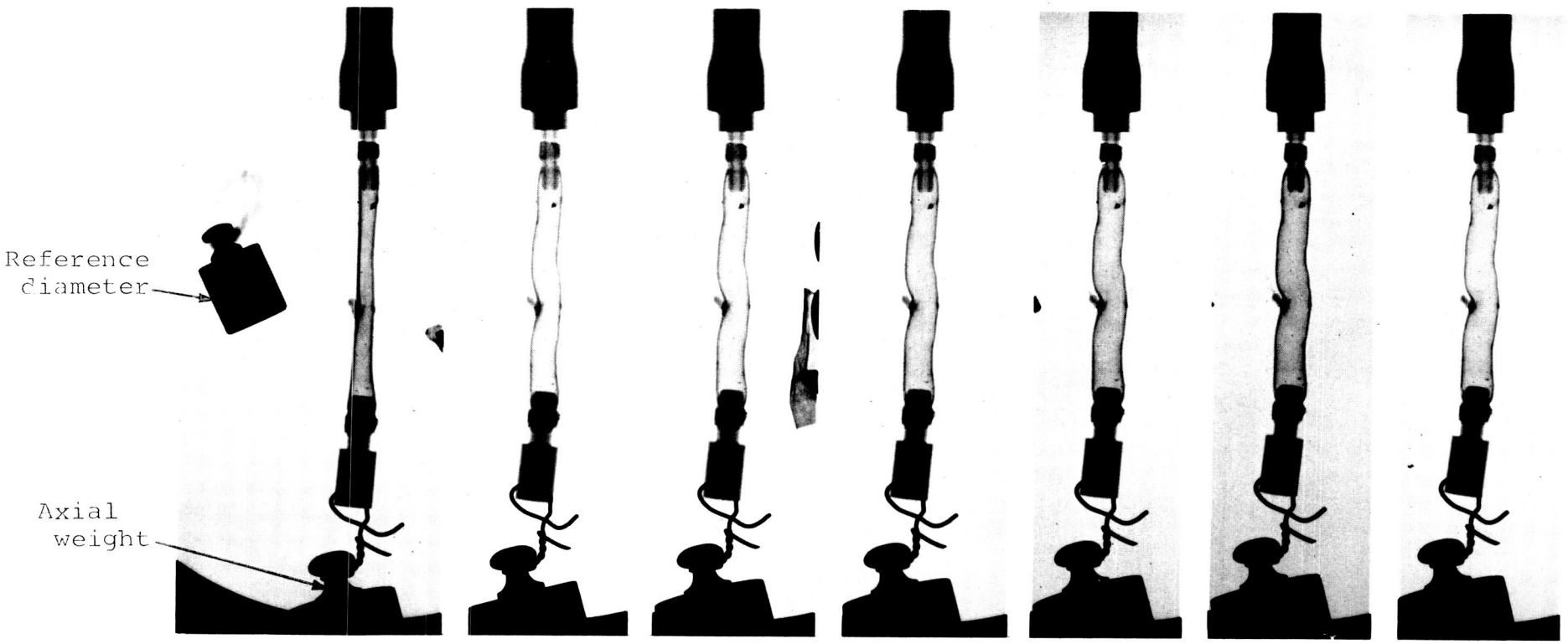

Figure 11.- X-ray photographs of Human Brachial IIIA for various internal pressures with a 50 gram axial weight.

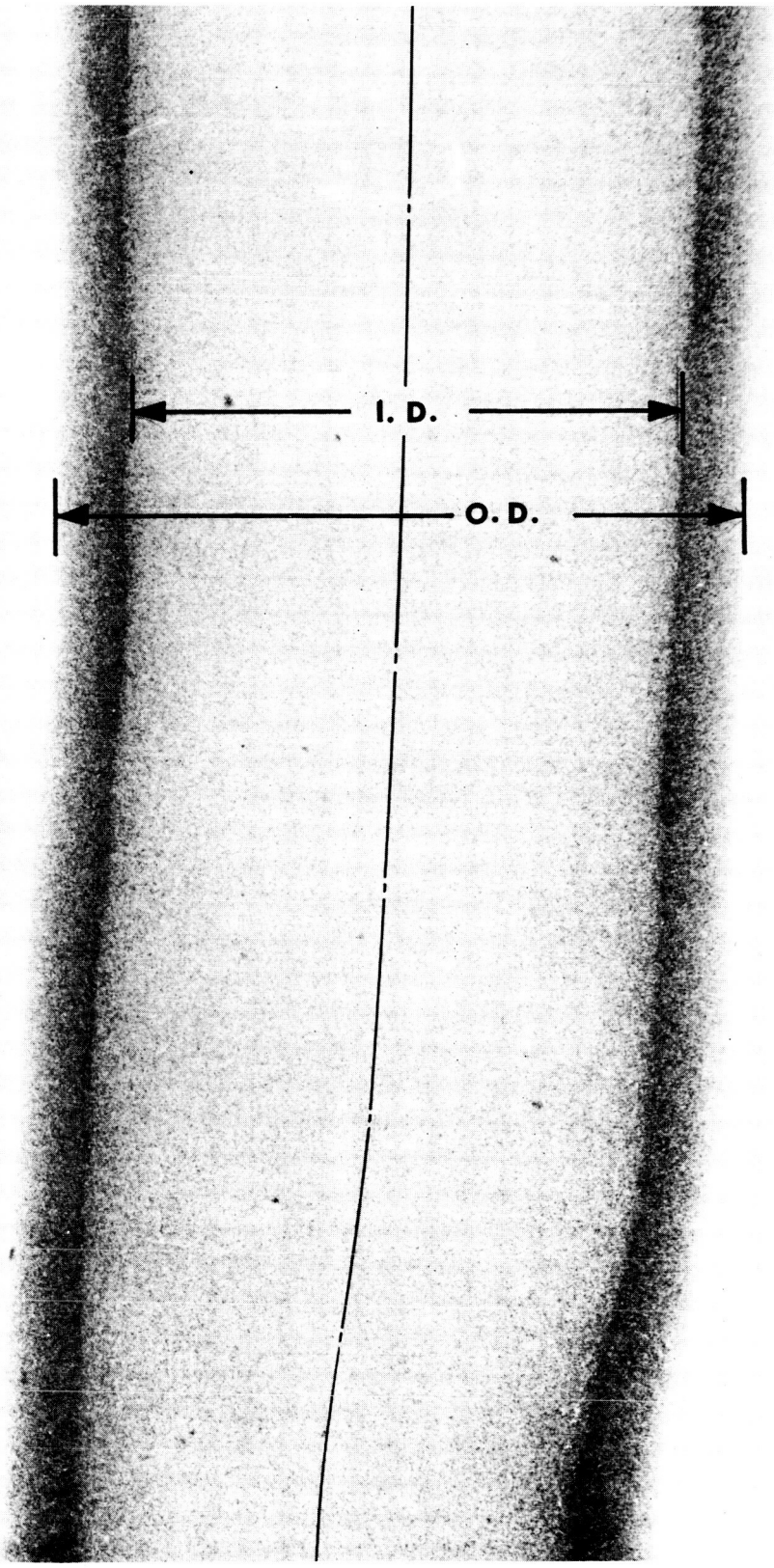

Figure 12.- Enlargement of X-ray negative for direct measurement.

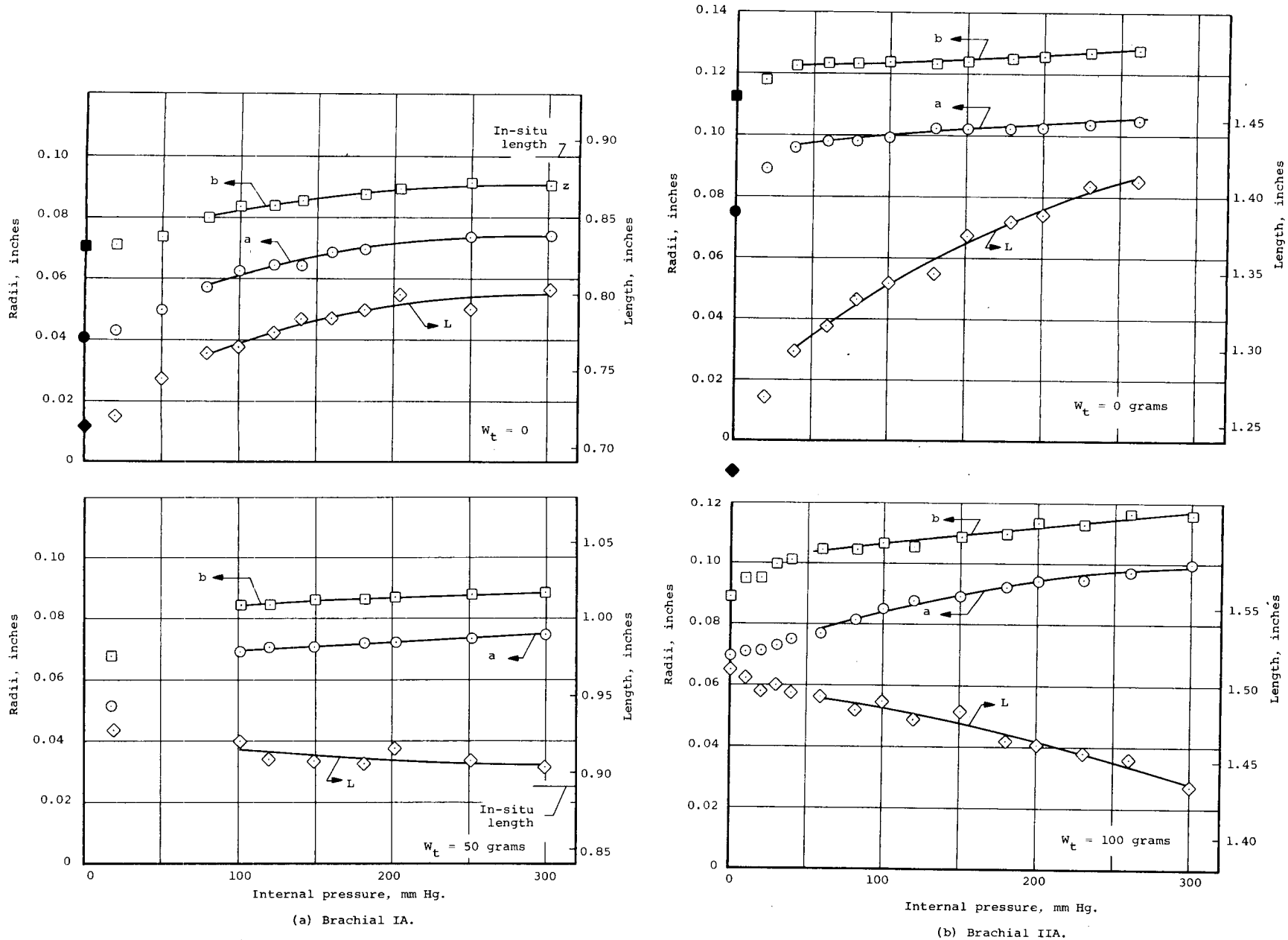

Figure 13.- Variation of dimensions with internal pressure for four Human Brachial arteries with and without axial loading.

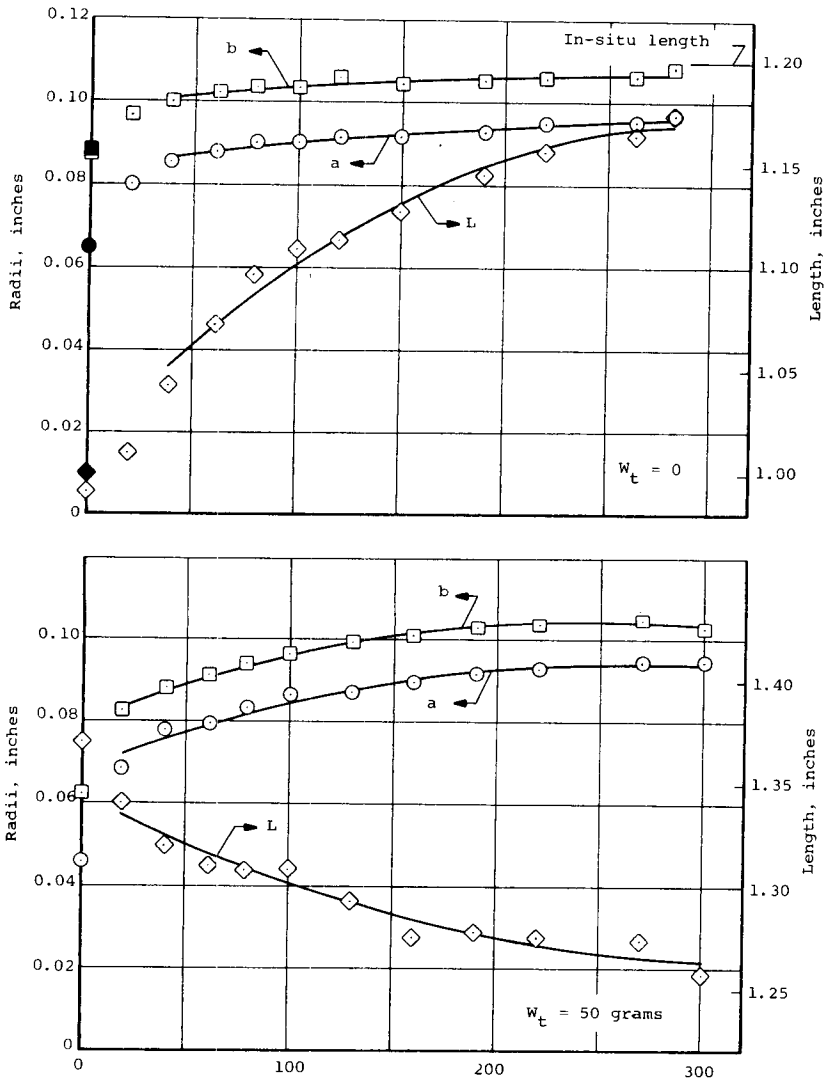

(c) Brachial IIIA.

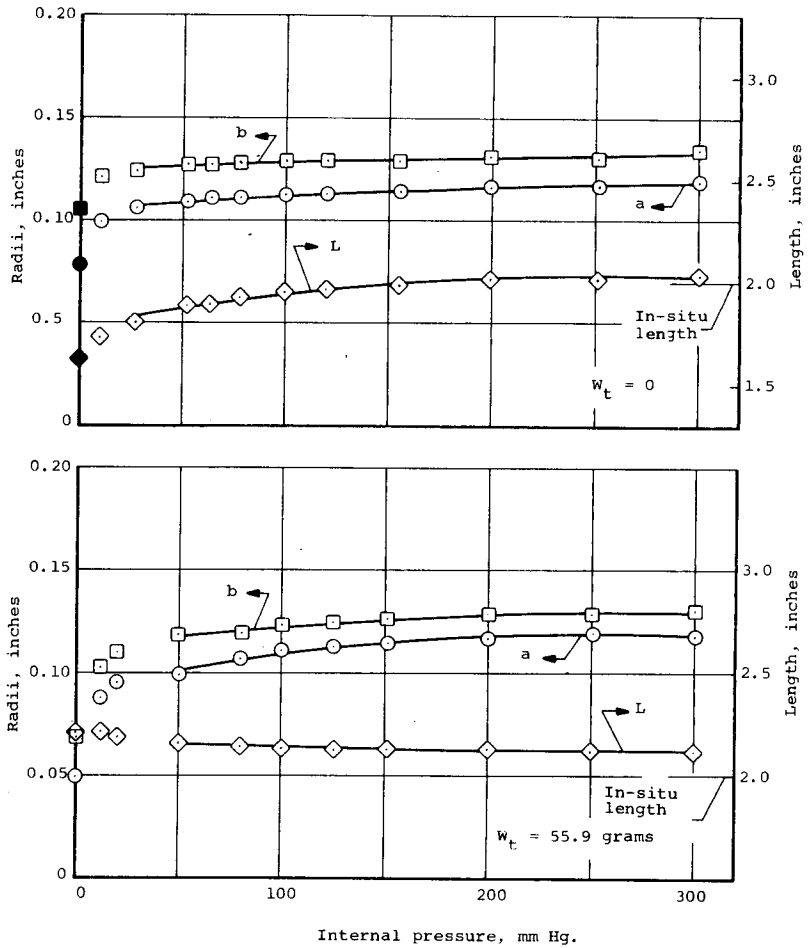

(d) Brachial IVA.

Figure 13.- Concluded.

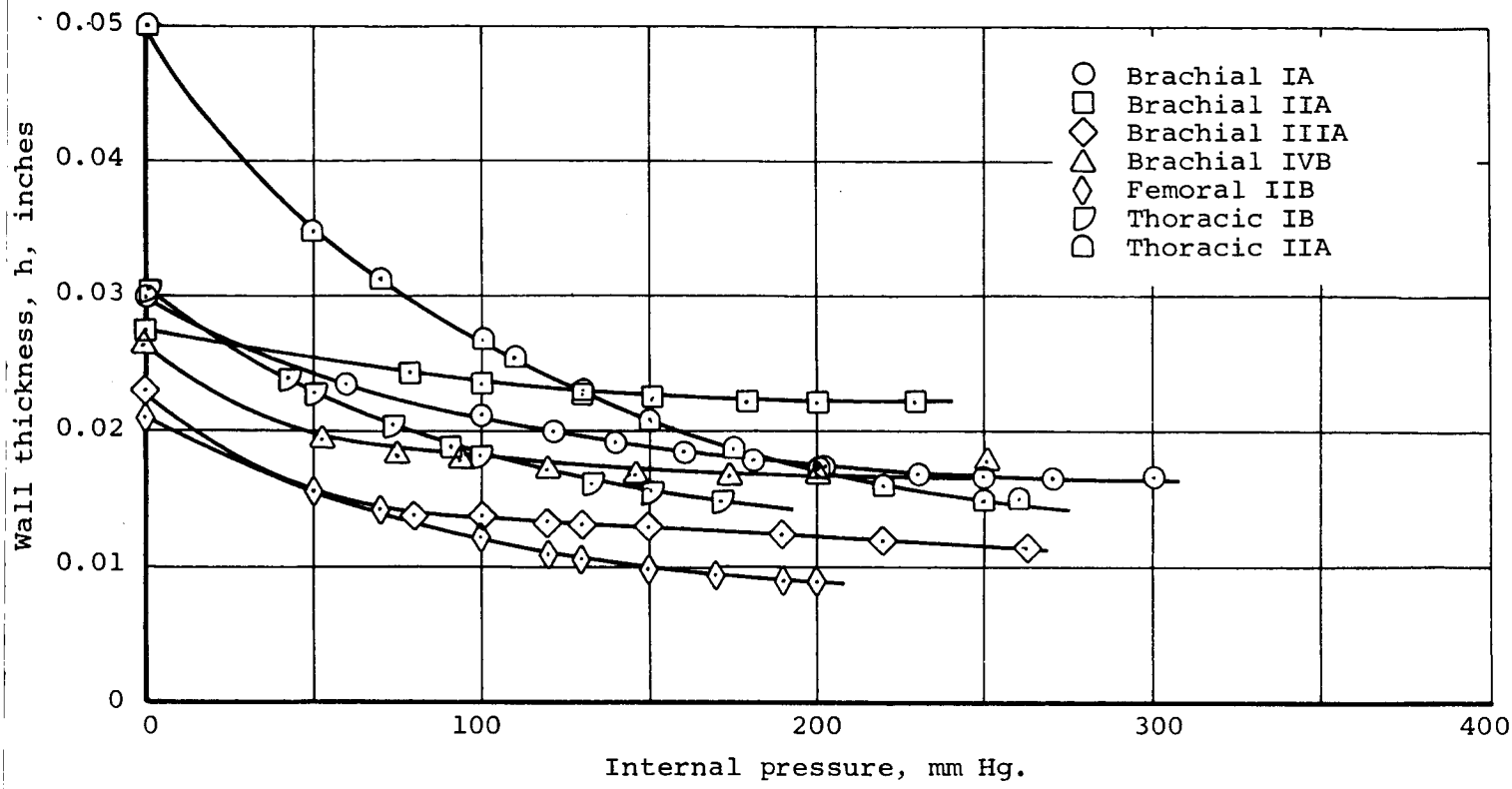

(a) No axial loading.

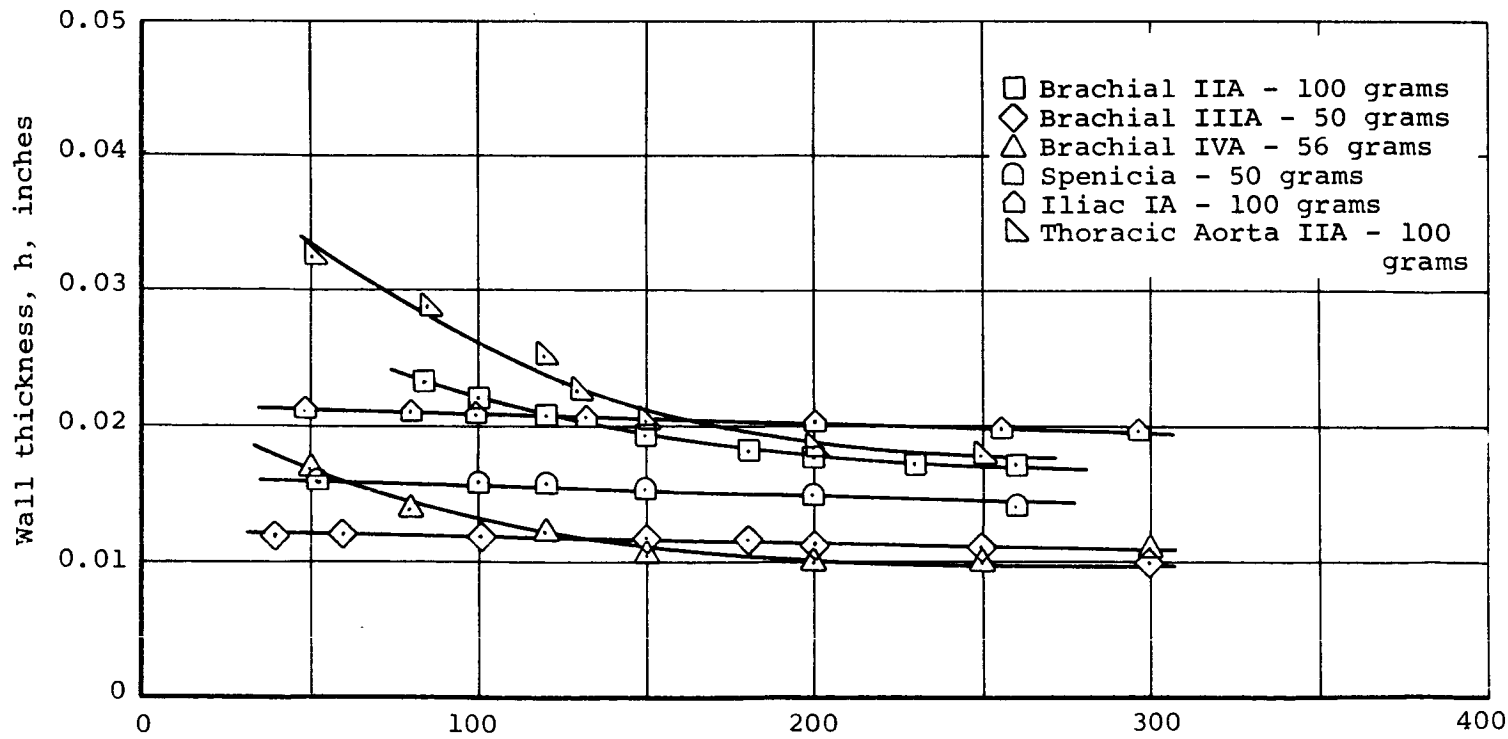

(b) Heavy axial loading.

Figure 15.- Variation of wall thickness with internal pressure for several arteries.

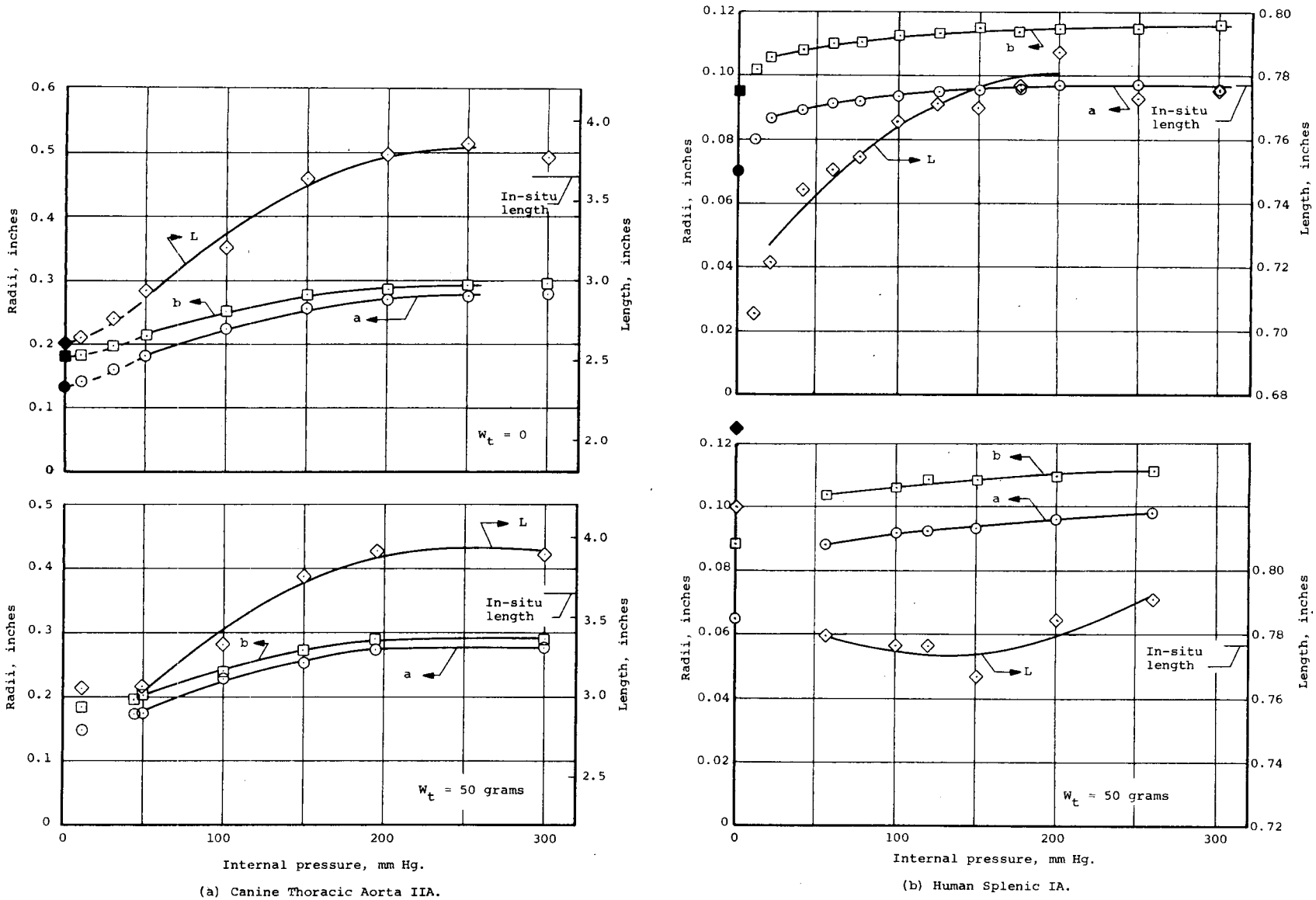

Figure 14.- Variation of dimensions with internal pressure for two different arteries with and without axial loading.

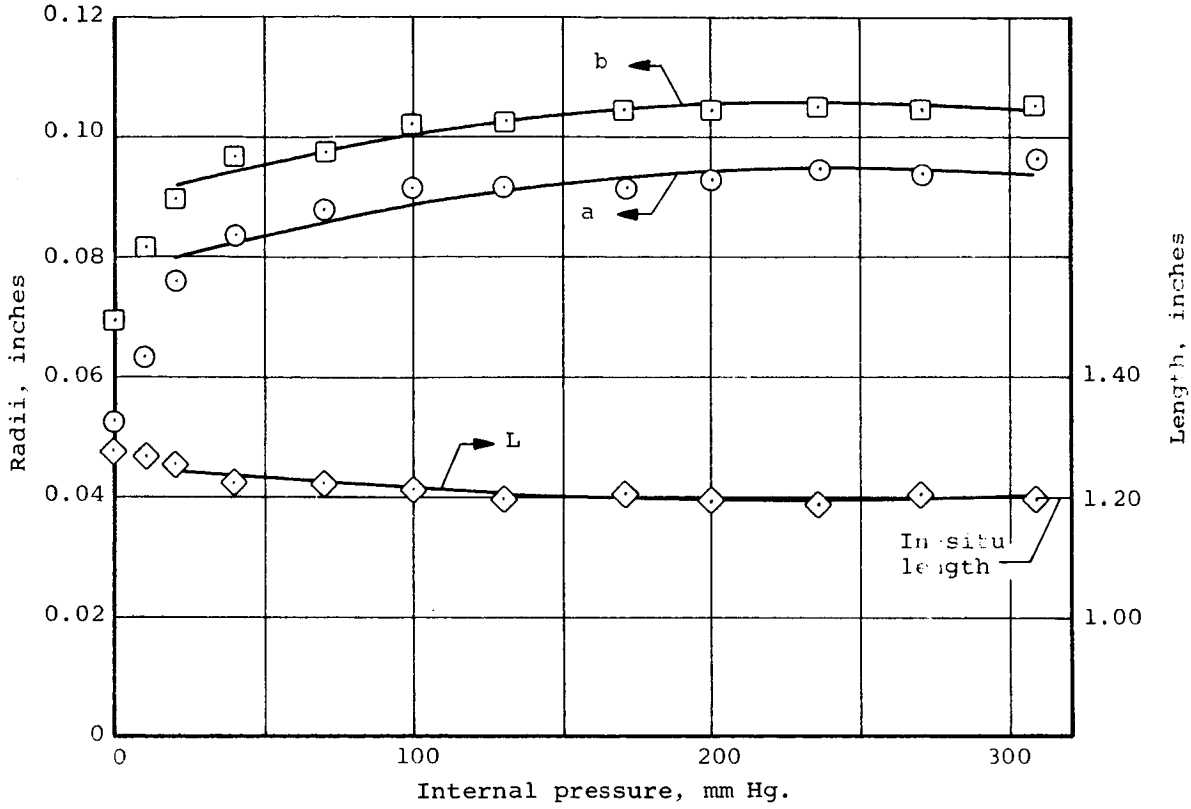

(a) Brachial IIIA, W_t = 20 grams.

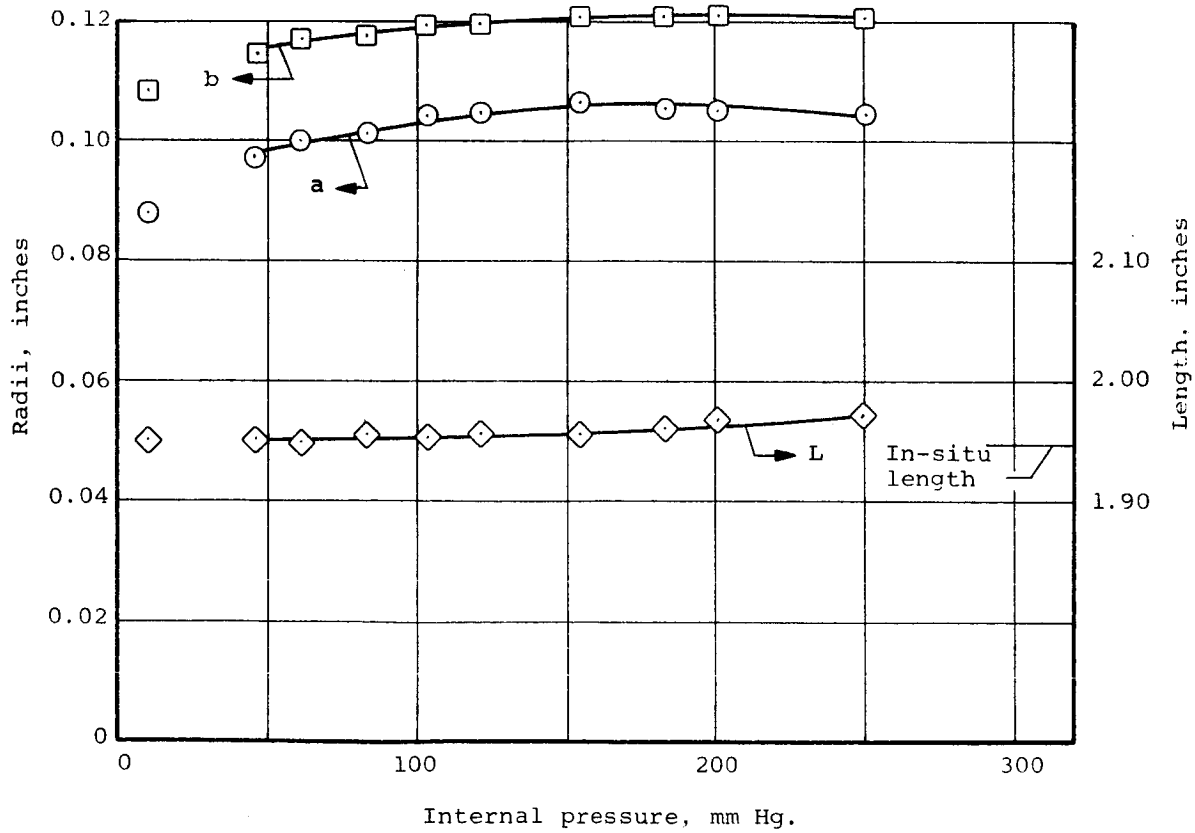

(b) Brachial IVB, W_t = 20 grams.

Figure 16.- Variation of dimensions with internal pressure with axial weight nearly equal to in-situ tethering force.

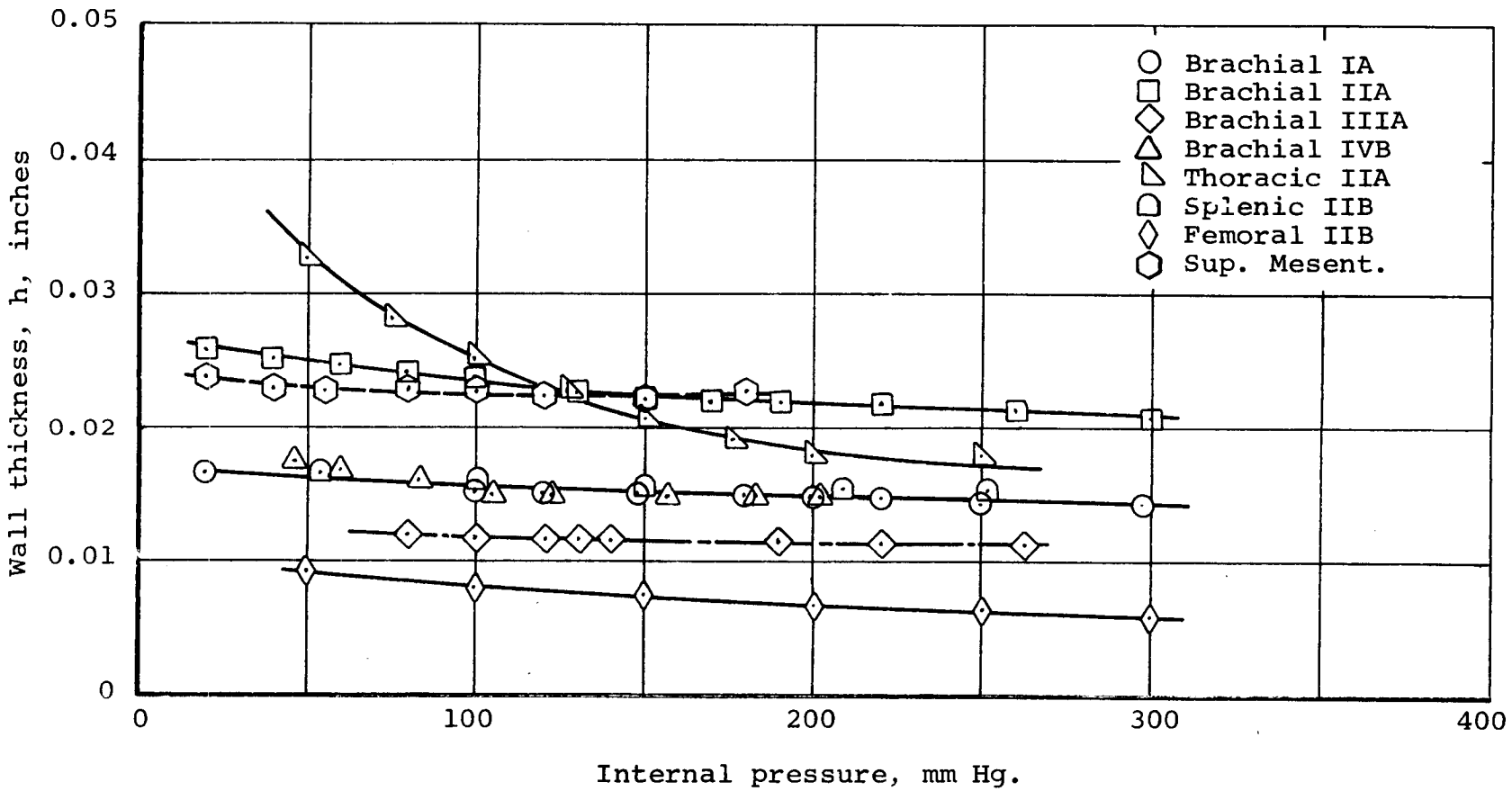

Figure 17.- Variation of wall thickness with internal pressure for several arteries stretched to their in-situ length.

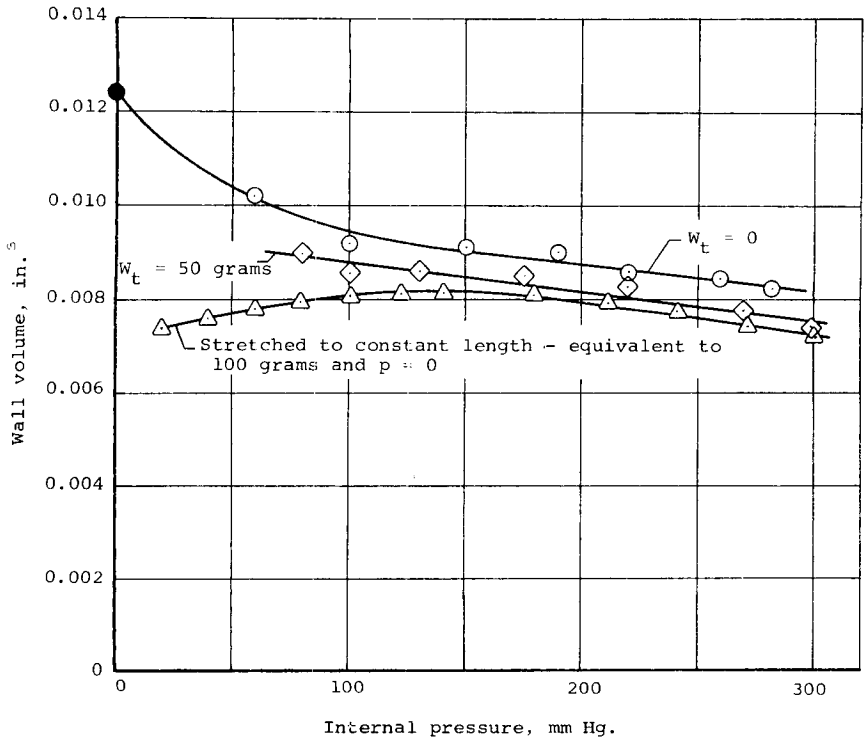

(a) Brachial IIIA.

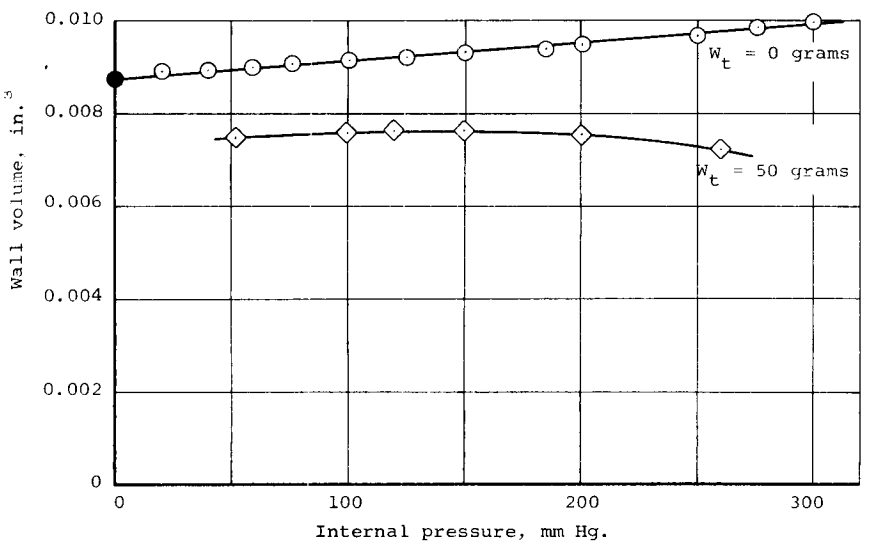

(b) Splenic IA.

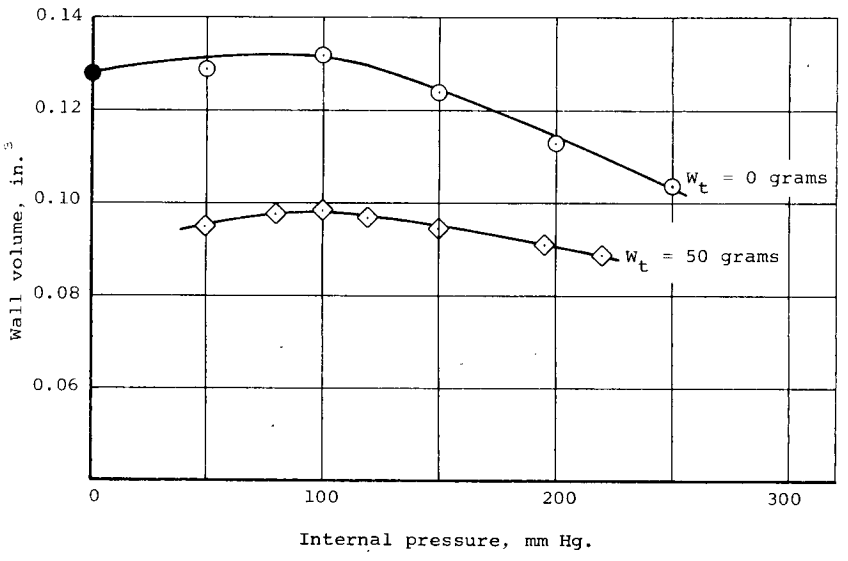

(c) Thoracic Aorta IIA.

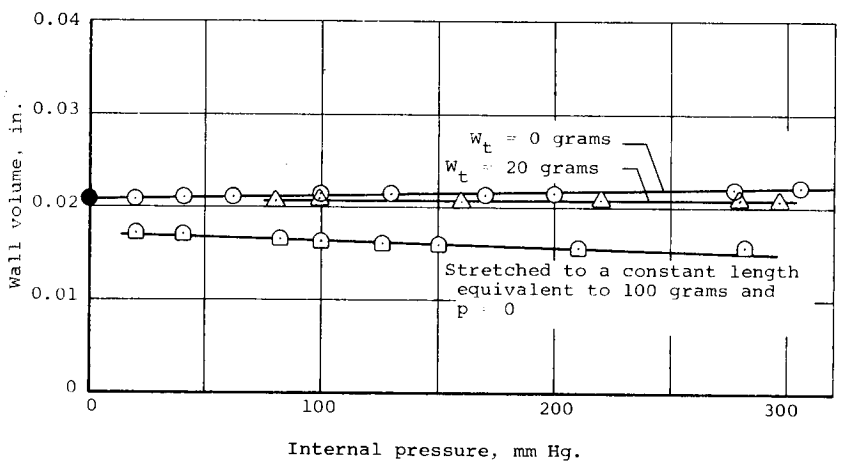

(d) External Iliac IA.

Figure 18.- Variation of wall volume with internal pressure for various axial weights.

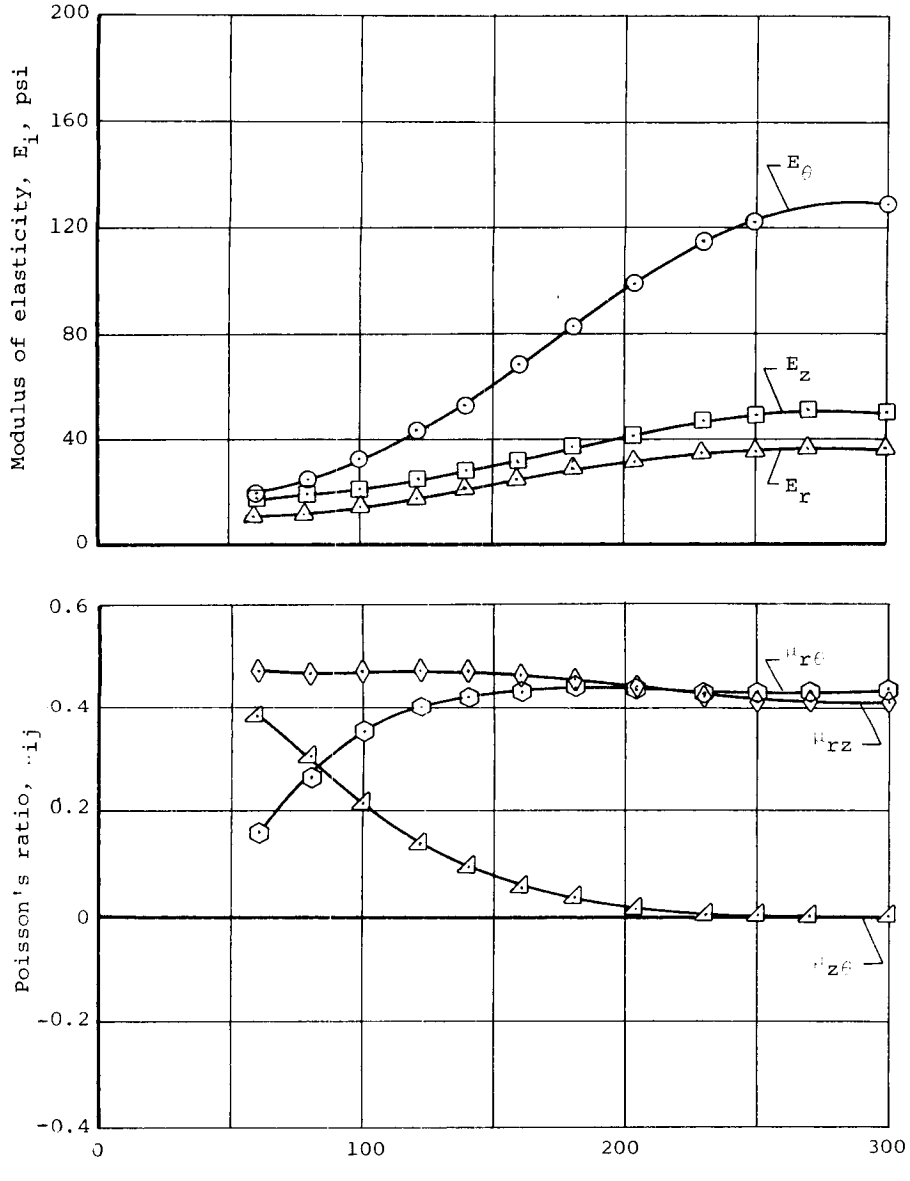

(a) Zero axial weight.

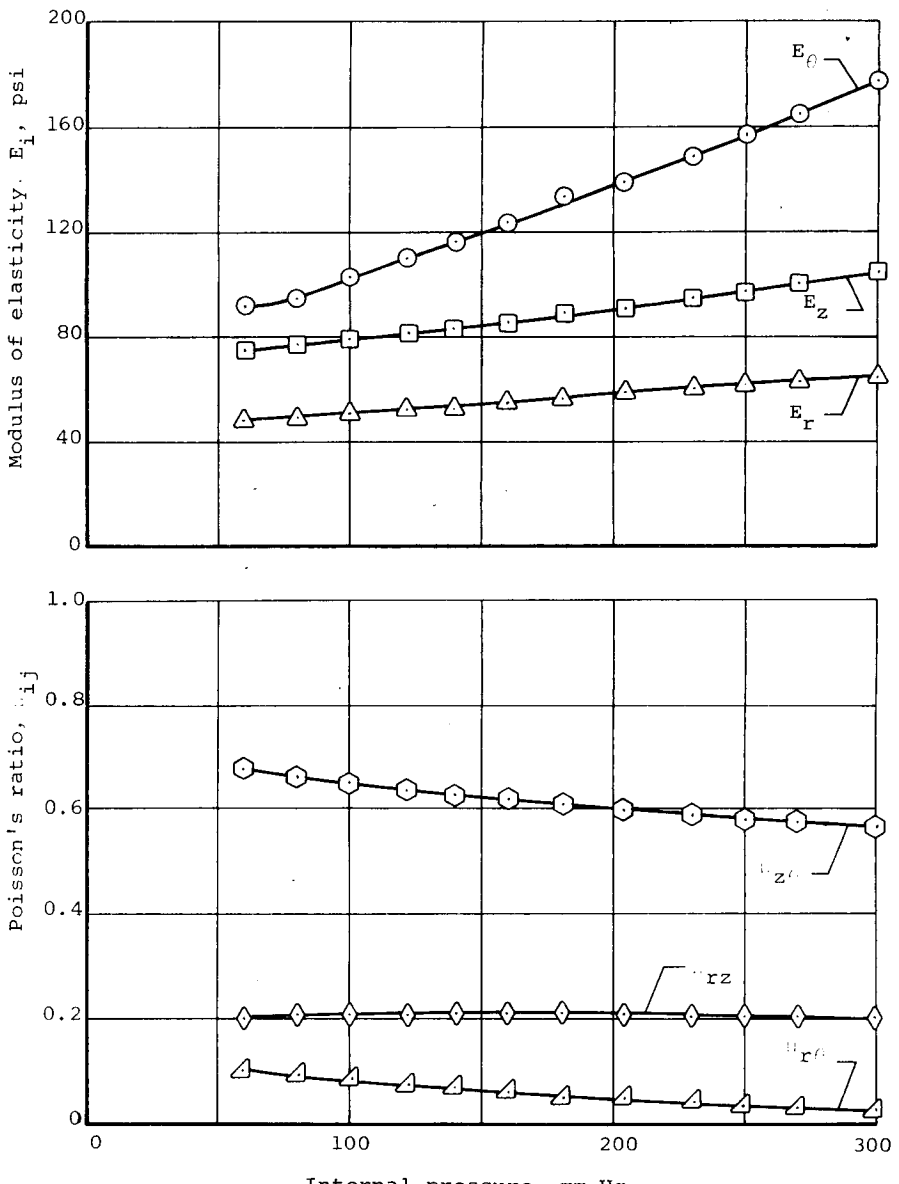

(b) 50 gram axial weight.

Figure 19.- Variation of Young's Moduli and Poisson's ratios with internal pressure for Brachial IA.

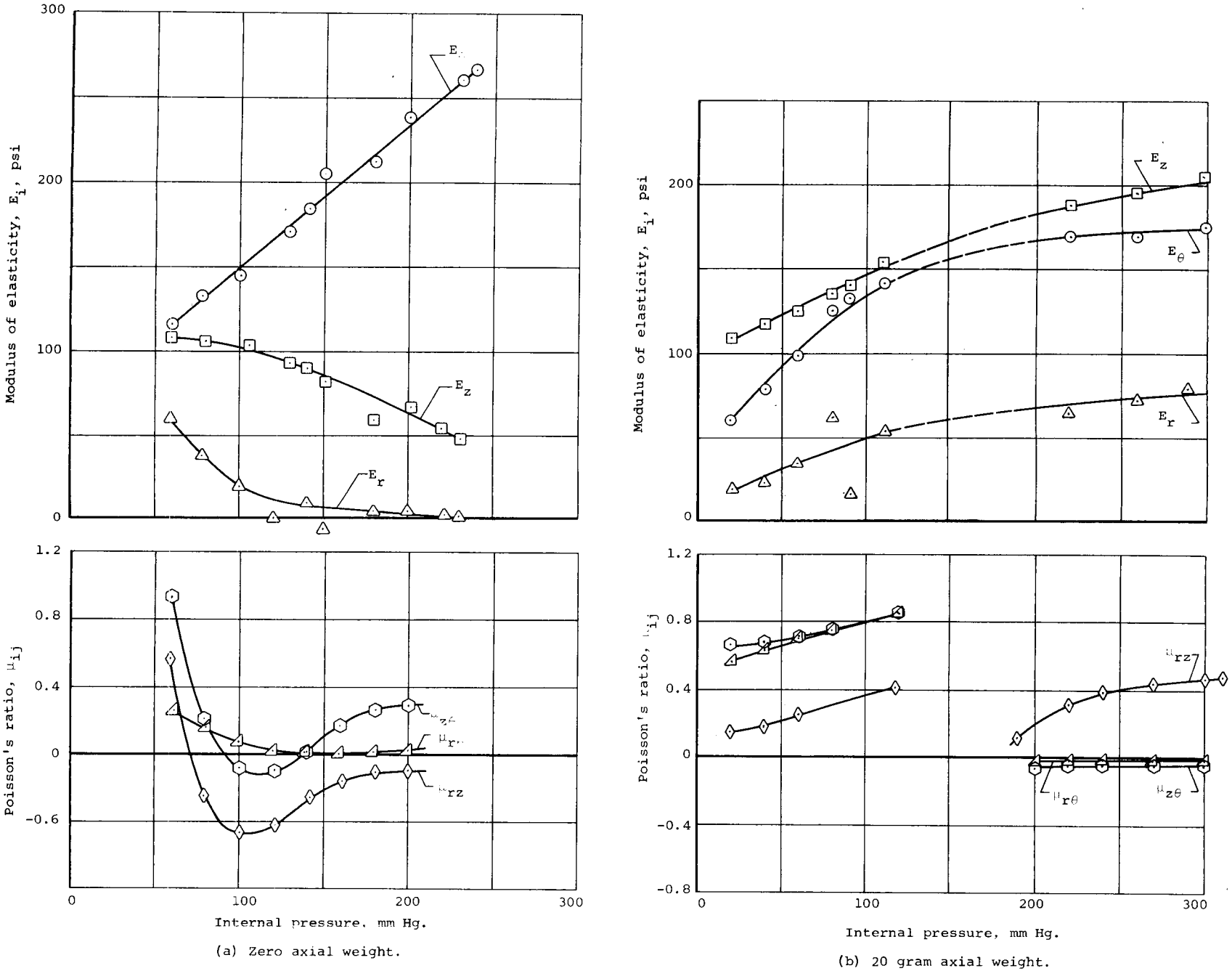

Figure 20.- Variation of Young's Moduli and Poisson's ratio with internal pressure for Brachial IIA.

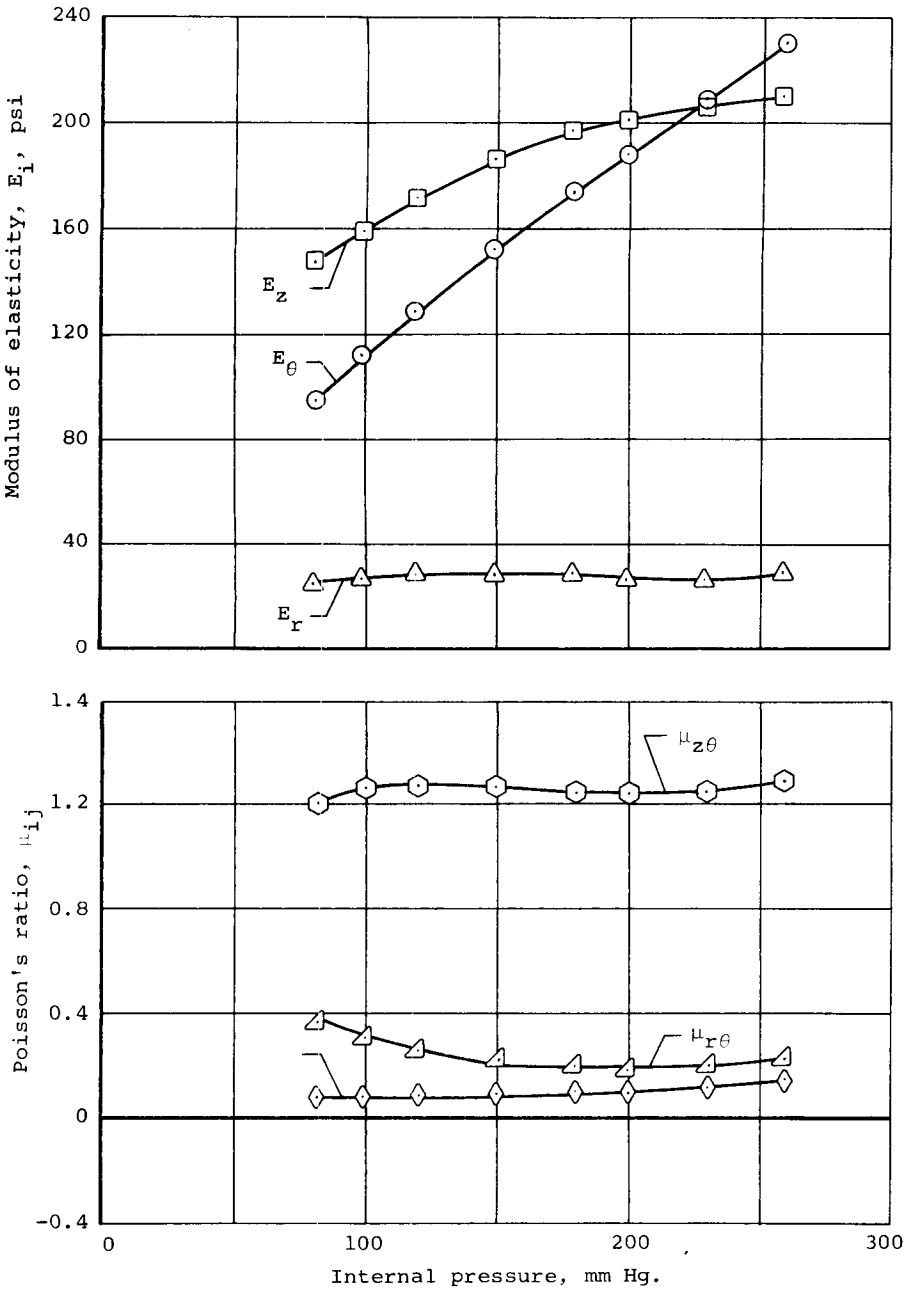

(c) 100 gram axial weight.

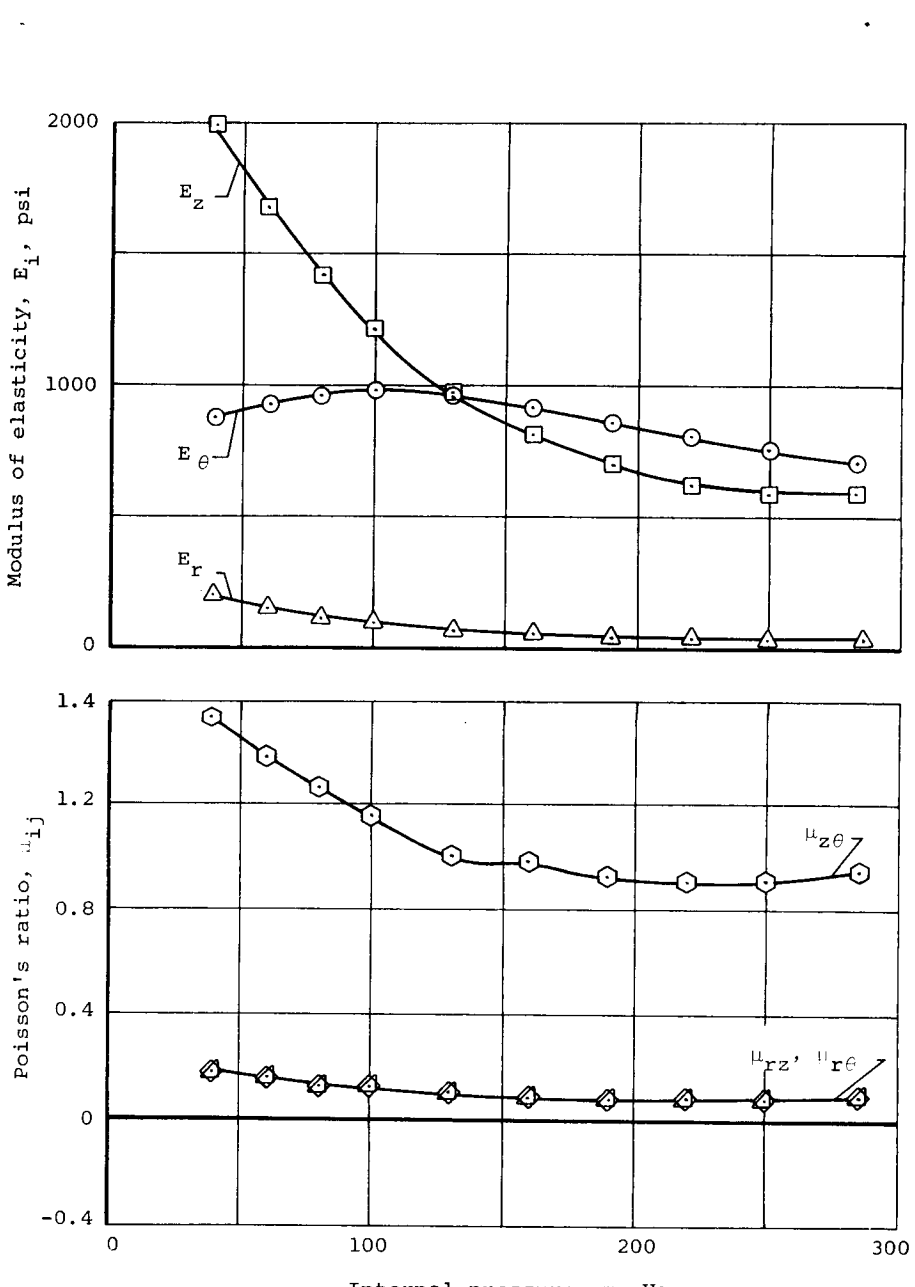

(d) Stretched to constant length.

Figure 20.- Concluded.

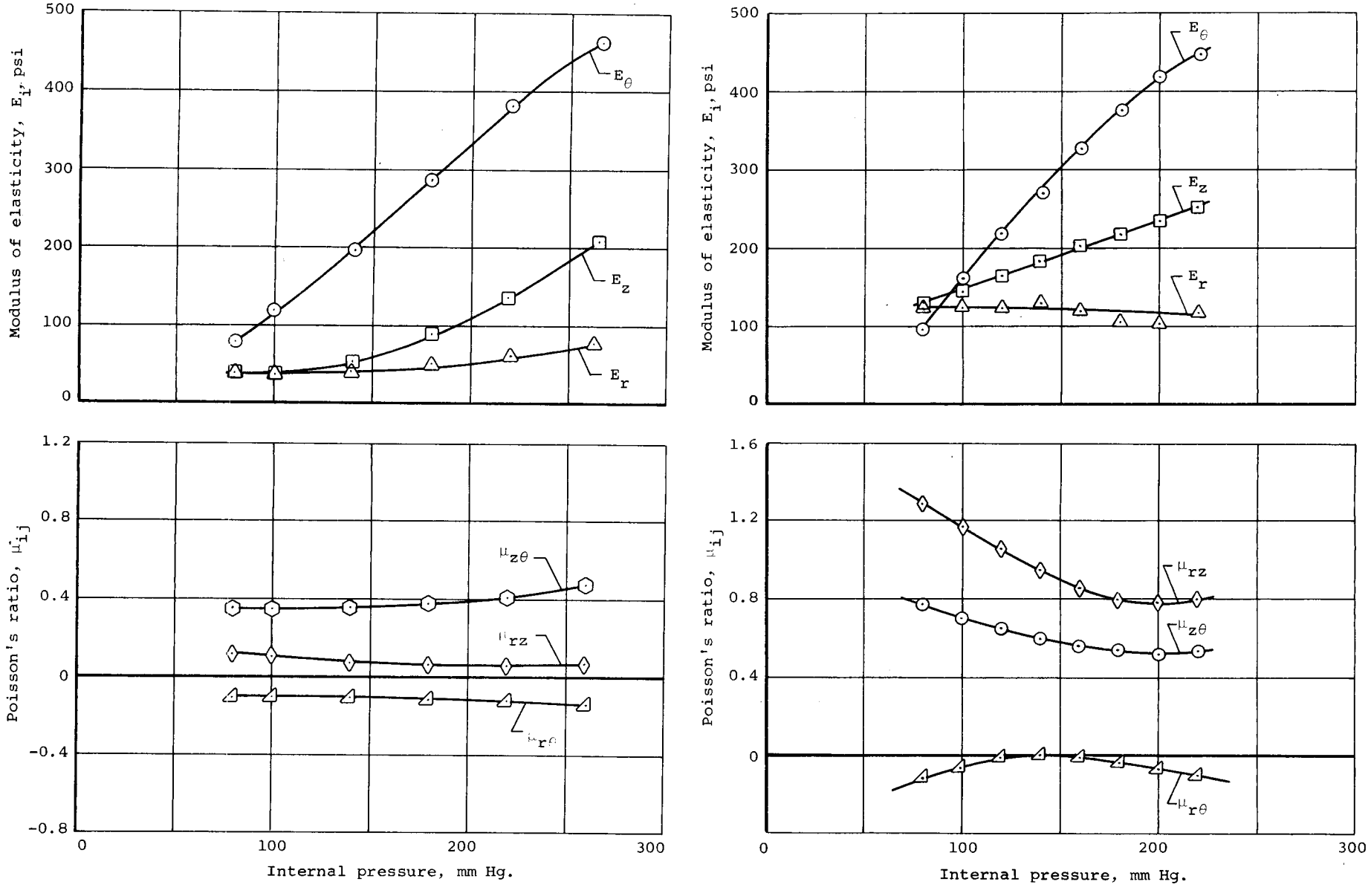

Figure 21.- Variation of Young's Moduli and Poisson's ratios with internal pressure for Brachial IIIA.

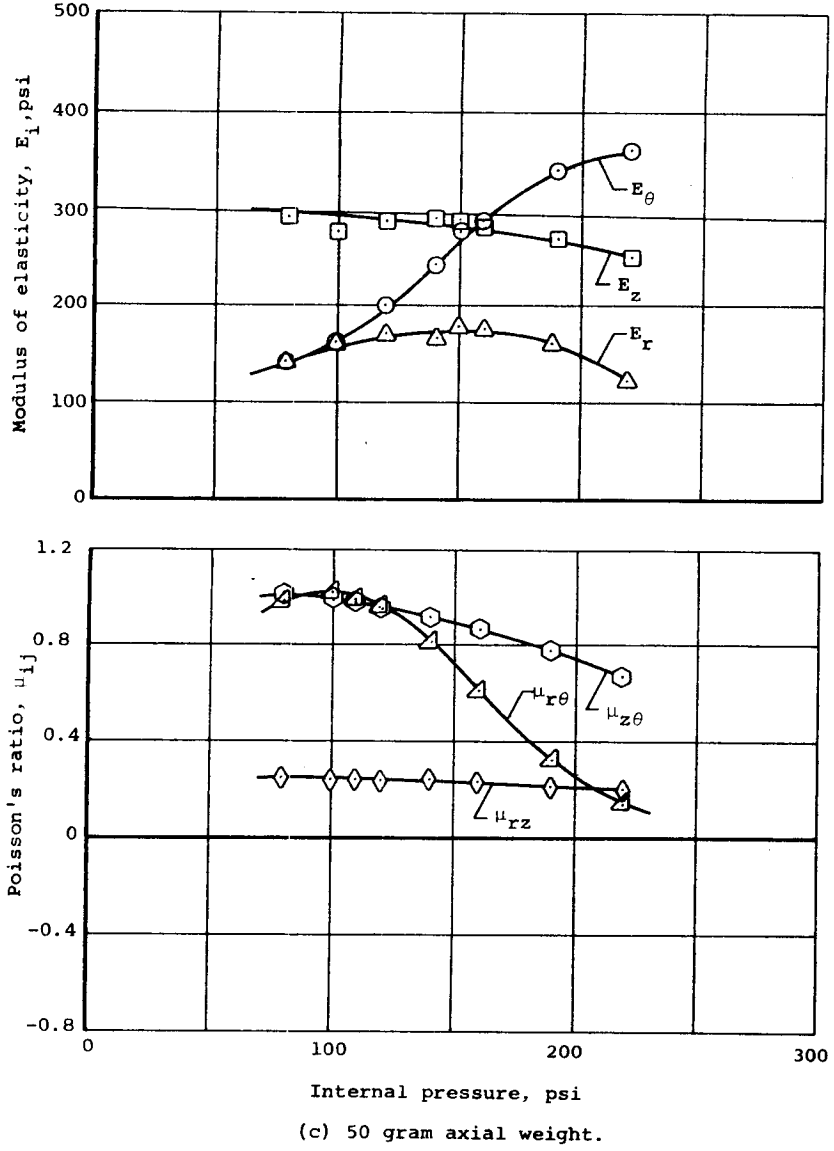

(c) 50 gram axial weight.

Figure 21.- Concluded.

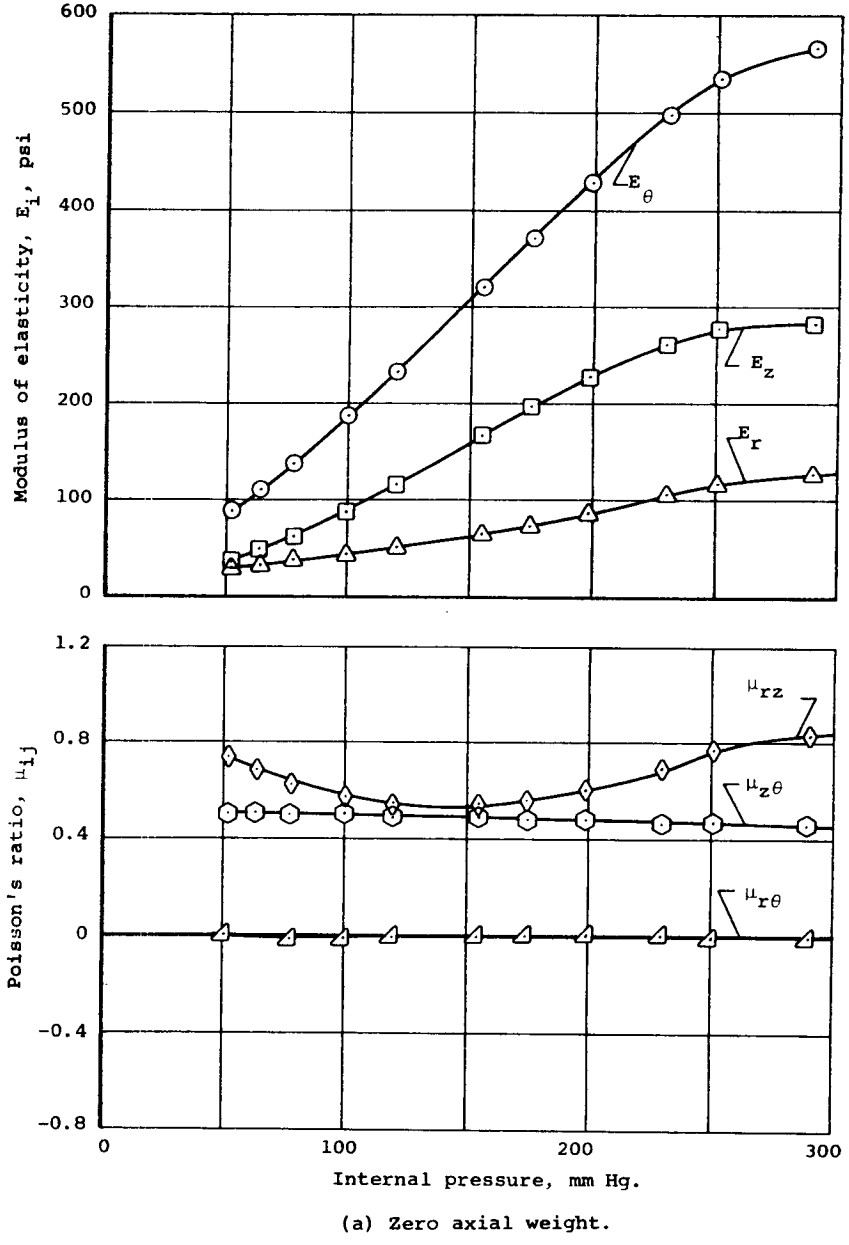

(a) Zero axial weight.

Figure 22.- Variation of Young's Moduli and Poisson's ratios with internal pressure for Brachial IVA.

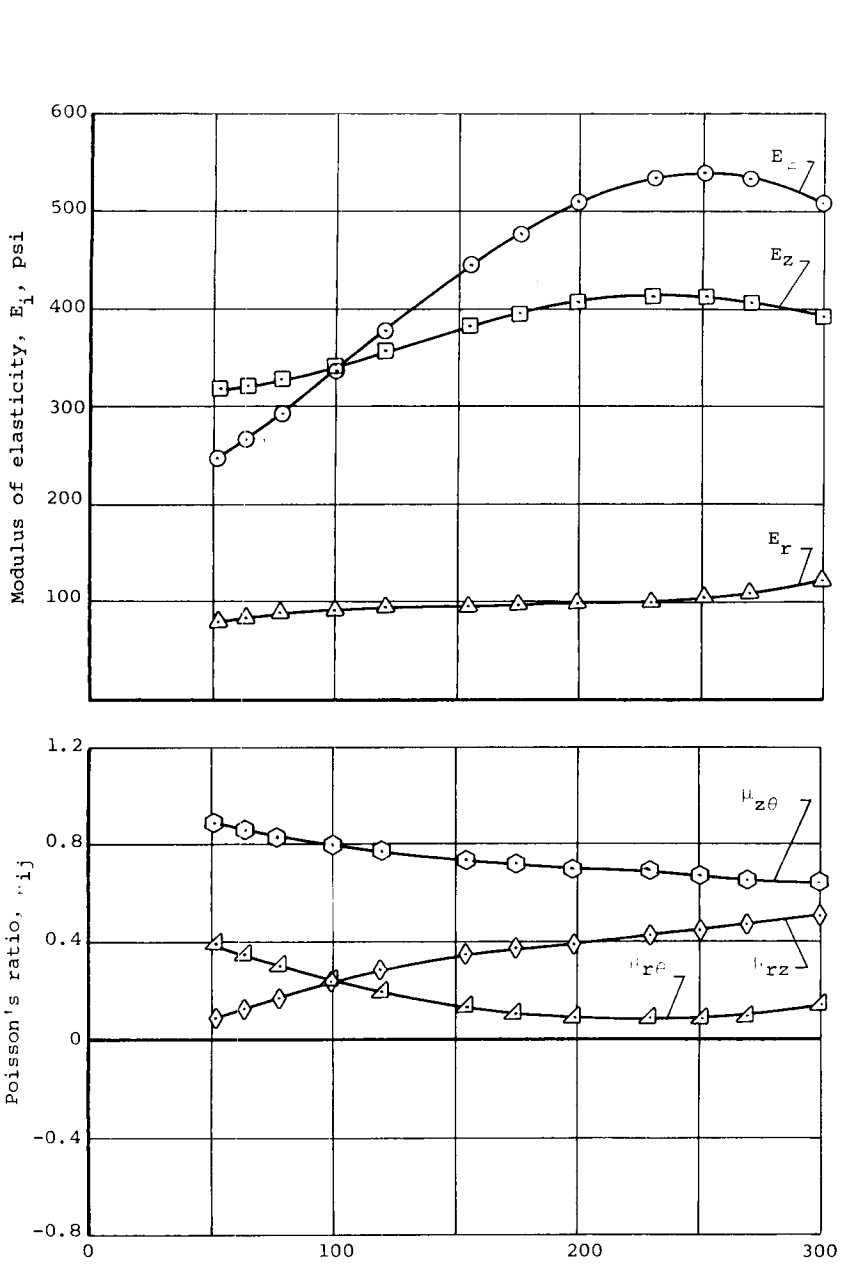

(b) 32.4 gram axial weight.

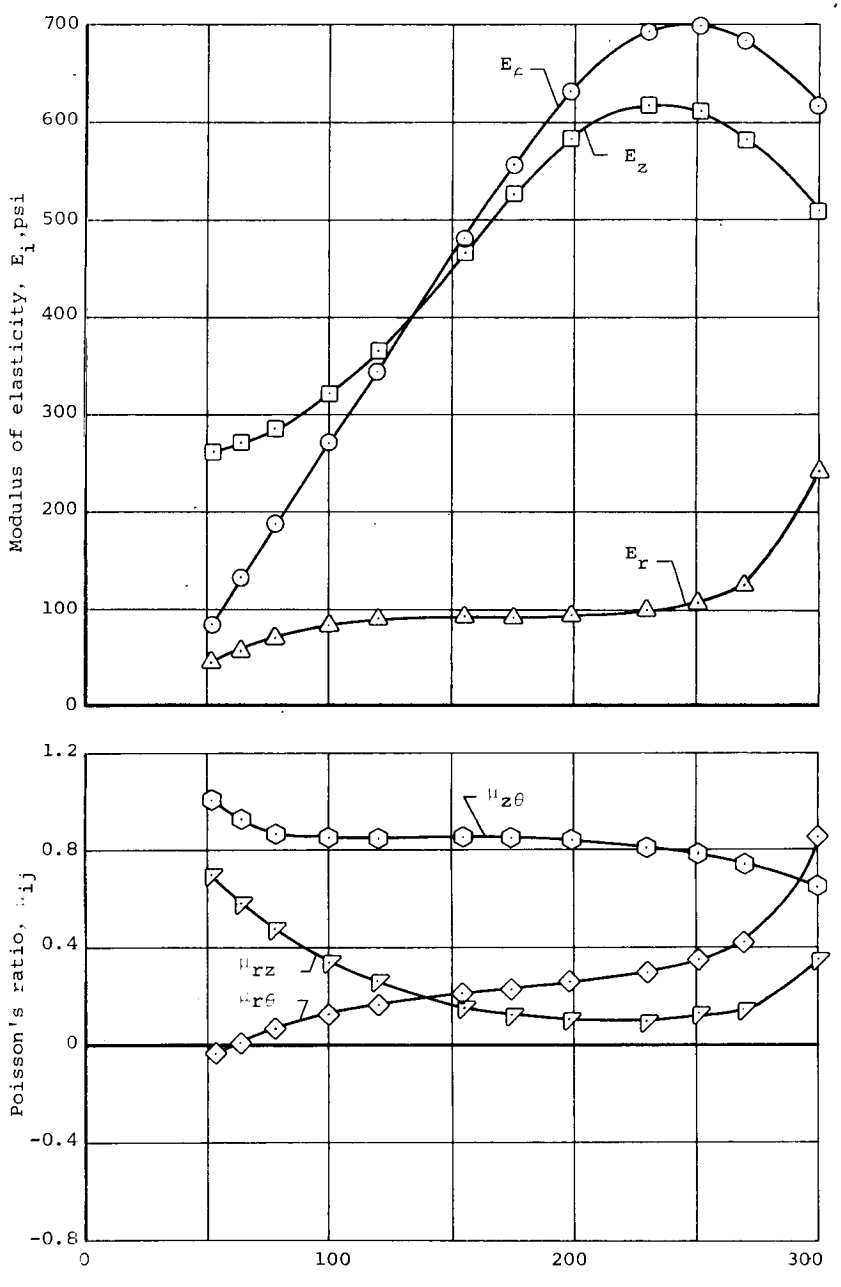

(c) 55.9 gram axial weight.

Figure 22.- Concluded.

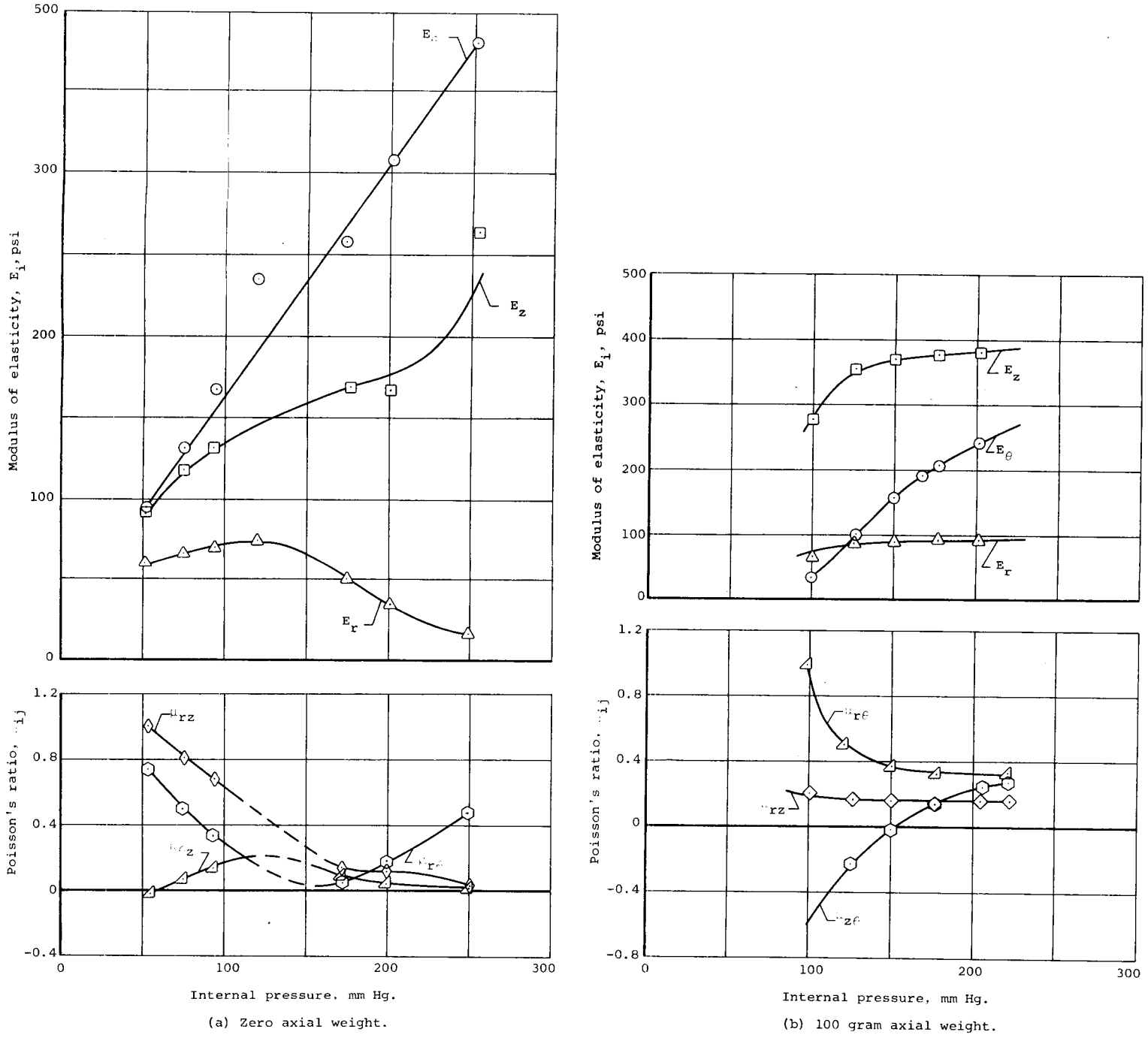

Figure 23.- Variation of Young's Moduli and Poisson's ratios with internal pressure for Brachial IVB.

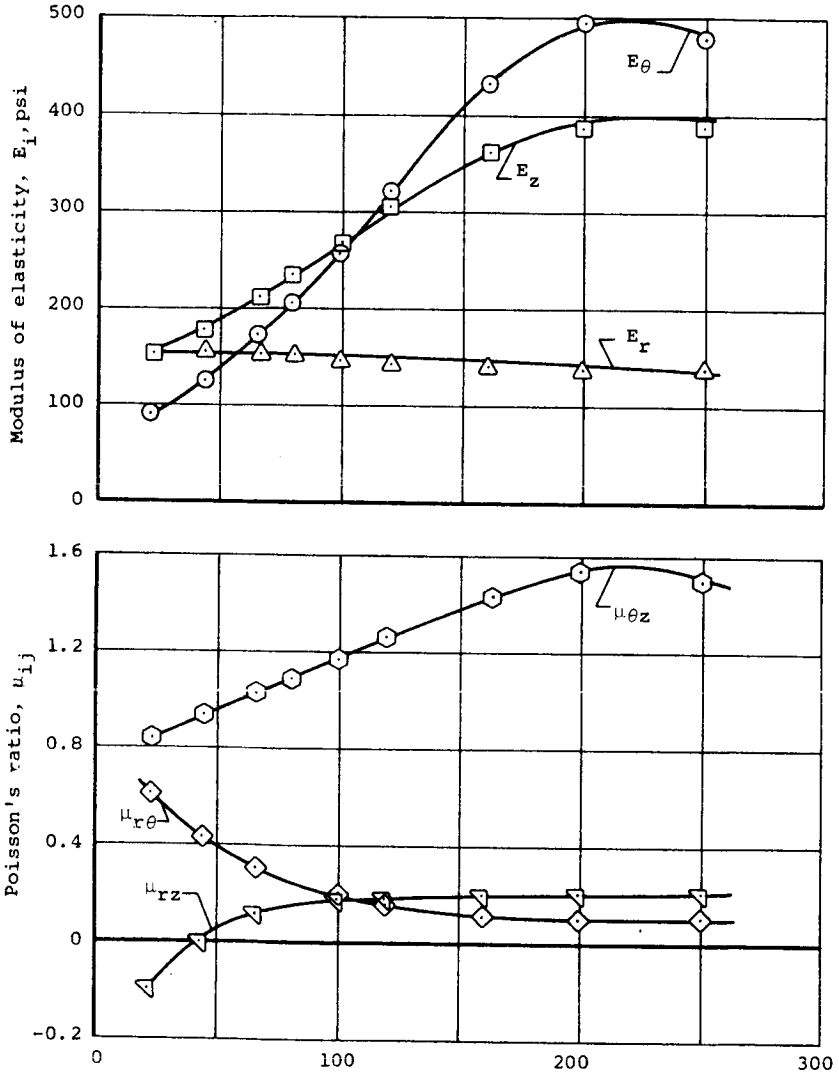

(c) Stretched to constant length.

Figure 23.- Concluded.

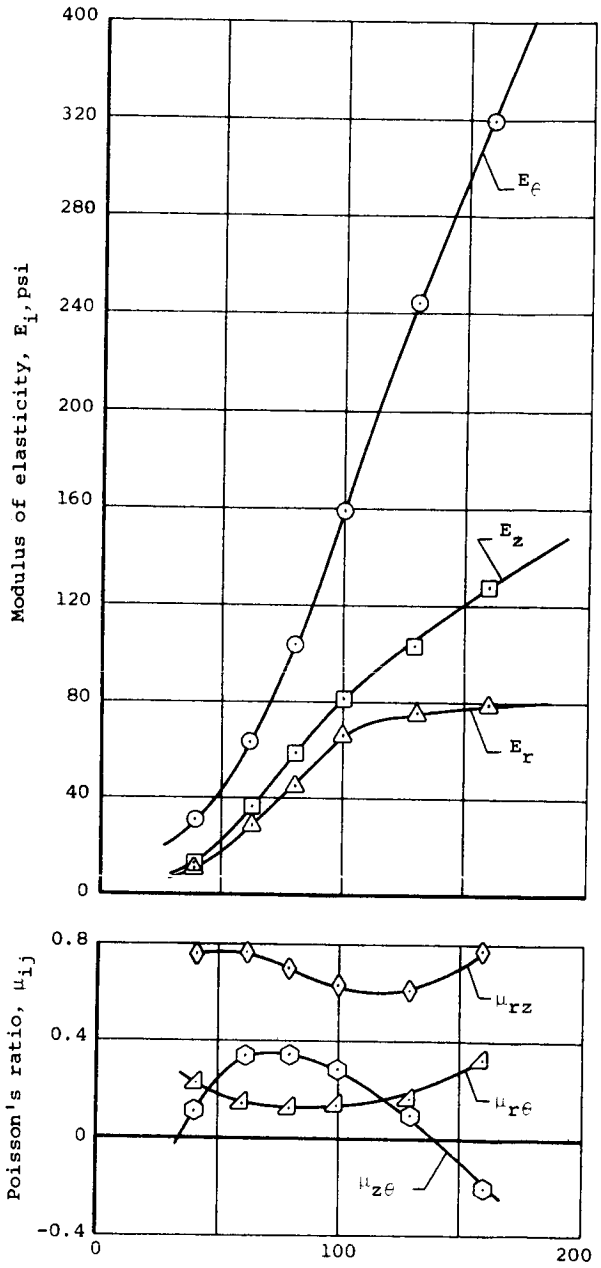

(a) Zero axial weight.

Figure 24.- Variation of Young's Moduli and Poisson's ratios with internal pressure for Iliac I.

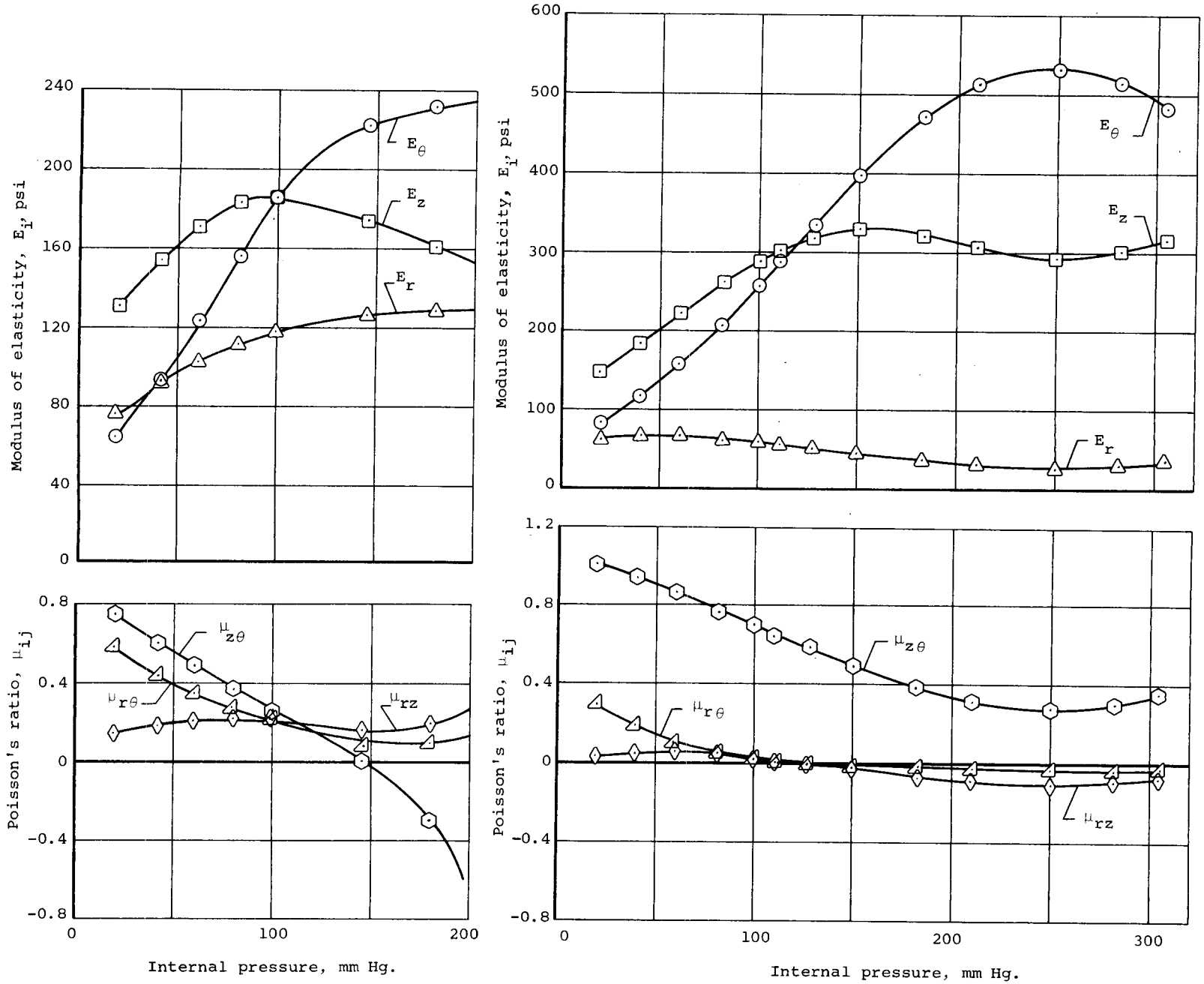

(b) 20 gram axial weight.

(c) Stretched to constant length.

Figure 24.- Concluded.

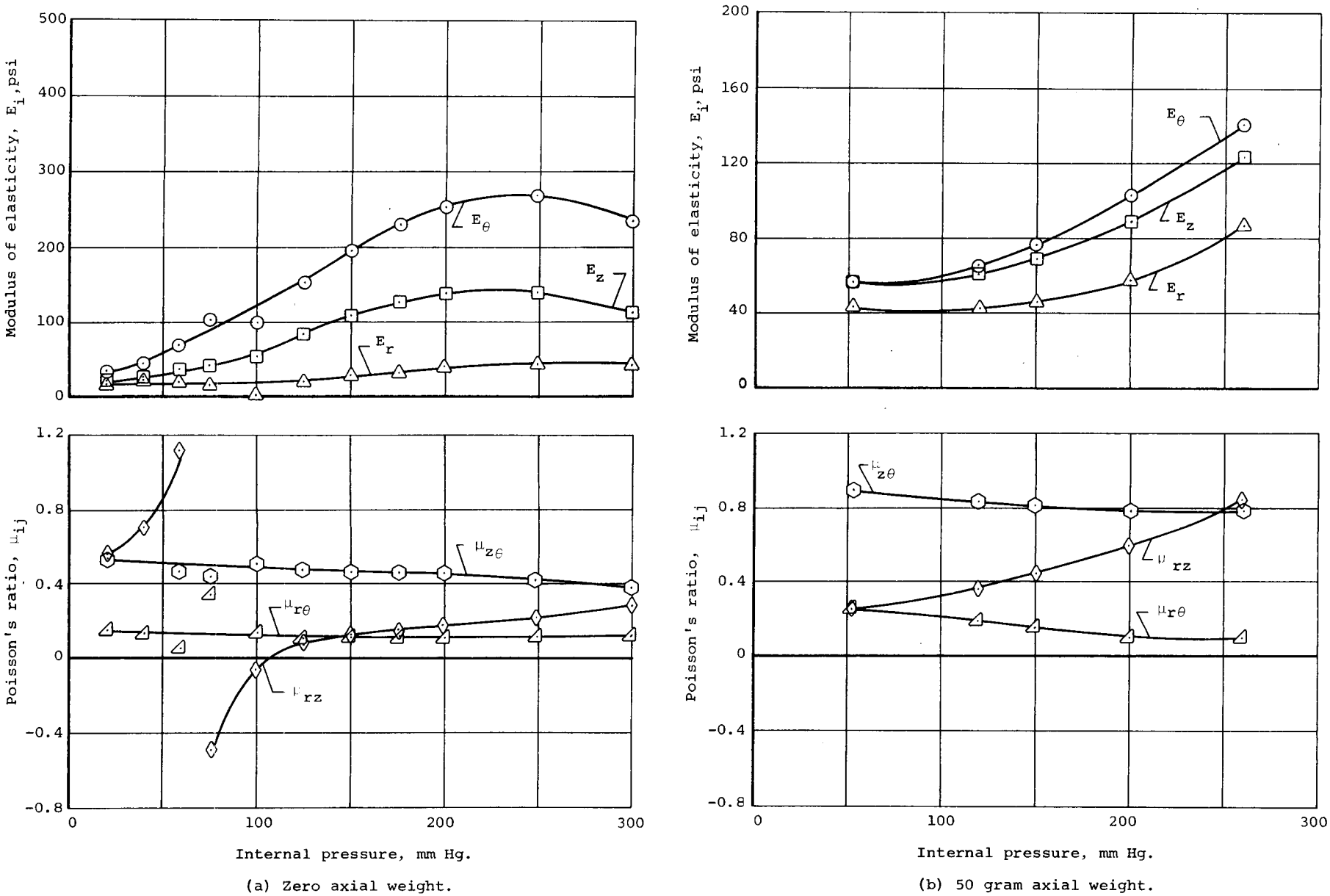

Figure 25.- Variation of Young's Moduli and Poisson's ratios with internal pressure for Splenic IA.

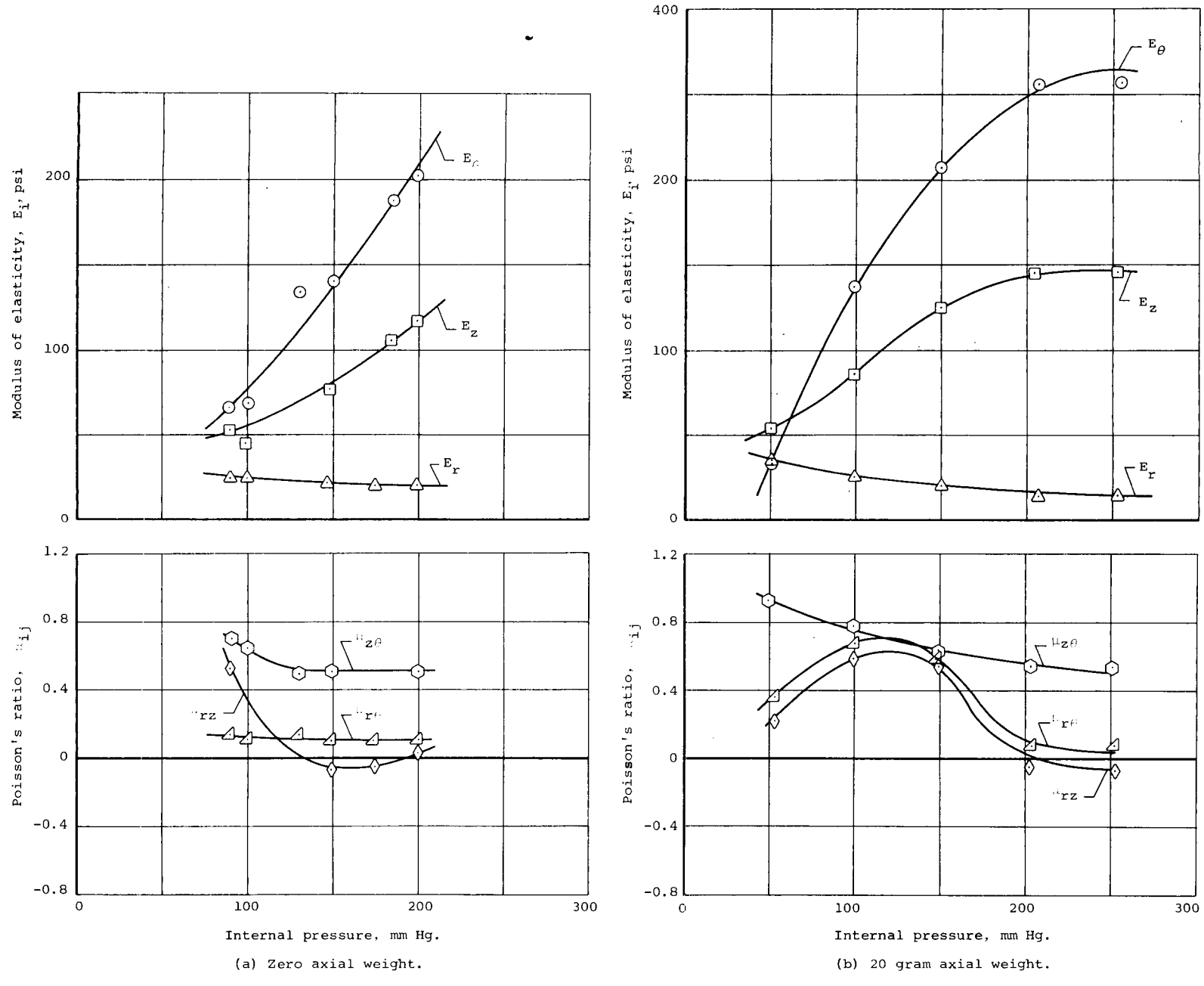

Figure 26.- Variation of Young's Moduli and Poisson's ratios with internal pressure for Splenic IB.

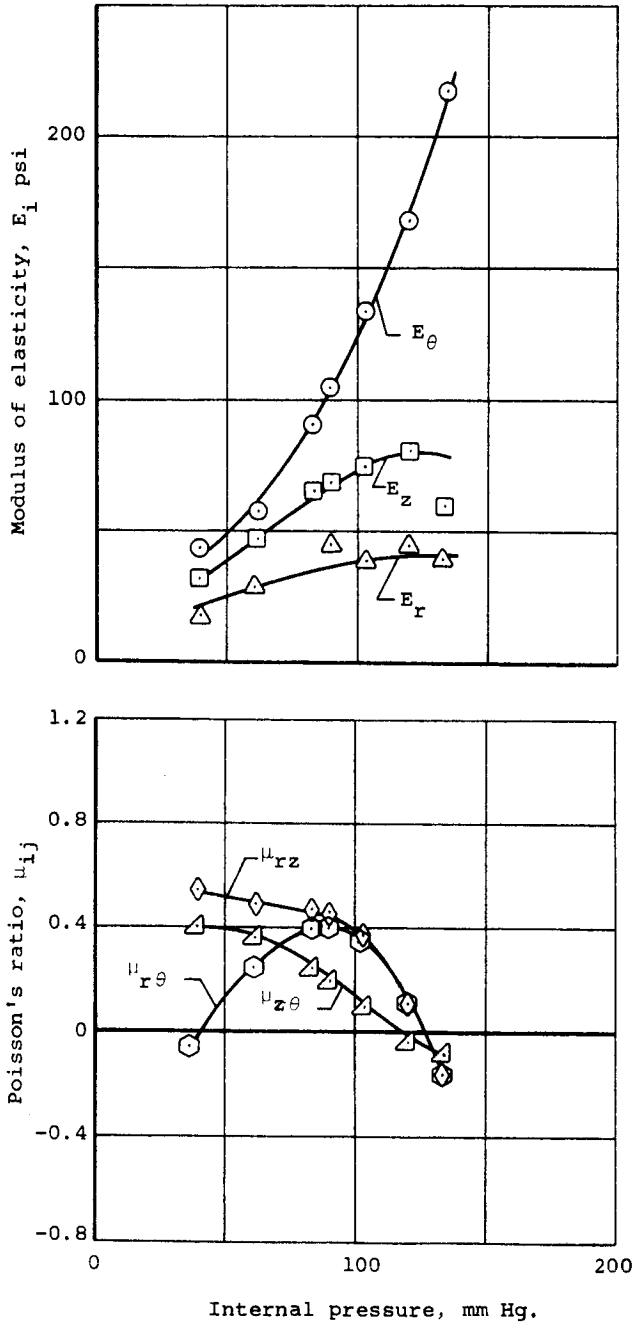

(a) Zero axial weight.

Figure 27.- Variation of Young's Moduli and Poisson's ratios with internal pressure for Thoracic Aorta IA.

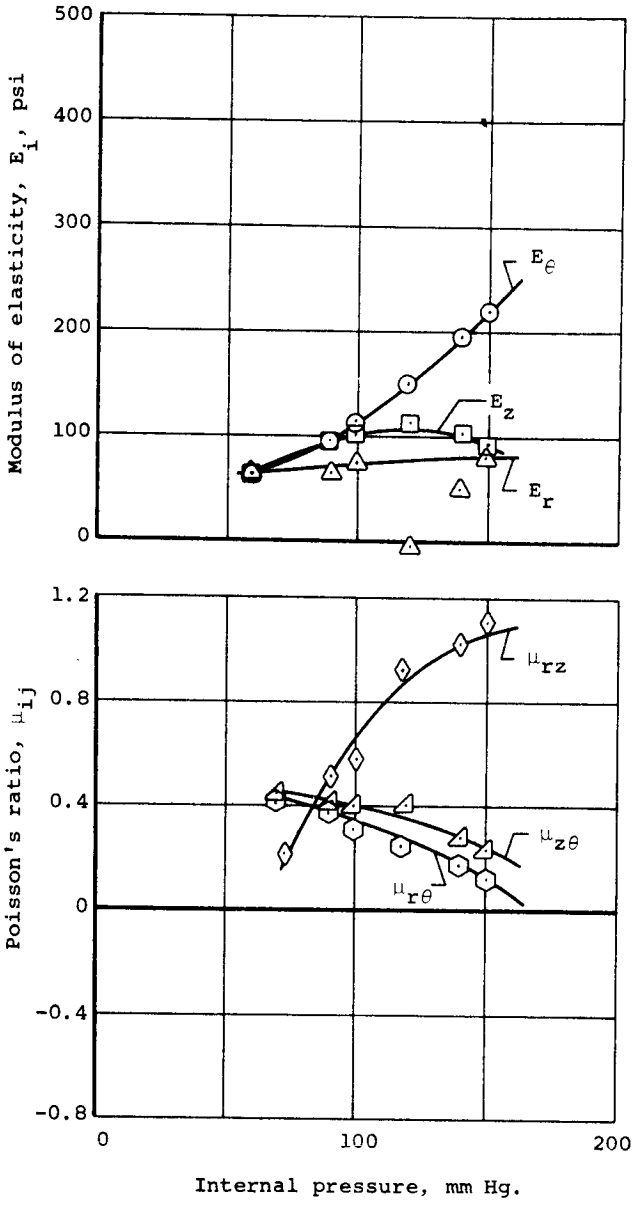

Figure 28.- Variation of Young's Moduli and Poisson's ratios with internal pressure for Thoracic Aorta IB, zero axial weight.

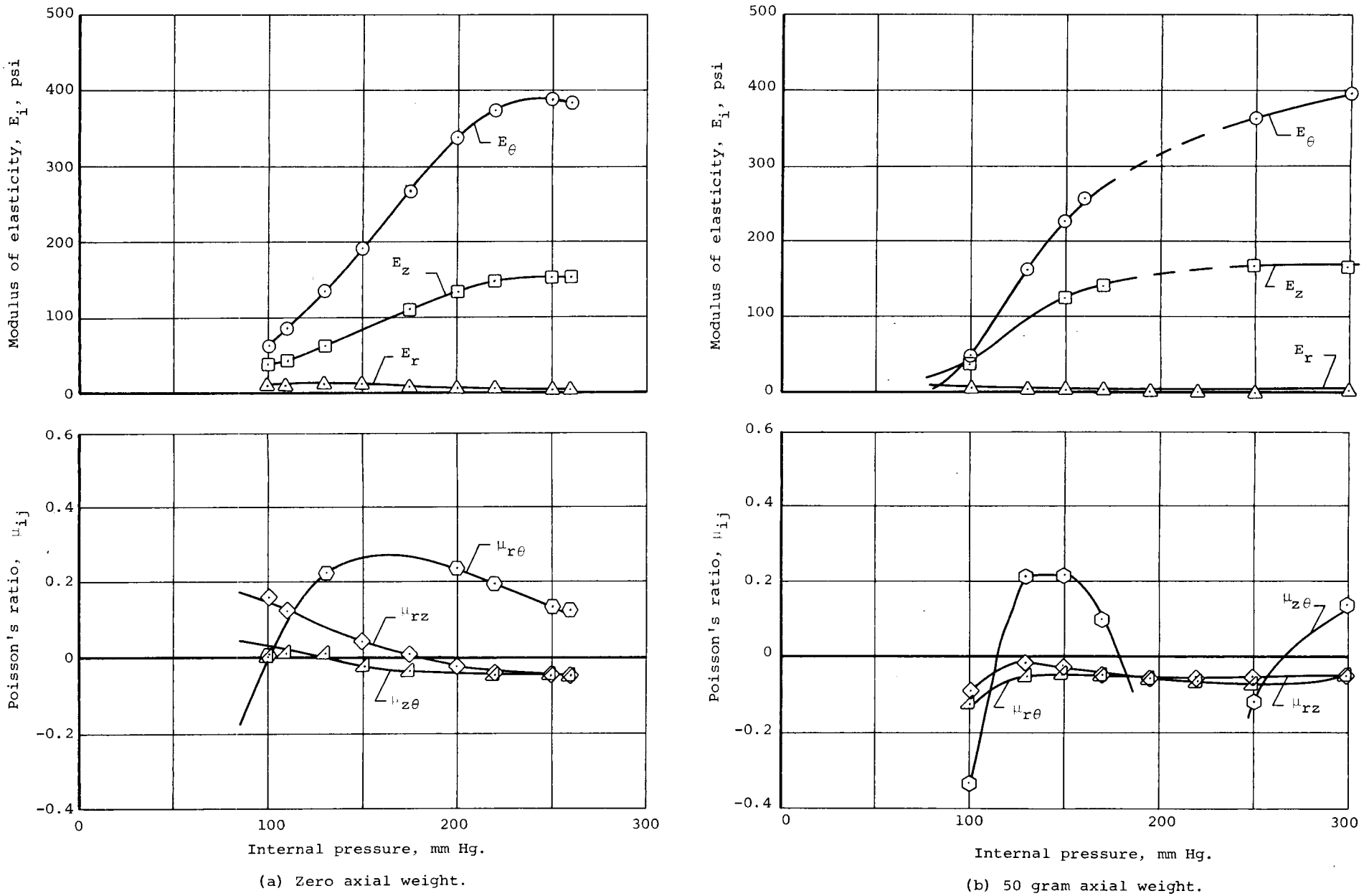

Figure 29.- Variation of Young's Moduli and Poisson's ratios with internal pressure for Thoracic Aorta IIA.

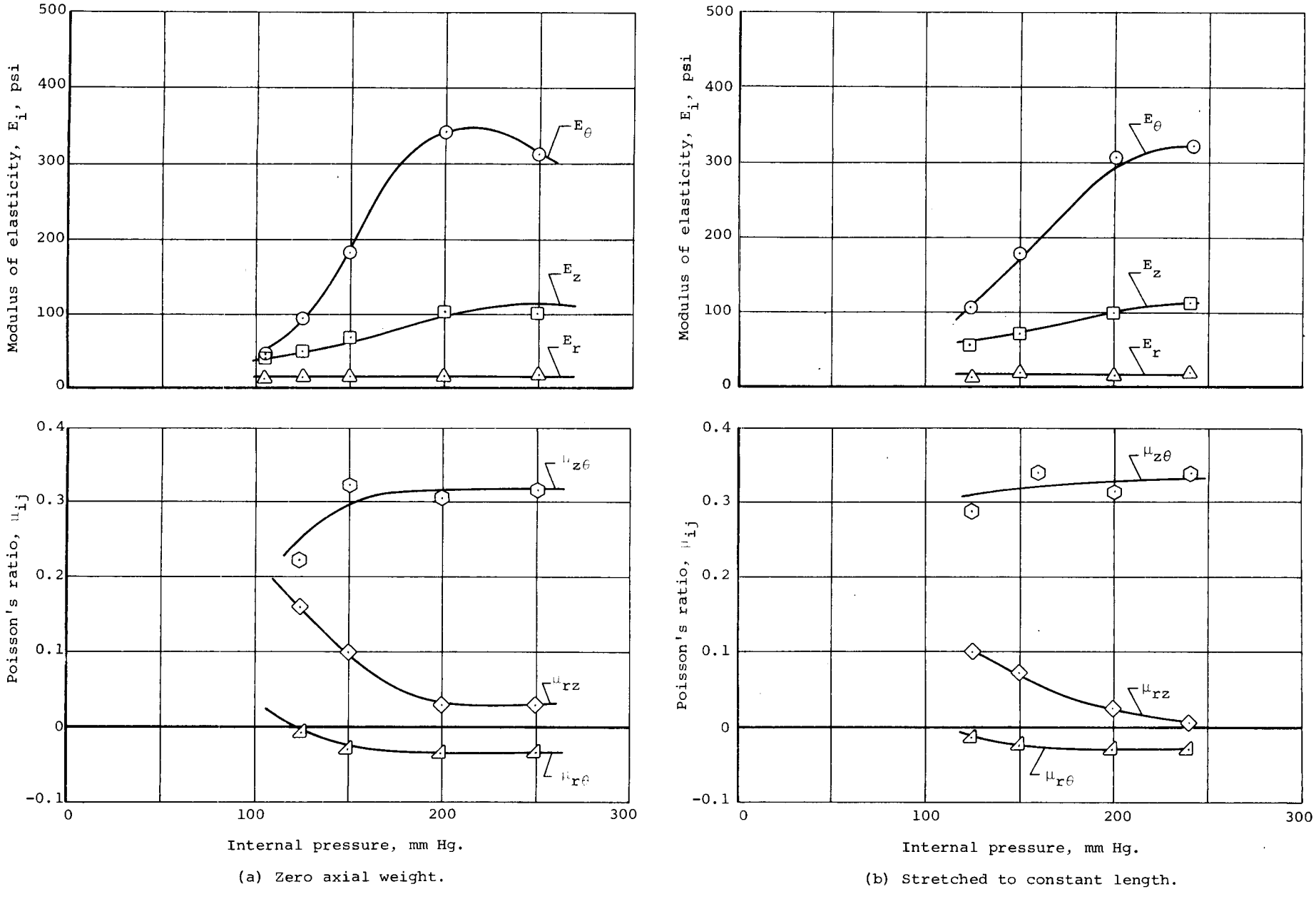

Figure 30.- Variation of Young's Moduli and Poisson's ratios with internal pressure for Thoracic Aorta IIB.

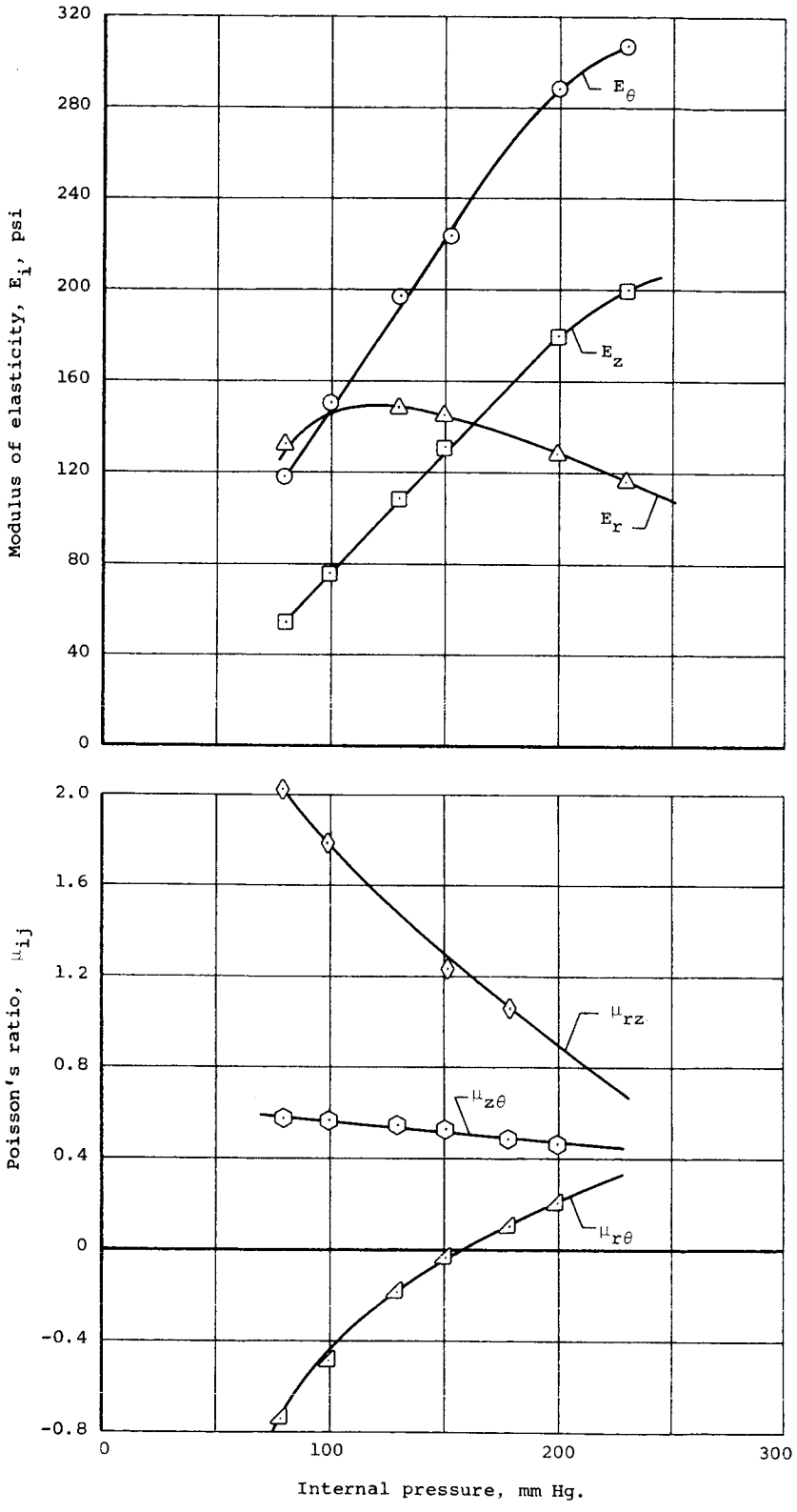

Figure 31.- Variation of Young's Moduli and Poisson's ratios with internal pressure for Superior Mesenteric IA, zero axial weight.

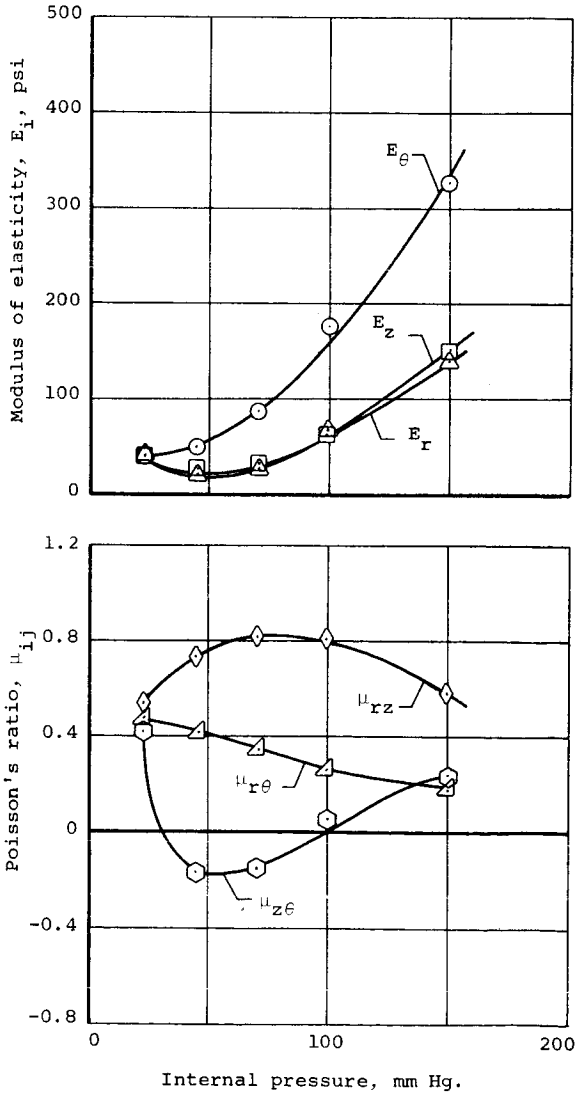

Figure 32.- Variation of Young's Moduli and Poisson's ratios with internal pressure for Femoral IA, zero axial weight.

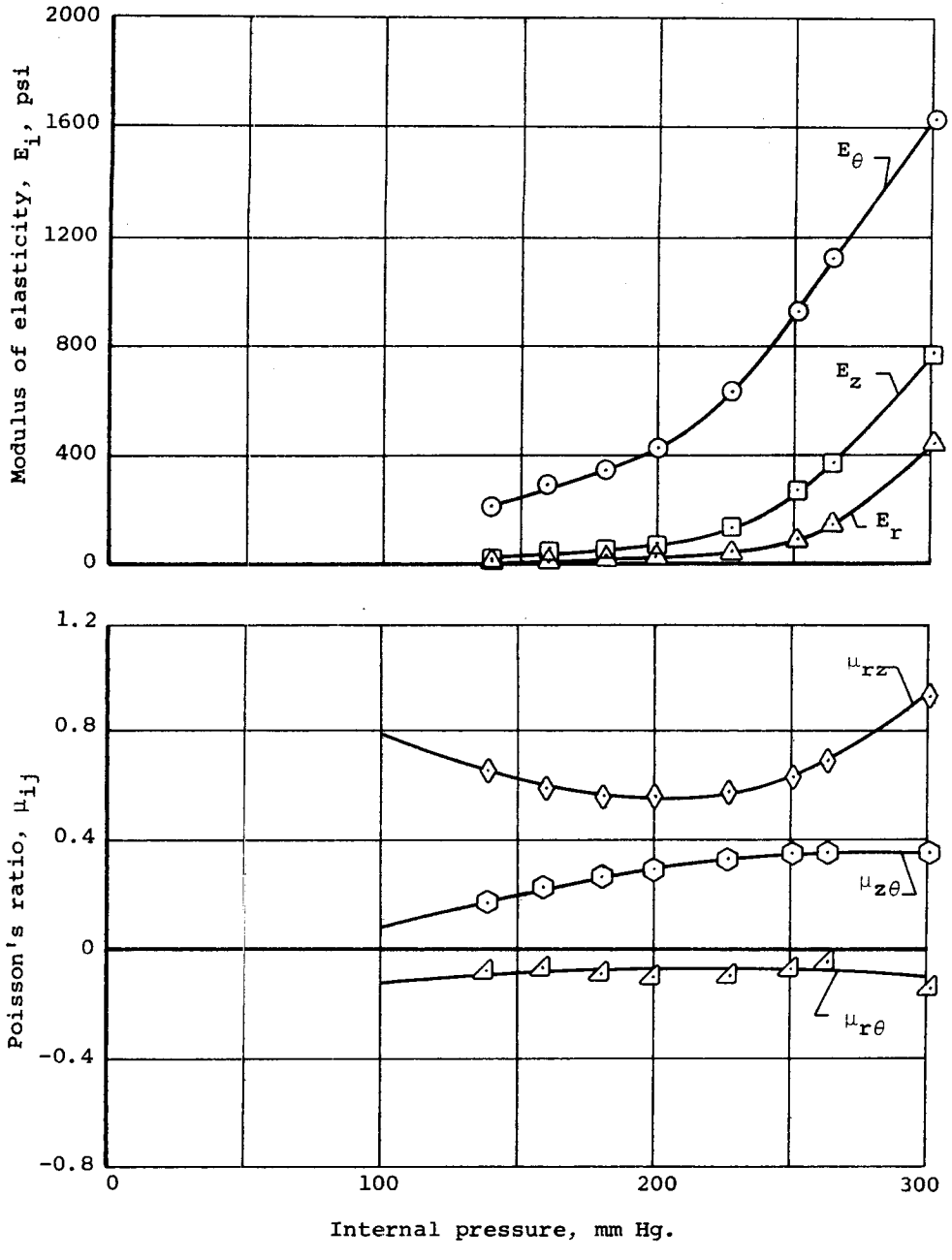

Figure 33.- Variation of Young's Moduli and Poisson's ratios with internal pressure for Femoral IIA, zero axial weight.

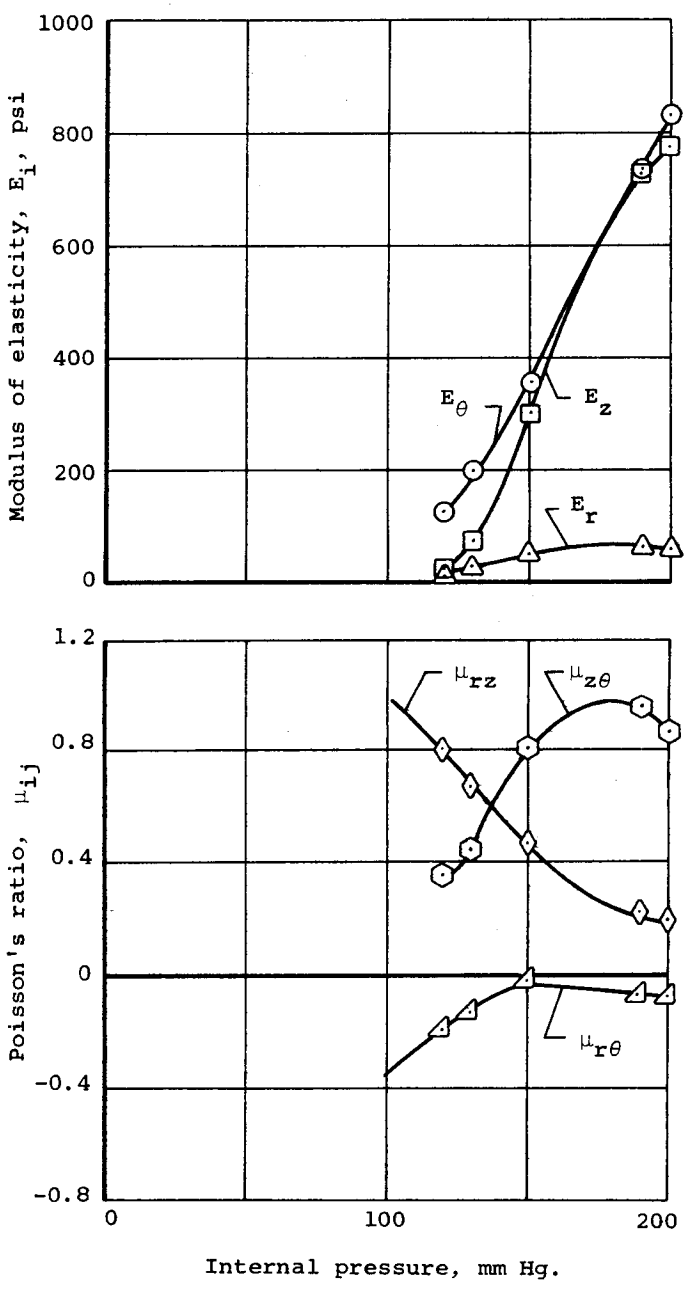

Figure 34.- Variation of Young's Moduli and Poisson's ratios with internal pressure for Femoral IIB, zero axial weight.

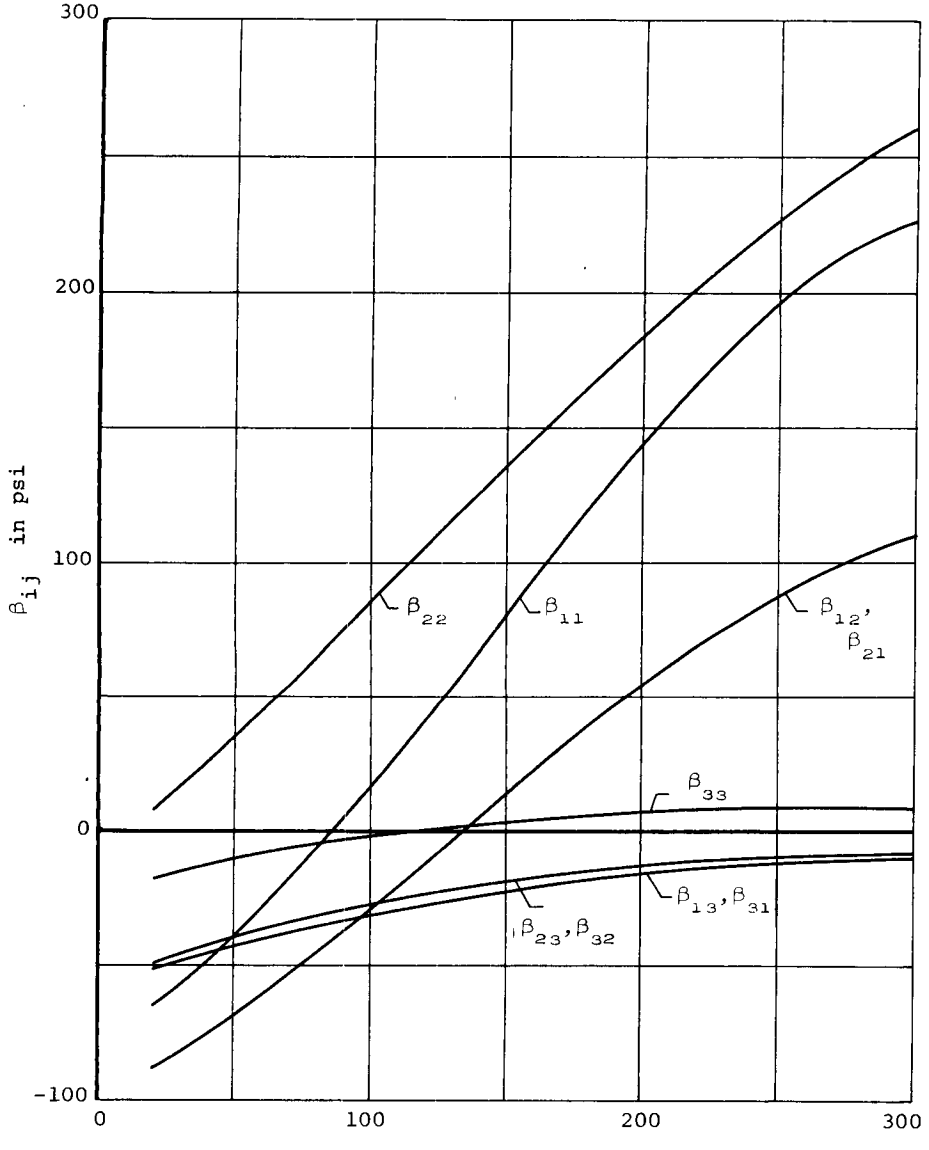

(a) Brachial IIA, 20 gram axial weight.

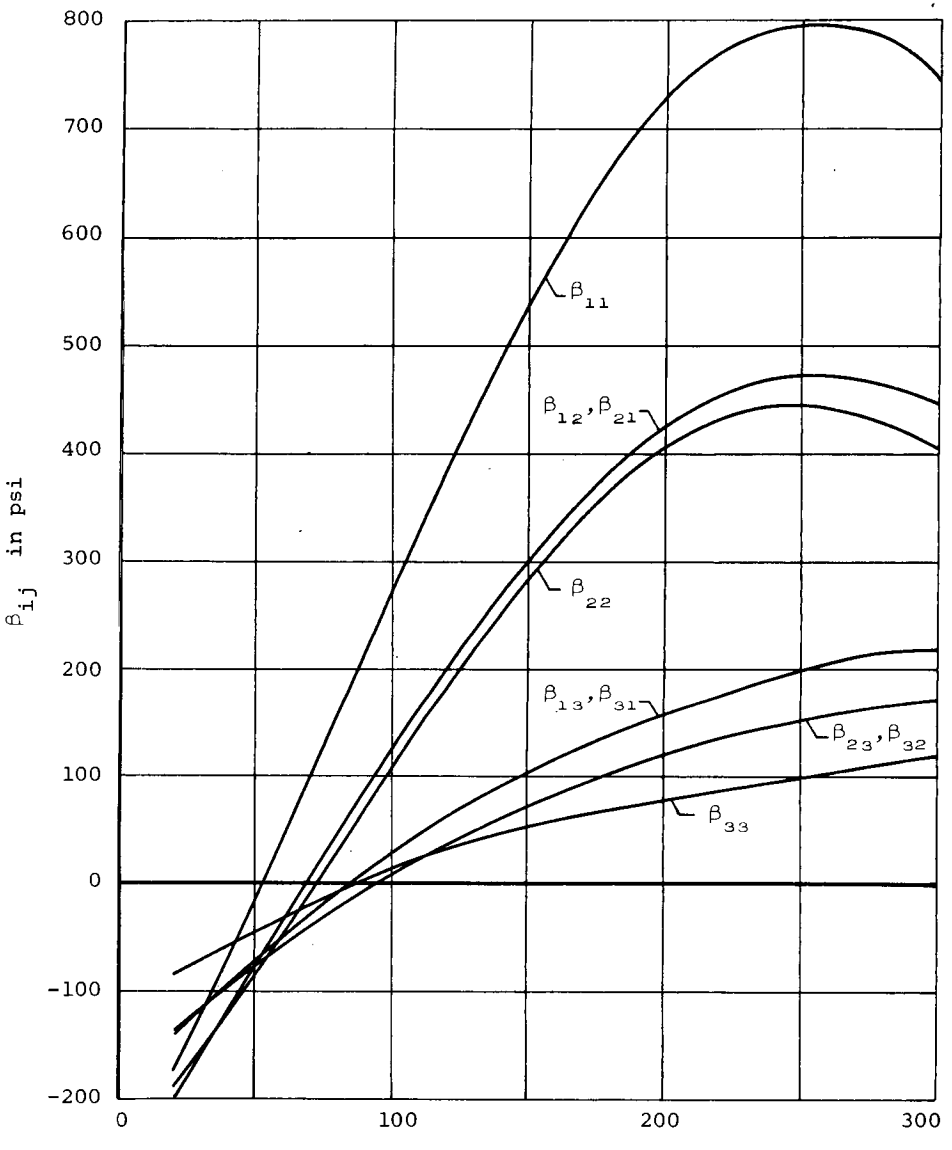

(b) Splenic IA, no axial weight.

Figure 35.- Variation of β_{ij} with internal pressure for two different specimens.

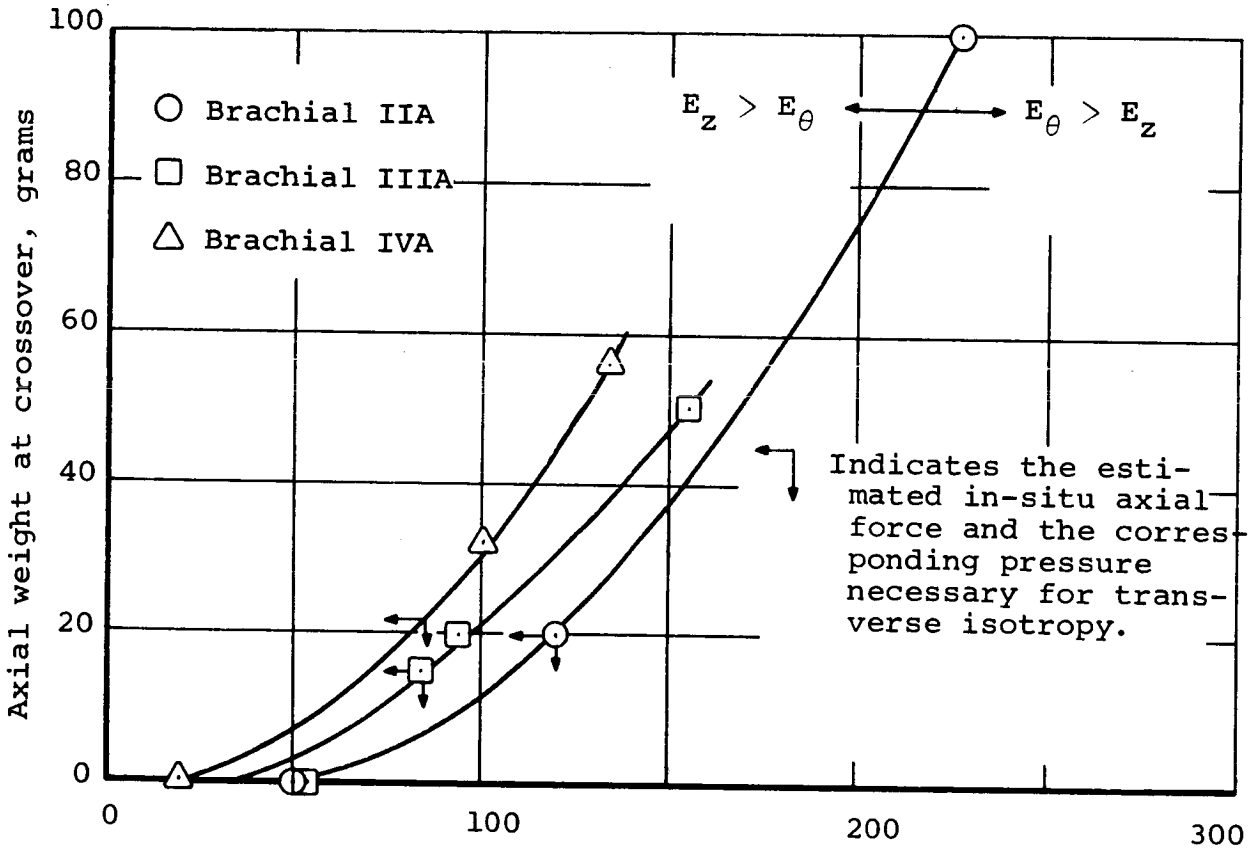

Figure 36.- Condition for transverse isotropy for three different Brachial arteries.

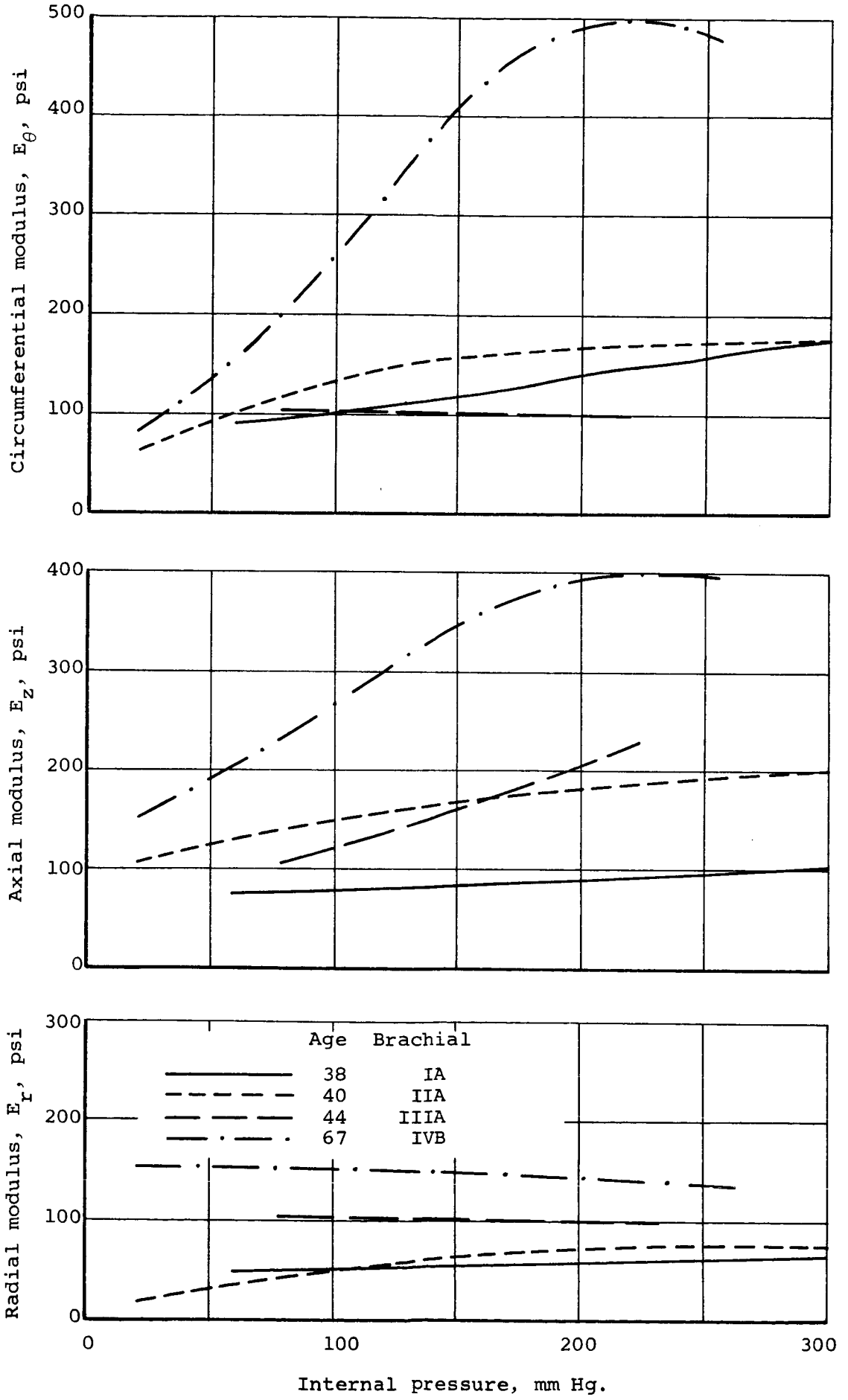

Figure 37.- Variation of the elastic moduli of elasticity for four different Brachial arteries stretched to their in-situ length, showing the effect of age.

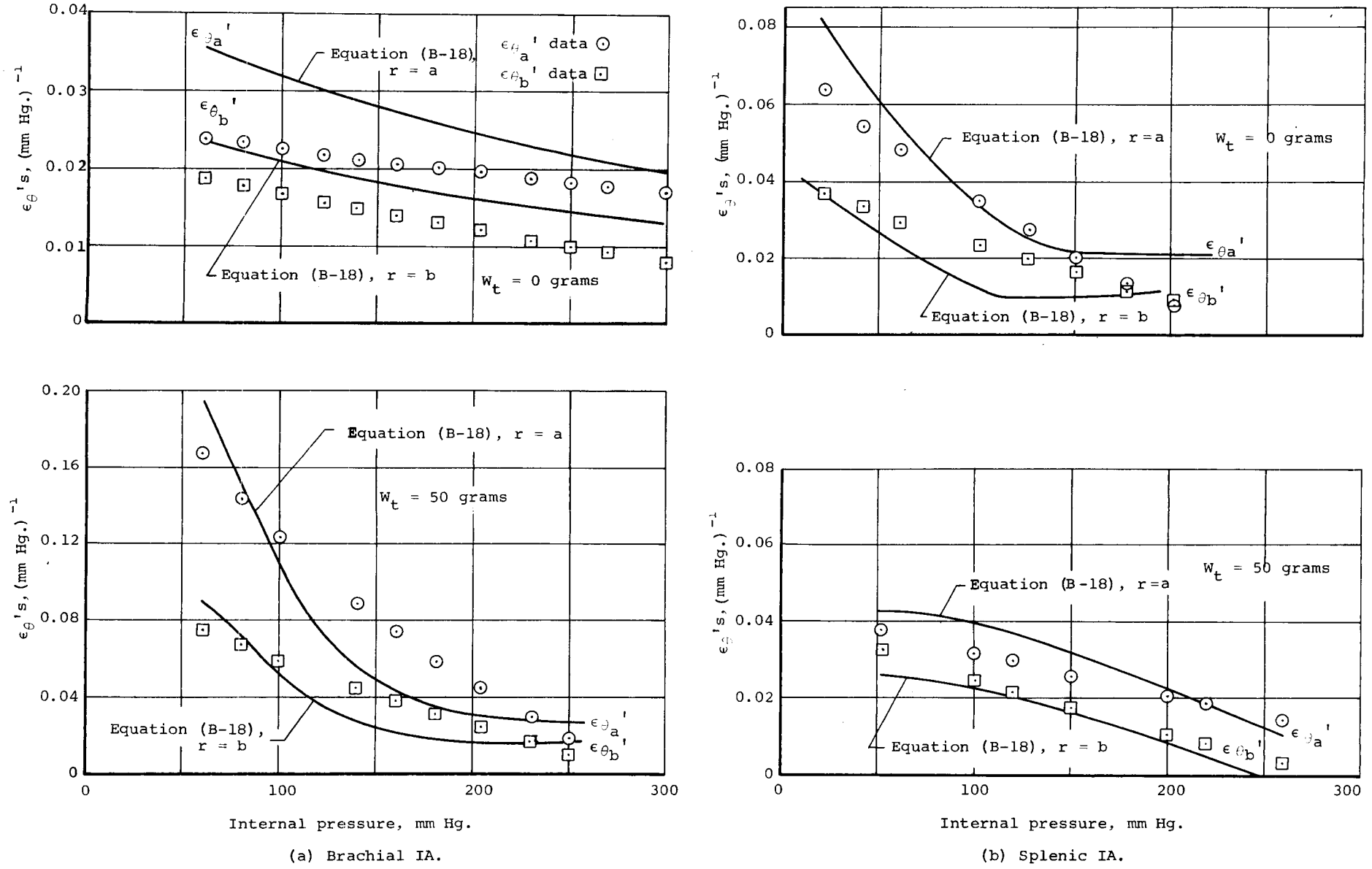

(a) Brachial IA.

(b) Splenic IA.

Figure 38.- Comparison of the computed and the measured circumferential strain.

APPENDIX A

DETERMINATION OF THE β CONSTANTS

The form of the β_{ij} was given in Equation (27) as

$$\beta_{ij} = \lambda_j \frac{\partial \sigma_{ii}}{\partial \lambda_j} \qquad (i,j = 1,2,3) \tag{A-1}$$

which is convenient for machine computation. The various partial derivatives, obtained directly from Equation (13) are given by

$$\left.\begin{aligned}
\frac{\partial \sigma_{11}}{\partial \lambda_1} &= 2\lambda_1\phi + \lambda_1^2 \frac{\partial \phi}{\partial \lambda_1} + \lambda_1^2(\lambda_2^2 + \lambda_3^2)\frac{\partial \psi}{\partial \lambda_1} + 2\lambda_1(\lambda_2^2 + \lambda_3^2)\psi + \frac{\partial P}{\partial \lambda_1} \\
\frac{\partial \sigma_{11}}{\partial \lambda_2} &= \lambda_1^2 \frac{\partial \phi}{\partial \lambda_2} + \lambda_1^2(\lambda_2^2 + \lambda_3^2)\frac{\partial \psi}{\partial \lambda_2} + 2\lambda_2\lambda_1^2\psi + \frac{\partial P}{\partial \lambda_2} \\
\frac{\partial \sigma_{11}}{\partial \lambda_3} &= \lambda_1^2 \frac{\partial \phi}{\partial \lambda_3} + \lambda_1^2(\lambda_2^2 + \lambda_3^2)\frac{\partial \psi}{\partial \lambda_3} + 2\lambda_1^2\lambda_3\psi + \frac{\partial P}{\partial \lambda_3} \\
\frac{\partial \sigma_{22}}{\partial \lambda_1} &= \lambda_2^2 \frac{\partial \phi}{\partial \lambda_1} + \lambda_2^2(\lambda_1^2 + \lambda_3^2)\frac{\partial \psi}{\partial \lambda_1} + 2\lambda_1\lambda_2^2\psi + \frac{\partial P}{\partial \lambda_1} \\
\frac{\partial \sigma_{22}}{\partial \lambda_2} &= 2\lambda_2\phi + \lambda_2^2 \frac{\partial \phi}{\partial \lambda_2} + \lambda_2^2(\lambda_1^2 + \lambda_3^2)\frac{\partial \psi}{\partial \lambda_2} + 2\lambda_2(\lambda_1^2 + \lambda_3^2)\psi + \frac{\partial P}{\partial \lambda_2} \\
\frac{\partial \sigma_{22}}{\partial \lambda_3} &= \lambda_2^2 \frac{\partial \phi}{\partial \lambda_3} + \lambda_2^2(\lambda_1^2 + \lambda_3^2)\frac{\partial \psi}{\partial \lambda_3} + 2\lambda_3\lambda_2^2\psi + \frac{\partial P}{\partial \lambda_3} \\
\frac{\partial \sigma_{33}}{\partial \lambda_1} &= \lambda_3^2 \frac{\partial \phi}{\partial \lambda_1} + \lambda_3^2(\lambda_1^2 + \lambda_2^2)\frac{\partial \psi}{\partial \lambda_1} + 2\lambda_1\lambda_3^2\psi + \frac{\partial P}{\partial \lambda_1} \\
\frac{\partial \sigma_{33}}{\partial \lambda_2} &= \lambda_3^2 \frac{\partial \phi}{\partial \lambda_2} + \lambda_3^2(\lambda_1^2 + \lambda_2^2)\frac{\partial \psi}{\partial \lambda_2} + 2\lambda_2\lambda_3^2\psi + \frac{\partial P}{\partial \lambda_2} \\
\frac{\partial \sigma_{33}}{\partial \lambda_3} &= \lambda_3^2 \frac{\partial \phi}{\partial \lambda_3} + 2\lambda_3\phi + \lambda_3^2(\lambda_1^2 + \lambda_2^2)\frac{\partial \psi}{\partial \lambda_3} + 2\lambda_3(\lambda_1^2 + \lambda_2^2)\psi + \frac{\partial P}{\partial \lambda_3}
\end{aligned}\right\} \tag{A-2}$$

where ϕ, ψ, and P are given by Equation (14). The derivatives of these functions are then given as

$$\left.\begin{aligned}
\frac{\partial \phi}{\partial \lambda_i} &= \frac{2}{\sqrt{I_3}} \frac{\partial^2 W}{\partial I_1 \partial \lambda_i} - \frac{\phi}{2I_3} \frac{\partial I_3}{\partial \lambda_i} \\
\frac{\partial \psi}{\partial \lambda_i} &= \frac{2}{\sqrt{I_3}} \frac{\partial^2 W}{\partial I_2 \partial \lambda_i} - \frac{\psi}{2I_3} \frac{\partial I_3}{\partial \lambda_i} \\
\frac{\partial P}{\partial \lambda_i} &= 2\sqrt{I_3} \frac{\partial^2 W}{\partial I_3 \partial \lambda_i} + \frac{P}{2I_3} \frac{\partial I_3}{\partial \lambda_i}
\end{aligned}\right\} \qquad \text{(A-3)}$$

The second-order partial derivatives, $\partial^2 W/\partial I_i \partial \lambda_j$, are determined by differentiation of $\partial W/\partial I_i$ (Eq. (19)) with respect to the extention ratio λ_j, that is,

$$\frac{\partial^2 W}{\partial I_i \partial \lambda_j} = K_i \frac{\partial I_i}{\partial \lambda_j} \quad (i,j = 1,2,3) \qquad \text{(A-4)}$$

where

$$\left.\begin{aligned}
K_1 &= 2\left[B_2 + 3B_3 (I_1 - 3)\right] \\
K_2 &= 2\left[C_2 + 3C_3 (I_2 - 3)\right] \\
K_3 &= 2\left[D_2 + 3D_3 (I_3 - 1)\right]
\end{aligned}\right\} \qquad \text{(A-5)}$$

The remaining derivatives $\partial I_i/\partial \lambda_j$ are determined by differentiating the strain invariants with respect to the extention ratios λ_j. Hence, the β_{ij} are finally obtained by substitution of Equations (A-2), (A-3), (A-4), and (A-5) into Equation (A-1).

APPENDIX B

DISPLACEMENT SOLUTION OF A THICK-WALLED TUBE

B.1 DEVELOPMENT OF THE STRAIN EQUATIONS

The analysis presented in Section 3 was a nonlinear membrane analysis in which the variation of stresses across the tube wall was neglected. By virtue of this approximation, it was possible to extract all of the elastic coefficients β_{ij} from experimental measurements of the internal pressure, axial load, and resulting deformations. As a check on that analysis, we shall present here the analysis of a thick-walled, homogeneous[8], anistropic tube subjected to internal pressure and axial tension. Since the variation of stress through the tube wall cannot be measured directly, it is not possible to use this analysis to extract the elastic constants from the experimental data. However, the thick-walled analysis can be used as a check on the membrane analysis by using the β_{ij} computed from the latter in the stress-strain relations obtained from the thick-walled analysis. These stresses and strains can then be checked against the experimental data.

The equilibrium equations for an axisymmetric body (see Fig. 6) are given, in cylindrical coordinates (Ref. 35), as

$$\frac{\partial \sigma_r}{\partial r} + \frac{\partial \tau_{rz}}{\partial z} + \frac{\sigma_r - \sigma_\theta}{r} = 0 \qquad \text{(B-1)}$$

and

$$\frac{\partial \tau_{rz}}{\partial r} + \frac{\partial \sigma_z}{\partial z} + \frac{\tau_{rz}}{r} = 0 \qquad \text{(B-2)}$$

We now assume that the shear stresses τ_{rz} and the shear strains are zero and that the normal stresses are functions only of the radial coordinate r. Equation (B-2) is then automatically satisfied and Equation (B-1) becomes

$$\frac{d\sigma_r}{dr} + \frac{\sigma_r - \sigma_\theta}{r} = 0 \qquad \text{(B-3)}$$

---

[8] It should be noted that, in a thick-wall analysis, the assumption of homogeneity may actually be less realistic than in the membrane analysis, in view of the nonhomogeneous material wall. However, the thick-wall analysis does permit a radial variation of stresses and strains which the membrane analysis does not allow.

The strains are given in terms of displacements (Ref. 35) by

$$\epsilon_r = \frac{du}{dr}; \quad \epsilon_\theta = \frac{u}{r}; \quad \epsilon_z = \frac{w}{z} \tag{B-4}$$

and ϵ_z was observed experimentally to be constant through the wall. Since the normal stresses and strains are assumed to be a function only of the radial coordinate r, the material automatically satisfies the compatibility equations, (see Ref. 35).

The stress-strain equations for a linear, cylindrically anisotropic material can be expressed in terms of the elastic constants β's by

$$\left.\begin{aligned} \sigma_\theta &= \beta_{11}\epsilon_\theta + \beta_{12}\epsilon_z + \beta_{13}\epsilon_r \\ \sigma_z &= \beta_{12}\epsilon_\theta + \beta_{22}\epsilon_z + \beta_{23}\epsilon_r \\ \sigma_r &= \beta_{13}\epsilon_\theta + \beta_{23}\epsilon_z + \beta_{33}\epsilon_r \end{aligned}\right\} \tag{B-5}$$

This equation is based upon the assumption that the components of strain are linear functions of the stresses and pass through the origin. However, if the stress-strain relationship is nonlinear, then Equation (B-5) is meaningless, so, rather than discuss absolute stresses, we must discuss the local rates of change (perturbations) of the stresses and strains σ and ϵ, and thereby determine the differential strains. In order to do this, we assume that the elastic constants β_{ij} are defined as the local values and are not strong functions of the pressure; that is, we assume that

$$\frac{\partial \beta_{ij}}{\partial p} \cong 0 \tag{B-6}$$

This assumption permits us to write the stress-strain equation in the form

$$\left.\begin{aligned} \left.\frac{\partial \sigma_\theta}{\partial p}\right|_{p_1} &= \beta_{11}\left.\frac{\partial \epsilon_\theta}{\partial p}\right|_{p_1} + \beta_{12}\left.\frac{\partial \epsilon_z}{\partial p}\right|_{p_1} + \beta_{13}\left.\frac{\partial \epsilon_r}{\partial p}\right|_{p_1} \\ \left.\frac{\partial \sigma_z}{\partial p}\right|_{p_1} &= \beta_{12}\left.\frac{\partial \epsilon_\theta}{\partial p}\right|_{p_1} + \beta_{22}\left.\frac{\partial \epsilon_z}{\partial p}\right|_{p_1} + \beta_{23}\left.\frac{\partial \epsilon_r}{\partial p}\right|_{p_1} \\ \left.\frac{\partial \sigma_r}{\partial p}\right|_{p_1} &= \beta_{13}\left.\frac{\partial \theta}{\partial p}\right|_{p_1} + \beta_{23}\left.\frac{\partial \epsilon_z}{\partial p}\right|_{p_1} + \beta_{33}\left.\frac{\partial \epsilon_r}{\partial p}\right|_{p_1} \end{aligned}\right\} \tag{B-7}$$

where the derivatives are evaluated at some pressure p_1.

Equation (B-7) is more simply written as

$$\left.\begin{aligned} \sigma_\theta' &= \beta_{11}\epsilon_\theta' + \beta_{12}\epsilon_z' + \beta_{13}\epsilon_r' \\ \sigma_z' &= \beta_{12}\epsilon_\theta' + \beta_{22}\epsilon_z' + \beta_{23}\epsilon_r' \\ \sigma_r' &= \beta_{13}\epsilon_\theta' + \beta_{23}\epsilon_z' + \beta_{33}\epsilon_r' \end{aligned}\right\} \qquad \text{(B-8)}$$

where $\epsilon_\theta' = \partial\epsilon_\theta/\partial p$, $\epsilon_z' = \partial\epsilon_z/\partial p$, and $\epsilon_r' = \partial\epsilon_r/\partial p$.

The differentiation of equilibrium Equation (B-3) with respect to pressure yields

$$\frac{d\sigma_r'}{dr} + \frac{\sigma_r' - \sigma_\theta'}{r} = 0 \qquad \text{(B-9)}$$

Now, by substituting the strain-displacement Equations (B-4) and the stress-strain Equations (B-5) into the equilibrium Equation (B-9), we obtain the following second-order, ordinary differential equation for the radial displacement u' as a function of r:

$$\frac{d^2u'}{dr^2} + \frac{1}{r}\frac{du'}{dr} - k^2\,\frac{u'}{r^2} + A\,\epsilon_z' = 0 \qquad \text{(B-10)}$$

where

$$k^2 = \beta_{11}/\beta_{33} \quad \text{and} \quad A = (\beta_{23} - \beta_{13})/\beta_{33} \qquad \text{(B-11)}$$

The solution of Equation (B-10) has the form

$$u' = F_1\, r^k + F_2 r^{-k} + Fr \qquad \text{(B-12)}$$

where the constants F_1 and F_2 must be determined from the boundary conditions, and F is defined by

$$F = -A\epsilon_z'/(1 - k^2) \qquad \text{(B-13)}$$

The two boundary conditions which are used to evaluate F_1 and F_2 are the values of radial stress (equal to minus the pressure) at the inner and outer wall. Thus, in terms of the local derivatives, we have

$$\sigma_r' = 0 \text{ at } r = b, \text{ and } \sigma_r' = -1 \text{ at } r = a \qquad \text{(B-14)}$$

By substituting the solution of the differential equation (Eq. (B-12)) into the stress-strain equation (Eq. (B-8)), and employing these boundary conditions, we find that F_1 and F_2 are given by

$$F_1 = \frac{\dfrac{\gamma^{k+1}\left[1 + B\epsilon_z'(1 - \gamma^{k-1})\right]}{(1 - \gamma^{2k})} - B\epsilon_z'}{b^{k-1}(\beta_{13} + k\,\beta_{33})} \tag{B-15}$$

and

$$F_2 = \frac{(-1)\ a^{k+1}\left[1 + B\epsilon_z'\ (1 - \gamma^{k-1})\right]}{(1 - \gamma^{2k})(\beta_{13} - k\,\beta_{33})} \tag{B-16}$$

where

$$\gamma = a/b$$

$$B = \beta_{23} - \frac{A}{1 - k^2}\,(\beta_{33} + \beta_{13}) \tag{B-17}$$

Hence, the stresses and strains can finally be written in terms of the radial coordinate by substituting Equations (B-15), (B-16), (B-4), (B-13), and (B-12) into Equation (B-8). Thus, we have

$$\left.\begin{aligned}
\epsilon_z' &= \text{constant} \\
\epsilon_\theta' &= F_1 r^{k-1} + F_2 r^{-k-1} - \frac{A\epsilon_z'}{1 - k^2} \\
\epsilon_r' &= F_1\,kr^{k-1} - F_2 kr^{-k-1} - \frac{A\epsilon_z'}{1 - k^2} \\
\sigma_r' &= F_1 r^{k-1}(\beta_{13} + k\,\beta_{33}) + \frac{F_2}{r^{k+1}}\,(\beta_{13} - k\,\beta_{33}) + B\epsilon_z' \\
\sigma_\theta' &= F_1 r^{k-1}(\beta_{11} + k\,\beta_{13}) + \frac{F_2}{r^{k+1}}\,(\beta_{11} - k\,\beta_{13}) + H\epsilon_z' \\
\sigma_z' &= F_1 r^{k-1}(\beta_{12} + k\,\beta_{23}) + \frac{F_2}{r^{k+1}}\,(\beta_{12} - k\,\beta_{23}) + G\epsilon_z'
\end{aligned}\right\} \tag{B-18}$$

where the constants H and G are given by

$$\left.\begin{aligned} H &= \beta_{12} - \frac{A}{1 - k^2}(\beta_{13} + \beta_{11}) \\ G &= \beta_{11} - \frac{A}{1 - k^2}(\beta_{23} + \beta_{12}) \end{aligned}\right\} \qquad \text{(B-19)}$$

Equations (B-18) will be used to check the validity of the elastic constants β_{ij} generated by the nonlinear membrane theory of Section 3. This check is completed by comparing the computed values of ϵ_θ' at the inner and outer radii (a and b) with the values calculated directly from the experimental data. The experimental strains, ϵ_{θ_a}' and ϵ_{θ_b}' are given locally by

$$\left.\begin{aligned} \epsilon_{\theta_a}' &= \frac{1}{a}\frac{\partial a}{\partial p} \\ \epsilon_{\theta_b}' &= \frac{1}{b}\frac{\partial b}{\partial p} \end{aligned}\right\} \qquad \text{(B-20)}$$

These expressions are easily evaluated from the a and b curve-fit Equations (36), so that they become

$$\left.\begin{aligned} \epsilon_{\theta_a}' &= \frac{a_2 + 2a_3 p}{a_1 + a_2 p + a_3 p^2} \\ \epsilon_{\theta_b}' &= \frac{b_2 + 2b_3 p}{b_1 + b_2 p + b_3 p^2} \end{aligned}\right\} \qquad \text{(B-21)}$$

Figure 38 presents the values of ϵ_{θ_a}' and ϵ_{θ_b}' computed from the thick-tube analysis (Eqs. (B-18)) for two different arteries, each of which was exposed to two different axial weights. The experimentally determined values of ϵ_{θ_a}' and ϵ_{θ_b}' are also shown.

Since experimental uncertainties (Ref. 41) in calculating the experimental ϵ_θ's are fairly high (20 to 30 percent), it is difficult to say a great deal concerning the results except that the experimental data are in approximate agreement with the theoretical values. In view of the highly nonlinear equations involved in computing these theoretical strains, and in view of the nonhomogeneous arterial wall, the agreement is considered sufficiently close to conclude that this approach adequately checks the β's computed from the membrane analysis. It also appears that the thick tube effects do not warrant additional consideration at this time, since the theory roughly predicts the strains at both the inner and outer walls.

B.2 INCOMPRESSIBILITY

The condition of incompressibility is given by setting Equation (39) to zero and written here in terms of ϵ_r', ϵ_θ', and ϵ_z' as

$$\epsilon_r' + \epsilon_\theta' + \epsilon_z' \equiv 0 \tag{B-22}$$

By substituting the strain Equations (B-18) into the above, we observe that

$$F_1 r^{k-1}(1 + k) + F_2(1 - k)r^{-k-1} - \epsilon_z' \left[2A(1 - k^2)^{-1} - 1\right] \equiv 0 \tag{B-23}$$

If the test material is truly a homogeneous, incompressible material, then Equation (B-23) must hold for any value of the radial coordinate r. However, the only conditions which will satisfy Equation (B-23) for all values of r are either

$$k \equiv 1 \quad \text{and} \quad A \equiv 0 \tag{B-24}$$

or

$$\beta_{11} \equiv \beta_{33} \quad \text{and} \quad \beta_{13} \equiv \beta_{23}$$

but these are the conditions for isotropy and/or transverse isotropy in the $r\theta$ plane, respectively. Hence, only isotropic or transversely isotropic ($r\theta$ plane) material can be incompressible; all other homogeneous, transversely isotropic (rz and θz planes) and anisotropic materials must be compressible.

Under certain loading conditions, arteries behave as transversely isotropic materials in the θz plane, but this is <u>not</u> the condition for incompressibility discussed above. Consequently, arteries are compressible except for extremely small loading (below the physiological range) where they behave isotropically.

APPENDIX C

COMMENTS ON β_{ij} AND W

C.1 CHECKS ON THE COMPUTED β_{ij} and W

It is often very helpful to be able to have an instant check of the computed W's (strain energy) and β_{ij}'s (elastic constants) to eliminate unnecessary computing if errors are present. Two such checks exist, one for the β's and one for W's.

The β's can be quickly checked by observing whether reciprocity[9] exists, that is, $\beta_{ij} = \beta_{ji}$. Since all nine β's are calculated individually (see Table VI for sample output), this comparison is a convenient and quick check. In the present work, if the β's did not check within 10 percent, the data were not considered admissible, and the W function was re-evaluated.

It should be noted that reciprocity also exists for the α's, as well as the β's.

The magnitude of the stored strain energy W for the unweighted specimens can be evaluated by considering the work done by the air in distending the specimen. The isothermal work W_a done on the gas inside the artery can be expressed as

$$W_a = -\int_{V_1}^{V_i} p_i \, dV \tag{C-1}$$

where the internal pressure p_i can be related to the internal volume V_i by the equation of state, that is

$$p_i V_i = R_o T_i \tag{C-2}$$

In this case, the pressure is <u>absolute</u> pressure and not gage pressure. By substituting (C-2) into (C-1) and integrating, we find that W_a is given by

---

[9]The proof of reciprocity can be found in most elasticity texts (see Refs. 31, 33, or 34).

$$W_a = -R_o T_i \ln \frac{p_i}{p_1} \qquad \text{(C-3)}$$

or

$$W_a = -p_i V_i \ln \frac{p_i}{p_1}$$

If W_a is the work done on the gas, then the stored strain energy is equal to $-W_a$ the work done by the gas on the walls. However, since W is given as the strain energy per unit volume, we must divide $-W_a$ by the volume of the arterial wall V, which finally yields W. The value of the W then should be given as

$$W = \frac{-W_a}{V} = \frac{p_i\, a^2}{(b^2 - a^2)} \ln \frac{p_i}{p_1} \qquad \text{(C-4)}$$

where p_i is the internal pressure corresponding to the radii a and b, and p_1 is atmospheric pressure (14.7 psia).

This check of W is also presented in Table VI (noted as W (check)) for comparison with the value obtained from the W function curve fit. Equation (C-4) offers only an approximate check because the errors involved in measuring the pressures are too great to allow an accurate computation of the logarithm. Therefore, if the value of W computed from (C-4) agreed within an order of magnitude with the value computed from Equations (18), the data were considered acceptable.

C.2 FINALIZED ELASTIC CONSTANTS

All of the finalized elastic constants presented herein were obtained by averaging the β_{ij} where reciprocity should exist; that is, since β_{12} should equal β_{21}, an average value was used in their place. The net result of this averaging is shown in Table VI. In general, the finalized moduli and Poisson's ratio only changed by 1 to 2 percent from their values before averaging.